Memristor Circuit Equations with Periodic Forcing

Makoto Itoh[1]
1-19-20-203, Arae, Jonan-ku,
Fukuoka, 814-0101 JAPAN
Email: itoh-makoto@jcom.home.ne.jp

Abstract
In this paper, we show that the dynamics of a wide variety of nonlinear systems such as engineering, physical, chemical, biological, and ecological systems, can be simulated or modeled by the dynamics of memristor circuits. It has the advantage that we can apply nonlinear circuit theory to analyze the dynamics of memristor circuits. Applying an external source to these memristor circuits, they exhibit complex behavior, such as chaos and non-periodic oscillation. If the memristor circuits have an integral invariant, they can exhibit quasi-periodic or non-periodic behavior by the sinusoidal forcing. Their behavior greatly depends on the initial conditions, the parameters, and the maximum step size of the numerical integration. Furthermore, an overflow is likely to occur due to the numerical instability in long-time simulations. In order to generate a non-periodic oscillation, we have to choose the initial conditions, the parameters, and the maximum step size, carefully. We also show that we can reconstruct chaotic attractors by using the terminal voltage and current of the memristor. Furthermore, in many memristor circuits, the active memristor switches between passive and active modes of operation, depending on its terminal voltage. We can measure its complexity order by defining the binary coding for the operation modes. By using this coding, we show that the memristor's operation modes exhibit the higher complexity, in the forced memristor Toda lattice equations and the forced memristor Van der Pol equations. Furthermore, the memristor has the special operation modes in the memristor Chua circuit.

Keywords
memristor; chaos; quasi-periodic; non-periodic; numerical instability; integral invariant; attractor reconstruction; passive; active; instantaneous power; complexity order; memristor's operation modes; Chua circuit; Van der Pol oscillator; Hamilton's equations; Hamiltonian; Toda lattice equations; Lotka-Volterra equations; ecological predator-prey model; Rössler equations; Lorenz equations; Brusselator equations; Gierer-Meinhardt equations; Tyson-Kauffman equations; Oregonator equations; sine-Gordon equation; tennis racket equations; pendulum equations; CO_2 laser model.

1 Introduction

The dynamics of n-dimensional autonomous systems can be transformed into the dynamics of two-element *extended memristor* circuits. The internal state of the memristors in these two-element circuits have the same dynamics as n-dimensional autonomous systems [1]. Thus, the memristors are essential dynamical elements needed in the modeling of complex nonlinear dynamical phenomena. In this paper, based on the above research results, we show that the dynamics of a wide variety of nonlinear systems, not only in physical and engineering systems, but also in biological and chemical systems and, even, in ecological systems, can

[1]After retirement from Fukuoka Institute of Technology, he has continued to study the nonlinear dynamics on memristors.

be simulated or modeled by the dynamics of memristor circuits. It has the advantage that we can apply nonlinear circuit theory to analyze the dynamics of memristor circuits.

It is known that the dynamics of Chua's circuit and Van der Pol oscillator can be realized by using an ideal active memristor and some linear elements [2]. However, almost nonlinear systems can not satisfy the circuits equations without change. Thus, in order to transform their nonlinear equations into the memristor circuit equations, we use two methods, one is the exponential coordinate transformation, and the other is the time-scaling change [1, 3, 4]. The resulting memristor circuits have the same dynamics as the nonlinear systems. Furthermore, by connecting an external periodic forcing to these memristor circuits, they can exhibit complex behavior, such as chaos and non-periodic oscillation. If the memristor circuits have an integral invariant, then they can exhibit quasi-periodic or non-periodic behavior, which greatly depends on the initial conditions, the circuit parameters, and the maximum step size of the numerical integration. Furthermore, an overflow (outside the range of data) is likely to occur due to the numerical instability in long-time simulations. Thus, in order to generate a non-periodic oscillation, we have to choose the initial conditions, the parameters, and the maximum step size, carefully. Furthermore, noise may considerably affect the behavior of physical circuits.

We also show that if we plot the terminal voltage against current of the memristor in the circuits, we can get the reconstruction of chaotic attractor on the two-dimensional plane. Furthermore, if we plot the instantaneous power p versus the terminal voltage v of the active memristor, then the $v-p$ locus lies in the first and the third quadrants, and it is pinched at the origin in many memristor circuits. It looks exactly like the $i-v$ loci of the passive memristor when a periodic source is supplied. Thus, the active memristor switches between passive and active modes of operation depending on its terminal voltage. However, in the forced memristor Toda lattice equations, the $v-p$ locus exhibits more complicated behavior, that is, it switches between four modes of operation. In order to measure the *complexity order*, we define the binary coding for the above memristor's operation modes. By using this coding, we show that the memristor's operation modes exhibit the higher complexity, in the forced memristor Toda lattice equations and the forced memristor Van der Pol equations. Furthermore, in the memristor Chua circuit, the active memristor exhibits the special operation modes, which is quite different from the other memristor circuits.

2 Three-element Memristor Circuit

Let us consider the three-element memristor circuit in Figure 1, which consists of an inductor L, a battery E, and a current-controlled extended memristor.

The terminal voltage v_M and the terminal current i_M of the current-controlled extended memristor are described by

V-I characteristics of the extended memristor

$$\begin{aligned} v_M &= \hat{R}(\boldsymbol{x},\ i_M)\, i_M, \\ &\quad \hat{R}(\boldsymbol{x},\ 0) \neq \infty, \\ \frac{d\boldsymbol{x}}{dt} &= \tilde{\boldsymbol{f}}(\boldsymbol{x},\ i_M). \end{aligned} \tag{1}$$

Here, $\boldsymbol{x} = (x_1, x_2, \cdots, x_n) \in \mathbb{R}^n$, $\hat{R}(\boldsymbol{x},\ i_M)$ is a continuous scalar-valued function, and $\tilde{\boldsymbol{f}} = (\tilde{f}_1, \tilde{f}_2, \cdots, \tilde{f}_n) : \mathbb{R}^n \to \mathbb{R}^n$ (see Appendix A).

The dynamics of the above three-element memristor circuit is given by

Three-element memristor circuit equations

$$\begin{aligned} L\frac{di}{dt} &= -v_M + E = -\hat{R}(\boldsymbol{x},\ i)\, i + E, \\ \frac{d\boldsymbol{x}}{dt} &= \tilde{\boldsymbol{f}}(\boldsymbol{x},\ i), \end{aligned} \tag{2}$$

where L denotes the inductance of the inductor, E denotes the voltage of the battery, and $i_M = i$.

Assume that $n = 1$ and $L = 1$. Then Eq. (2) can be recast into the form

Three-element memristor circuit equations with $n = 1$ and $L = 1$

$$\begin{aligned} \frac{di}{dt} &= -v_M + E = -\hat{R}(x,\ i)\, i + E, \\ \frac{dx}{dt} &= \tilde{f}_1(x,\ i), \end{aligned} \tag{3}$$

where $\boldsymbol{x} = x$ and $\tilde{\boldsymbol{f}} = \tilde{f}_1$.

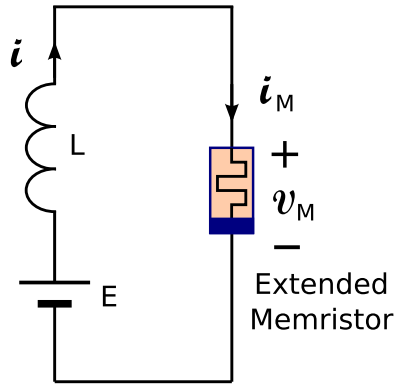

Figure 1: A three-element memristor circuit which consists of an inductor L, a battery E, and a current-controlled extended memristor (right side).

2.1 Brusselator equations

The Brusselator is a theoretical model for a type of autocatalytic reaction. The dynamics of the Brusselator is given by

Brusselator equations

$$\begin{aligned} \frac{du}{dt} &= A + \big\{uv - (B+1)\big\}u, \\ \frac{dv}{dt} &= B\,u - u^2\,v, \end{aligned} \tag{4}$$

where A and B are constants.

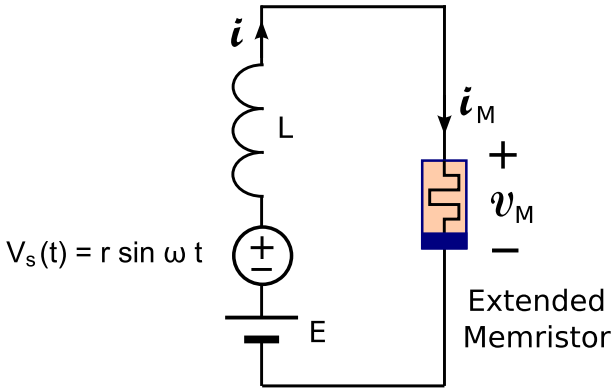

Figure 2: Four-element memristor circuit driven by a periodic voltage source $v_s(t) = r\sin(\omega t)$, where r and ω are constants.

Consider the three-element memristor circuit in Figure 1 with $L = 1$. Then the dynamics of this circuit is given by Eq. (3). Assume that Eq. (3) satisfies

$$\begin{aligned} E &= A, \\ \hat{R}(x,\, i) &= -\big\{i\,x - (B+1)\big\}, \\ \tilde{f}_1(x, i) &= Bi - i^2\,x. \end{aligned} \tag{5}$$

Then we obtain

Memristor Brusselator equations

$$\begin{aligned} \frac{di}{dt} &= A + \big\{ix - (B+1)\big\}i, \\ \frac{dx}{dt} &= B\,i - i^2\,x, \end{aligned} \tag{6}$$

where A and B are constants.

Equations (4) and (6) are equivalent if we change the variables

$$i = u,\ x = v. \tag{7}$$

The terminal voltage v_M and the terminal current i_M of the current-controlled extended memristor in Figure 1 are given by

V-I characteristics of the extended memristor

$$\begin{aligned} v_M &= \hat{R}(x,\, i_M)\, i_M = -\big\{i_M\,x - (B+1)\big\}i_M, \\ &\quad \hat{R}(x,\, 0) \neq \infty, \\ \frac{dx}{dt} &= B\,i_M - {i_M}^2\,x, \end{aligned} \tag{8}$$

where $\hat{R}(x,\, i_M) = -\big\{i_M\,x - (B+1)\big\}$ and $i_M = i$.

It follows that the Brusselator equations (4) can be realized by the three-element memristor circuit in Figure 1. Equations (4) and (6) exhibit periodic oscillation (limit cycle). When an external source is added as shown in Figure 2, the forced memristor Brusselator equations can exhibit chaotic oscillation [5]. The dynamics of this circuit is given by

Forced memristor Brusselator equations

$$\begin{aligned} \frac{di}{dt} &= A + \big\{ix - (B+1)\big\}i + r\sin(\omega t), \\ \frac{dx}{dt} &= B\,i - i^2\,x, \end{aligned} \tag{9}$$

where r and ω are constants.

We show the chaotic attractor, Poincaré map, and $i_M - v_M$ locus of Eq. (9) in Figures 3, 4, and 5(a), respectively. The following parameters are used in our computer simulations:

$$A = E = 0.4,\ B = 1.2,\ r = 0.05,\ \omega = 0.81. \tag{10}$$

The $i_M - v_M$ locus moves in the first quadrant, that is, it moves in the *passive* region, since the instantaneous power of the extended memristoris positive, that is,

$$P_M(t) \stackrel{\triangle}{=} i_M(t)\, v_M(t) > 0. \tag{11}$$

Hence, the instantaneous power $P_M(t)$ is dissipated in the extended memristor, which is delivered from the forcing signal and the inductor. Furthermore, the $i_M - v_M$ locus is not pinched at the origin as shown in Figure 5(a), since the trajectory does not tend to the origin.

We define next the instantaneous power of the two circuit elements, that is, the instantaneous power of the extended memristor and the battery by

$$p_{ME}(t) \stackrel{\triangle}{=} i_M(t)\, v_{ME}(t), \tag{12}$$

where $v_{ME}(t) = v_M(t) - E$, and E denotes the voltage of the battery. That is, $v_{ME}(t)$ denotes the voltage across the extended memristor and the battery. We show the $v_{ME} - p_{ME}$ locus in Figure 5(b). Observe that the locus is pinched at the origin, and it lies in the first and the third quadrants. Thus, the instantaneous power $p_{ME}(t)$ delivered from the forced signal and the inductor is dissipated when $v_M(t) - E > 0$. However, the instantaneous power $p_{ME}(t)$ is *not* dissipated when $v_M(t) - E < 0$. We conclude as follow:

Behavior of the extended memristor

Assume that Eq. (9) exhibits chaotic oscillation. Then, we obtain the following results:

1. The extended memristor defined by Eq. (8) is operated as a *passive* element. The instantaneous power $P_M(t)$ of the memristor is dissipated in this extended memristor, which is delivered from the forcing signal and the inductor.

2. When $v_M(t) - E < 0$, the instantaneous power $p_{ME}(t)$ of the extended memristor and the battery is *not* dissipated. However, when $v_M(t) - E > 0$, the instantaneous power $p_{ME}(t)$ is dissipated.

Note that $x(t)$ in Eq. (8) is the internal state of the extended memristor. Thus, we might not be able to observe it. However, we can reconstruct the chaotic attractor into two dimensional Euclidean space (plane) by using

$$\Big(i(t),\ i'(t)\Big), \tag{13}$$

where $i'(t) \triangleq \dfrac{di(t)}{dt}$ (see [6] for more details). Furthermore, the $i_M - v_M$ locus in Figure 5(a) is considered to be the reconstruction of the chaotic attractor on the two-dimensional plane, since

$$\Big(i_M(t),\, v_M(t)\Big) \equiv \Big(i(t),\ -i'(t) + A + r\sin(\omega t)\Big), \tag{14}$$

where $i_M(t) = i(t)$. We show their trajectories and Poincaré maps in Figures 6 and 7, respectively. We can also reconstruct the chaotic attractor into the three-dimensional Euclidean space by using

$$\Big(i(t),\ i'(t),\ i''(t)\Big), \tag{15}$$

or

$$\Big(i_M(t),\, v_M(t),\, i''_M(t)\Big) \equiv \Big(i(t),\ -i'(t) + A + r\sin(\omega t),\, i''(t)\Big), \tag{16}$$

where $i''(t) \triangleq \dfrac{d^2 i(t)}{dt^2}$. We show the reconstructed three-dimensional attractors in Figure 8. We can apply the above reconstruction methods to other examples in this paper.

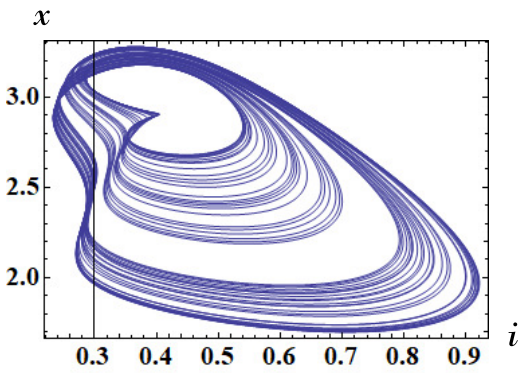

Figure 3: Chaotic attractor of the forced memristor Brusselator equations (9). Parameters: $A = 0.4,\ B = 1.2,\ r = 0.05,\ \omega = 0.81$. Initial conditions: $i(0) = 1.1,\ x(0) = 1.1$.

2.2 Diffusion-less Gierer-Meinhardt equations

Diffusion-less Gierer-Meinhardt equations [7, 8, 9] is defined by

Diffusion-less Gierer-Meinhardt equations

$$\begin{aligned} \frac{du}{dt} &= \frac{u^2}{v} - b\,u = \Big(\frac{u}{v} - b\Big)\,u, \\ \frac{dv}{dt} &= u^2 - c\,v, \end{aligned} \tag{17}$$

where b and c are constants.

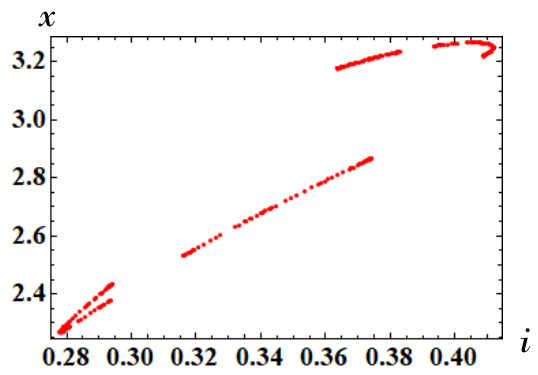

Figure 4: Poincaré map of the forced memristor Brusselator equations (9). Parameters: $A = 0.4,\ B = 1.2,\ r = 0.05,\ \omega = 0.81$. Initial conditions: $i(0) = 1.1,\ x(0) = 1.1$.

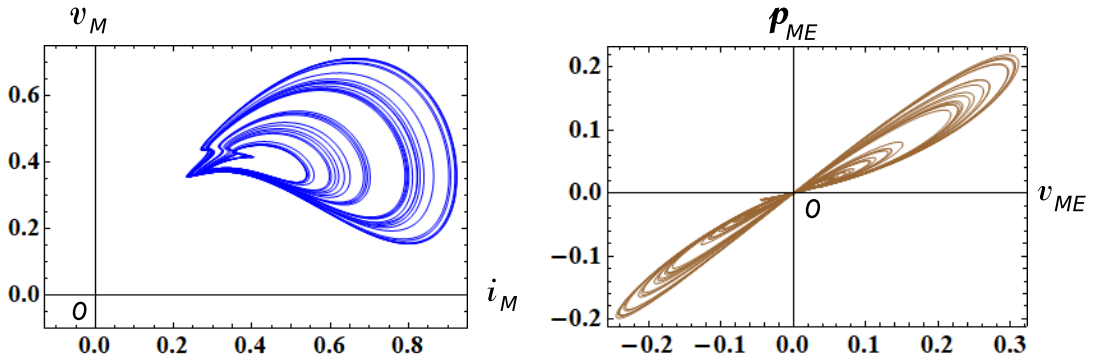

(a) $i_M - v_M$ locus (b) $i_{ME} - p_{ME}$ locus

Figure 5: The $i_M - v_M$ and $i_{ME} - p_{ME}$ loci of the forced memristor Brusselator equations (9). Here, v_M and i_M denote the terminal voltage and the terminal current of the current-controlled extended memristor, and $p_{ME}(t)$ are instantaneous powers defined by $p_{ME}(t) = i_M(t)\, v_{ME}(t)$. Observe that the $v_M - i_M$ locus is *not* pinched at the origin, and the locus lies in the first quadrant only. That is, it moves in the *passive* region. However, the $v_{ME} - p_{ME}$ locus is pinched at the origin, and it lies in the first and the third quadrants. Parameters: $A = 0.4,\ B = 1.2,\ r = 0.05,\ \omega = 0.81,\ d = 0.7$. Initial conditions: $i(0) = 1.1,\ x(0) = 1.1$.

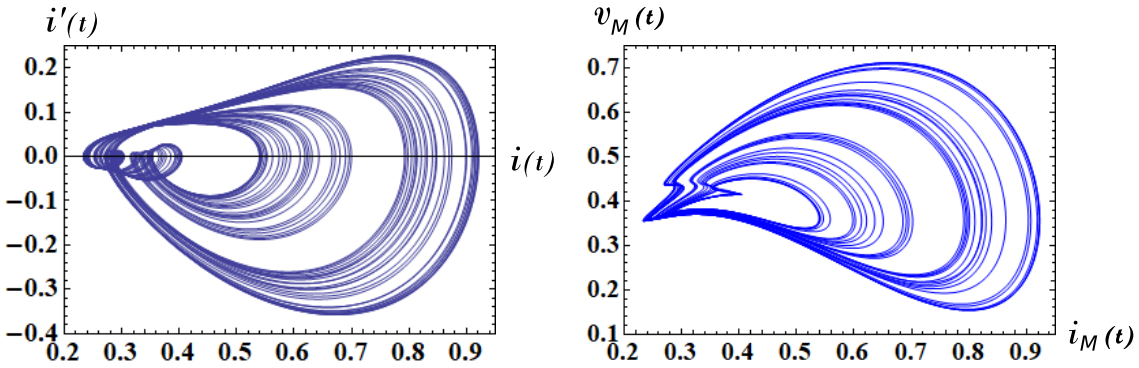

(a) $\big(i(t),\, i'(t)\big)$ reconstruction (b) $\big(i_M(t),\ v_M(t)\big)$ reconstruction

Figure 6: Reconstructed chaotic attractors using $\big(i(t),\, i'(t)\big)$ and $\big(i_M(t),\ v_M(t)\big)$, where v_M and i_M denote the terminal voltage and the terminal current of the current-controlled extended memristor. Parameters: $A = 0.4,\ B = 1.2,\ r = 0.05,\ \omega = 0.81$. Initial conditions: $i(0) = 1.1,\ x(0) = 1.1$.

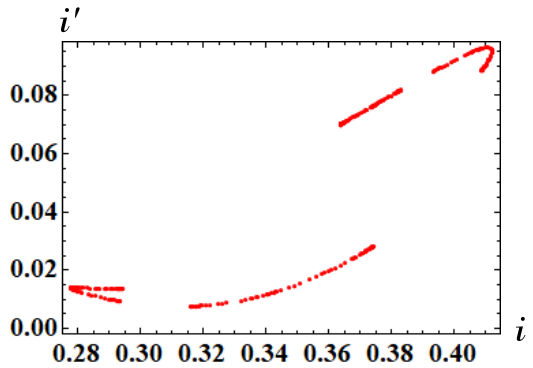

(a) Poincaré map for the attractor in Figure 6(a)

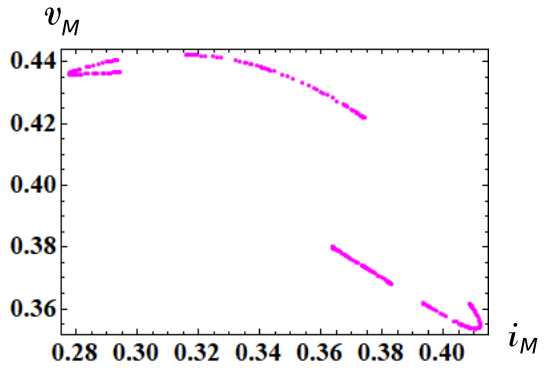

(b) Poincaré map for the attractor in Figure 6(b)

Figure 7: Poincaré maps for the reconstructed chaotic attractors in Figure 6. Observe that these two Poincaré maps are quite similar. Parameters: $A = 0.4,\ B = 1.2,\ r = 0.05,\ \omega = 0.81$. Initial conditions: $i(0) = 1.1,\ x(0) = 1.1$.

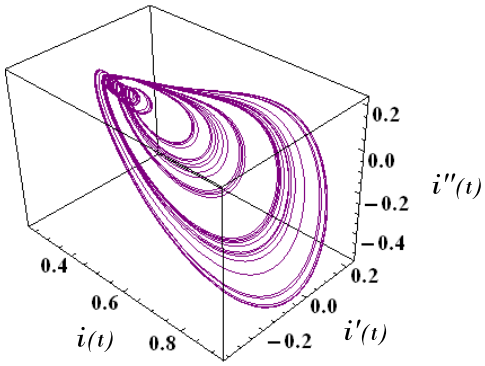

(a) $\big(i(t),\ i'(t),\ i''(t)\big)$ reconstruction

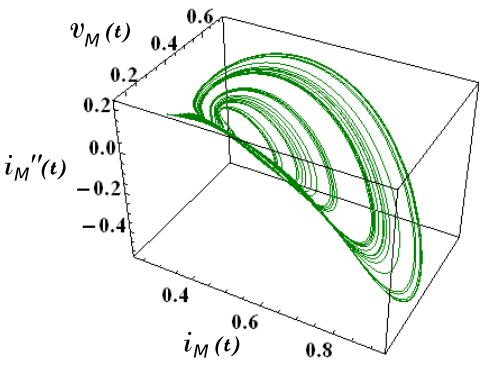

(b) $\big(i_M(t),\ v_M(t),\ {i_M}''(t)\big)$ reconstruction

Figure 8: Reconstructed chaotic attractor using $\big(i(t),\ i'(t)\ i''(t)\big)$ and $\big(i_M(t),\ v_M(t),\ {i_M}''(t)\big)$, where v_M and i_M denote the terminal voltage and the terminal current of the current-controlled extended memristor. Parameters: $A = 0.4,\ B = 1.2,\ r = 0.05,\ \omega = 0.81$. Initial conditions: $i(0) = 1.1,\ x(0) = 1.1$.

Let us consider the three-element memristor circuit in Figure 1. The dynamics of this circuit given by Eq. (3). Assume that Eq. (3) satisfies

$$\begin{aligned} E &= 0, \\ \hat{R}(x,i) &= -\left(\frac{i}{x} - b\right), \\ \tilde{f}_1(x,i) &= i^2 - c\,x. \end{aligned} \tag{18}$$

Then we obtain

Memristor diffusion-less Gierer-Meinhardt equations

$$\begin{aligned} \frac{di}{dt} &= \left(\frac{i}{x} - b\right) i, \\ \frac{dx}{dt} &= i^2 - c\,x, \end{aligned} \tag{19}$$

where b and c are constants.

Equations (17) and (19) are equivalent if we change the variables

$$i = u,\ x = v. \tag{20}$$

The terminal voltage v_M and the terminal current i_M of the current-controlled extended memristor in Figure 1 are given by

V-I characteristics of the extended memristor

$$\begin{aligned} v_M &= \hat{R}(x,\, i_M)\, i_M = -\left(\frac{i_M}{x} - b\right) i_M, \\ & \quad \hat{R}(x,\, 0) \neq \infty, \\ \frac{dx}{dt} &= {i_M}^2 - c\,x, \end{aligned} \tag{21}$$

where $\hat{R}(x,\, i_M) = -\left(\dfrac{i_M}{x} - b\right)$.

The above small-signal memristance $\hat{R}(x,\, i_M)$ satisfies

$$\lim_{x \to 0} |\hat{R}(x,\, i_M)| = \left| -\left(\frac{i_M}{x} - b\right) \right| = \infty, \tag{22}$$

when $i_M \neq 0$. In order to avoid this singularity, we use the different time-scaling [10]. That is, after time scaling by $d\tau = v\,dt$, Eqs. (17), (19), and (21) assume the equivalent forms

Diffusion-less Gierer-Meinhardt equations with time scaling

$$\begin{aligned} \frac{du}{d\tau} &= (u - bv)\, u, \\ \frac{dv}{d\tau} &= (u^2 - c\,v)v, \end{aligned} \tag{23}$$

where b and c are constants,

Memristor diffusion-less Gierer-Meinhardt equations with time scaling

$$\begin{aligned} \frac{di}{dt} &= (i - b\,x)i, \\ \frac{dx}{dt} &= (i^2 - c\,x)x, \end{aligned} \tag{24}$$

where b and c are constants,

and

V-I characteristics of the extended memristor

$$\begin{aligned} v_M &= \hat{R}(x,\, i_M)\, i_M = -(i_M - b\,x)\, i_M, \\ & \quad \hat{R}(x,\, 0) \neq \infty, \\ \frac{dx}{dt} &= ({i_M}^2 - c\,x)x, \end{aligned} \tag{25}$$

where $\hat{R}(x,\, i_M) = -(i_M - bx)$,

respectively. Similarly, Eq. (24) can be realized by the three-element memristor circuit in Figure 1, where

$$\begin{aligned} E &= 0, \\ \hat{R}(x, i) &= -(i - bx), \\ \tilde{f}_1(x, i) &= (i^2 - c\,x)\, x, \end{aligned} \tag{26}$$

Note that the above time scaling maps orbits between systems (17) and (23) in a one-to-one manner except at the singularity $v = 0$, although it may not preserve the time orientation of orbits.

Equations (17) and (24) exhibit periodic oscillation (limit cycle). When an external source is added as shown in Figure 2, the forced memristor circuit can exhibit chaotic oscillation. The dynamics of this circuit is given by

Forced memristor diffusion-less Gierer-Meinhardt equations with time scaling

$$\begin{aligned} \frac{di}{dt} &= (i - b\,x)i + r\sin(\omega t), \\ \frac{dx}{dt} &= (i^2 - c\,x)x, \end{aligned} \tag{27}$$

where r and ω are constants.

We show the chaotic attractor, Poincaré map, and $i_M - v_M$ locus of Eq. (27) in Figures 9, 10, and 11, respectively. The following parameters are used in our computer simulations:

$$b = 0.65,\ c = 0.796,\ r = 0.2,\ \omega = 0.5. \tag{28}$$

The $i_M - v_M$ locus in Figure 11 lies in the first and the fourth quadrants. Thus, the extended memristor defined by Eq. (25) is an active element. Let us next consider an instantaneous power defined by $p_M(t) = i_M(t)v_M(t)$. Then we obtain the $v_M - p_M$ locus in Figure 12. Observe that the locus is pinched at the origin, and the locus lies in the first and the third quadrants. Thus, when $v_M > 0$, the instantaneous power delivered from the forced signal and the inductor is dissipated in the memristor. However, when $v_M < 0$, the

instantaneous power delivered from the forced signal and the inductor is not dissipated in the memristor. Note that the $v_M - p_M$ locus in Figure 12 looks exactly like the $i_M - v_M$ locus of the "*passive*" memristor, whose locus lies in the first and the third quadrants [12]. Hence, the memristor switches between passive and active modes of operation, depending on its terminal voltage. We conclude as follow:

Switching behavior of the memristor

Assume that Eq. (27) exhibits chaotic oscillation. Then the extended memristor defined by Eq. (25) can switch between "passive" and "active" modes of operation, depending on its terminal voltage.

In order to obtain the results shown in Figures 9-12, we have to choose the initial conditions carefully. It is due to the fact that a periodic orbit (drawn in magenta)[2] coexists with a chaotic attractor (drawn in blue) as shown in Figure 13.

As stated in Sec. 2.1, we can reconstruct the chaotic attractor into two dimensional plane by using

$$(i(t),\ i'(t)). \tag{29}$$

Furthermore, the $i_M - v_M$ locus in Figure 11 is considered to be the reconstruction of the chaotic attractor on the two-dimensional plane, since

$$\Big(i_M(t),\, v_M(t)\Big) \equiv \Big(i(t),\ -i'(t) + r\sin(\omega t)\Big), \tag{30}$$

where $i_M(t) = i(t)$. We show their trajectories and Poincaré maps in Figures 14 and 15, respectively. We can also reconstruct the chaotic attractor into the three-dimensional Euclidean space by using

$$(i(t),\ i'(t)\ i''(t)), \tag{31}$$

or

$$\Big(i_M(t),\, v_M(t),\, i''_M(t)\Big) \equiv \Big(i(t),\ -i'(t) + r\sin(\omega t),\, i''(t)\Big). \tag{32}$$

We show the reconstructed three-dimensional attractors in Figure 16.

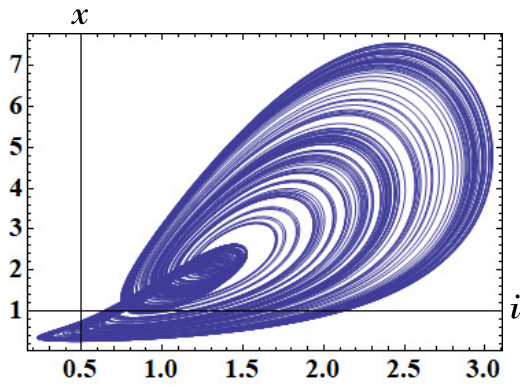

Figure 9: Chaotic attractor of the forced memristor diffusion-less Gierer-Meinhardt equations (27) with time scaling. Parameters: $b = 0.65,\ c = 0.796,\ r = 0.2,\ \omega = 0.5$. Initial conditions: $i(0) = 0.5,\ x(0) = 0.5$.

[2]Without loss of generality, we can use the terminology *"periodic orbit"* in order to describe a *"periodic trajectory"* of the *nonautonomous systems*, such as Eqs. (9) and (27) (see *"Duffing's Equation"* in Sec. 2.2 of [11])).

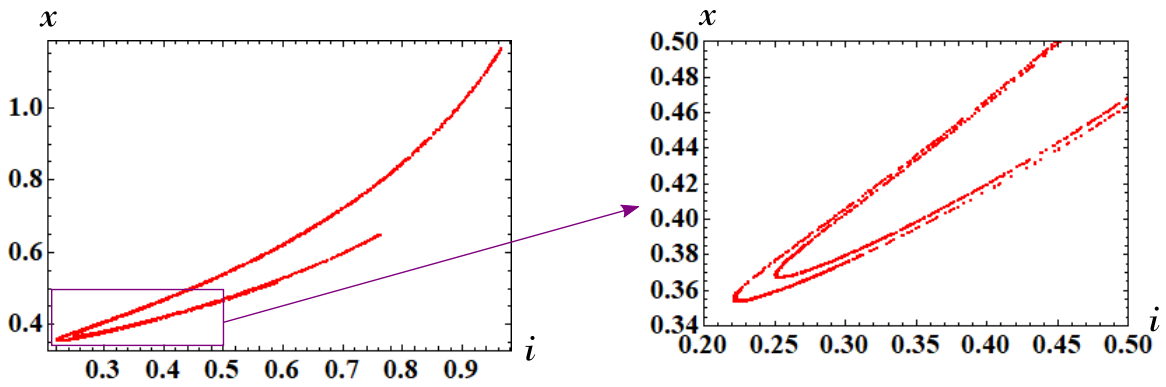

Figure 10: Poincaré map of the forced memristor diffusion-less Gierer-Meinhardt equations(27) with time scaling. The partially enlarged view of the locus is shown on the right side of Figure 10. Observe the folding action of the chaotic attractor. Parameters: $b = 0.65,\ c = 0.796,\ r = 0.2,\ \omega = 0.5$. Initial conditions: $i(0) = 0.5,\ x(0) = 0.5$.

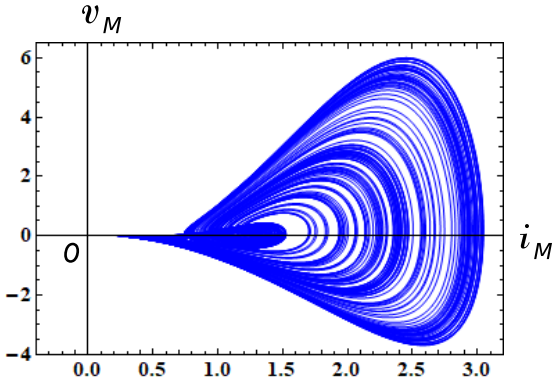

Figure 11: The $i_M - v_M$ locus of the forced memristor diffusion-less Gierer-Meinhardt equations (27) with time scaling. Here, v_M and i_M denote the terminal voltage and the terminal current of the current-controlled extended memristor. Observe that the extended memristor defined by Eq. (25) is an active element. Parameters: $b = 0.65,\ c = 0.796,\ r = 0.2,\ \omega = 0.5$. Initial conditions: $i(0) = 0.5,\ x(0) = 0.5$.

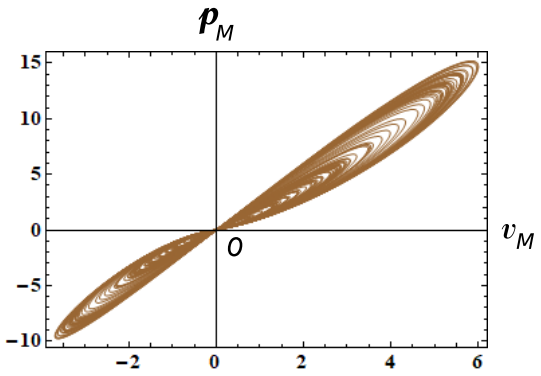

Figure 12: The $v_M - p_M$ locus of the forced memristor diffusion-less Gierer-Meinhardt equations (27) with time scaling. Here, $p_M(t)$ is an instantaneous power defined by $p_M(t) = i_M(t)v_M(t)$, and $v_M(t)$ and $i_M(t)$ denote the terminal voltage and the terminal current of the current-controlled extended memristor. Observe that the $v_M - p_M$ locus is pinched at the origin, and the locus lies in the first and the third quadrants. The memristor switches between passive and active modes of operation, depending on its terminal voltage $v_M(t)$. Parameters: $b = 0.65,\ c = 0.796,\ r = 0.2,\ \omega = 0.5$. Initial conditions: $i(0) = 0.5,\ x(0) = 0.5$.

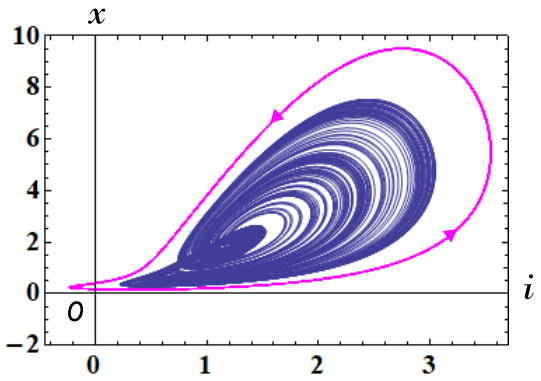

Figure 13: A periodic orbit (magenta) coexists with a chaotic attractor (blue). Parameters: $b = 0.65,\ c = 0.796,\ r = 0.2,\ \omega = 0.5$. Initial conditions for a chaotic attractor: $i(0) = 0.5,\ x(0) = 0.5$. Initial conditions for a periodic orbit: $i(0) = 0.5,\ x(0) = 0.1$.

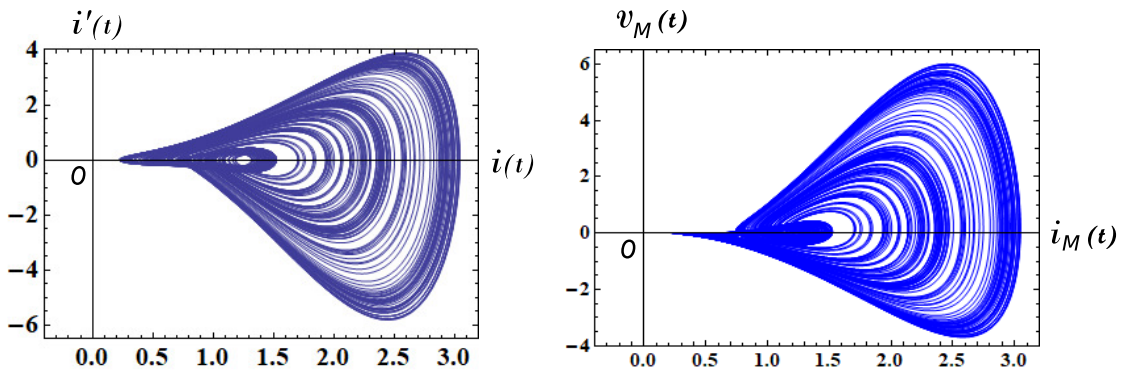

(a) $\big(i(t),\, i'(t)\big)$ reconstruction (b) $\big(i_M(t),\, v_M(t)\big)$ reconstruction

Figure 14: Reconstructed chaotic attractors using $\big(i(t),\, i'(t)\big)$ and $\big(i_M(t),\, v_M(t)\big)$, where v_M and i_M denote the terminal voltage and the terminal current of the current-controlled extended memristor. Parameters: $b = 0.65,\ c = 0.796,\ r = 0.2,\ \omega = 0.5$. Initial conditions: $i(0) = 0.5,\ x(0) = 0.5$.

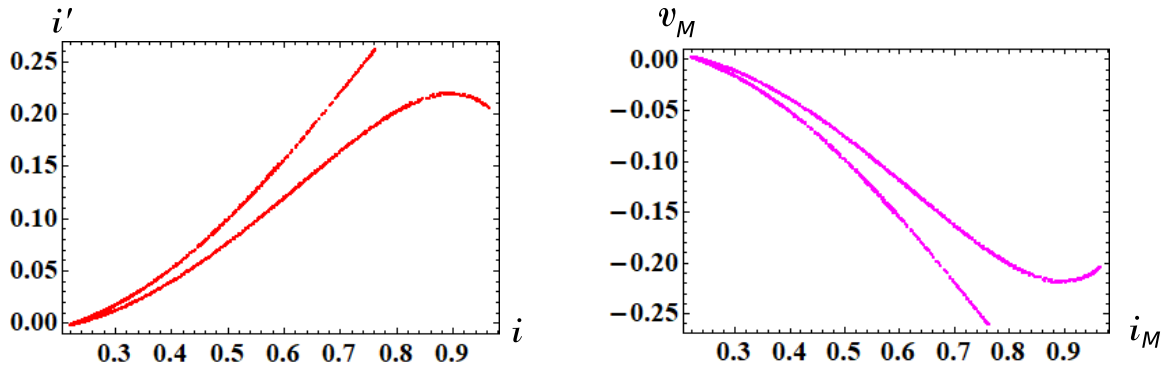

(a) Poincaré map for the attractor in Figure 14(a) (b) Poincaré map for the attractor in Figure 14(b)

Figure 15: Poincaré maps for the reconstructed chaotic attractors in Figure 14. Observe that these two Poincaré maps are quite similar. Parameters: $b = 0.65,\ c = 0.796,\ r = 0.2,\ \omega = 0.5$. Initial conditions: $i(0) = 0.5,\ x(0) = 0.5$.

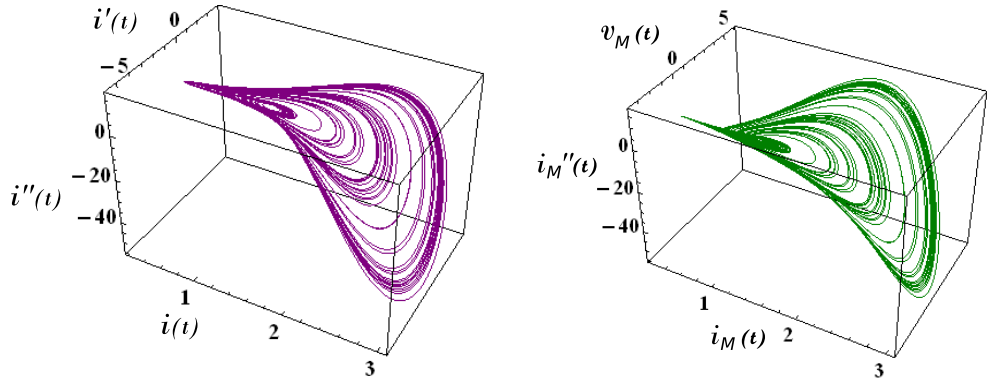

(a) $\big(i(t),\, i'(t),\, i''(t)\big)$ reconstruction (b) $\big(i_M(t),\, v_M(t),\, {i_M}''(t)\big)$ reconstruction

Figure 16: Reconstructed chaotic attractor using $\big(i(t),\, i'(t)\ i''(t)\big)$ and $\big(i_M(t),\, v_M(t),\, {i_M}''(t)\big)$, where v_M and i_M denote the terminal voltage and the terminal current of the current-controlled extended memristor. Parameters: $b = 0.65,\ c = 0.796,\ r = 0.2,\ \omega = 0.5$. Initial conditions: $i(0) = 0.5,\ x(0) = 0.5$.

2.3 Tyson-Kauffman equations

The dynamics of the Tyson-Kauffman equations [13] can be described by

Tyson-Kauffman equations

$$\begin{aligned} \frac{du}{dt} &= A - B\,u - u\,v^2 = A - (B + v^2)\,u, \\ \frac{dv}{dt} &= B\,u + u\,v^2 - v, \end{aligned} \tag{33}$$

where A and B are constants.

Consider the three-element memristor circuit in Figure 1. The dynamics of this circuit given by Eq. (3). Assume that Eq. (3) satisfies

$$\begin{aligned} E &= A, \\ \hat{R}(x,\, i) &= (B + x^2), \\ \tilde{f}_1(x, i) &= B\,i + i\,x^2 - x. \end{aligned} \tag{34}$$

Then we obtain

Memristor Tyson-Kauffman equations

$$\begin{aligned} \frac{di}{dt} &= A - (B + x^2)\,i, \\ \frac{dx}{dt} &= B\,i + i\,x^2 - x, \end{aligned} \tag{35}$$

where A and B are constants

Equations (33) and (35) are equivalent if we change the variables

$$i = u,\ x = v. \tag{36}$$

In this case, the extended memristor in Figure 1 is replaced by the generic memristor (see Appendix A). That is,

$$\hat{R}(x, i) = \tilde{R}(x) = (B + x^2). \tag{37}$$

The terminal voltage v_M and the terminal current i_M of the current-controlled generic memristor are described by

V-I characteristics of the generic memristor

$$\begin{aligned} v_M &= \tilde{R}(x)\,i_M = (B + x^2)\,i_M, \\ \frac{dx}{dt} &= B i_M - {i_M}^2 - x, \end{aligned} \tag{38}$$

where $\tilde{R}(x) = (B + x^2)$.

It follows that the Tyson-Kauffman equations (33) can be realized by the three-element memristor circuit in Figure 1. Equations (33) and (35) can exhibit periodic oscillation (limit cycle). When an external source is added as shown in Figure 2, the forced memristor Tyson-Kauffman equations can exhibit chaotic oscillation. The dynamics of the circuit is given by

Forced memristor Tyson-Kauffman equations

$$\begin{aligned} \frac{di}{dt} &= A - (B + x^2)\, i + r \sin(\omega t), \\ \frac{dx}{dt} &= B\, i + i\, x^2 - x, \end{aligned} \tag{39}$$

where r and ω are constants.

We show the chaotic attractors, Poincaré maps, and $i_M - v_M$ loci of Eq. (39) in Figures 17, 18, and 19, respectively. In our computer simulations, we used the following two kinds of the parameters:

$$\left.\begin{array}{lll} (a) & A = 0.5, \quad B = 0.00803, & C = 0.01, \\ & r = 0.5, \qquad \omega = 0.5, & \end{array}\right\} \tag{40}$$

and

$$\left.\begin{array}{lll} (b) & A = 0.5, \quad B = 0.0079, & C = 0.01, \\ & r = 0.55, \qquad \omega = 0.5. & \end{array}\right\} \tag{41}$$

Note that the locus in Figure 19(a) moves in the first quadrant, and the locus in Figure 19(b) moves in the first and third quadrants. That is, they move in the *passive* region, since the instantaneous power defined by

$$p_M(t) \stackrel{\triangle}{=} i_M(t)\, v_M(t), \tag{42}$$

is *not* negative. In this case, the power is dissipated in the generic memristor, which is delivered from the forcing signal and the inductor.

Let us define next the instantaneous power of the two circuit elements, as stated in Sec. 2.1. That is, we define the instantaneous power of the extended memristor and the battery by

$$p_{ME}(t) \stackrel{\triangle}{=} i_M(t)\, v_{ME}(t), \tag{43}$$

where $v_{ME}(t) = v_M(t) - E$, and E denotes the voltage of the battery. That is, $v_{ME}(t)$ denotes the voltage across the extended memristor and the battery. We show the $v_{ME} - p_{ME}$ locus in Figure 20. Observe that the locus is pinched at the origin, and it lies in the first and the third quadrants. Thus, the instantaneous power $p_{ME}(t)$ delivered from the forced signal and the inductor is dissipated when $v_M(t) - E > 0$. However, the instantaneous power $p_{ME}(t)$ is *not* dissipated when $v_M(t) - E < 0$. Thus, we conclude as follow:

Behavior of the generic memristor

Assume that Eq. (39) exhibits chaotic oscillation. Then, we obtain the following results:

1. The generic memristor defined by Eq. (38) is operated as a *passive* element. If we define the instantaneous power of the generic memristor by $p_M(t) \stackrel{\triangle}{=} i_M(t) v_M(t)$, then $p_M(t)$ is dissipated in this generic memristor, which is delivered from the forcing signal and the inductor.

2. If we define the instantaneous power of the two elements, that is, the instantaneous power of the generic memristor and the battery, by $p_{ME}(t) \stackrel{\triangle}{=} i_M(t)(v_M(t) - E)$, then $p_{ME}(t)$ is *not* dissipated when $v_M(t) - E < 0$. However, $p_{ME}(t)$ is dissipated when $v_M(t) - E > 0$.

As stated in Sec. 2.1, we can reconstruct the chaotic attractor into two dimensional plane by using

$$(i(t),\ i'(t)). \tag{44}$$

Furthermore, the $i_M - v_M$ loci in Figure 19 are considered to be the reconstruction of the chaotic attractor on the two-dimensional plane, since

$$\Big(i_M(t),\, v_M(t)\Big) \equiv \Big(i(t),\ -i'(t) + r\sin(\omega t)\Big), \tag{45}$$

where $i_M(t) = i(t)$. We show their trajectories and Poincaré maps in Figures 21 and 22, respectively. We can also reconstruct the chaotic attractor into the three-dimensional Euclidean space by using

$$(i(t),\ i'(t)\ i''(t)), \tag{46}$$

or

$$\Big(i_M(t),\, v_M(t),\, i''_M(t)\Big) \equiv \Big(i(t),\ -i'(t) + r\sin(\omega t),\, i''(t)\Big). \tag{47}$$

We show the reconstructed three-dimensional attractors in Figure 23.

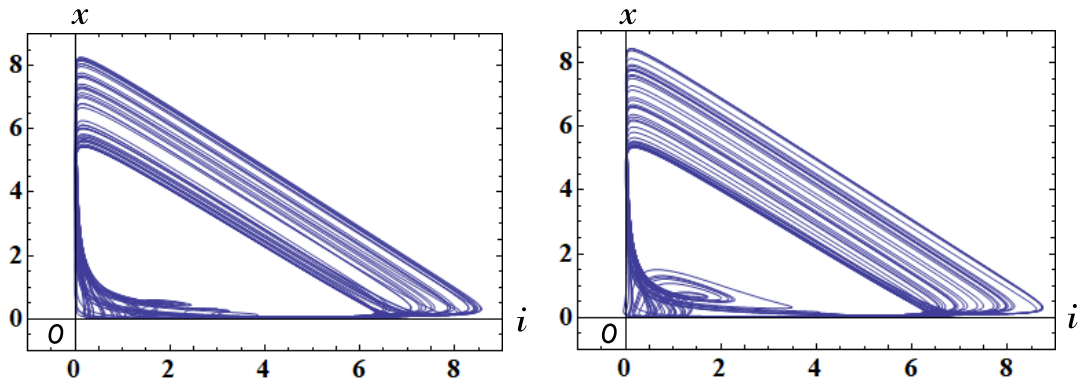

(a) (b)

Figure 17: Chaotic attractors of the forced memristor Tyson-Kauffman equations (39). Parameters: (a) $A = 0.5,\ B = 0.00803,\ r = 0.5,\ \omega = 0.5$. (b) $A = 0.5,\ B = 0.0079,\ r = 0.55,\ \omega = 0.5$. Initial conditions: $i(0) = 2.1,\ x(0) = 2.1$.

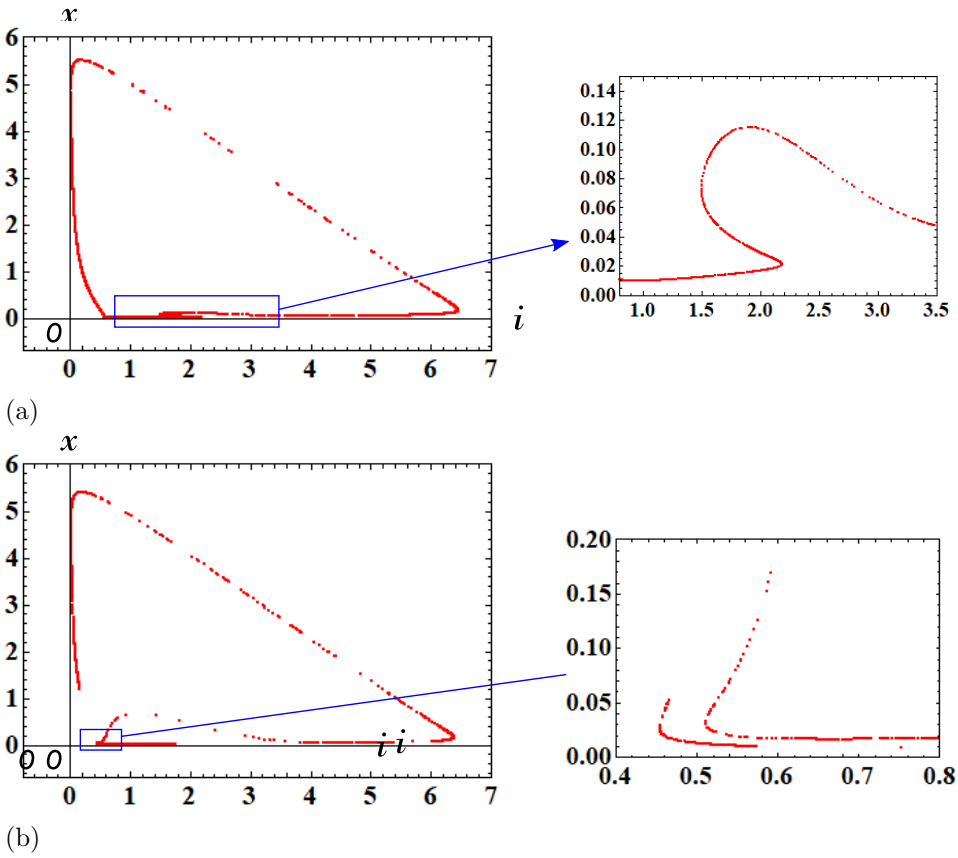

Figure 18: Poincaré maps of the forced memristor Tyson-Kauffman equations (39). The partially enlarged view of the locus is shown on the right side of Figure18. Parameters: (a) $A = 0.5,\ B = 0.00803,\ r = 0.5,\ \omega = 0.5$. (b) $A = 0.5,\ B = 0.0079,\ r = 0.55,\ \omega = 0.5$. Initial conditions: $i(0) = 2.1,\ x(0) = 2.1$.

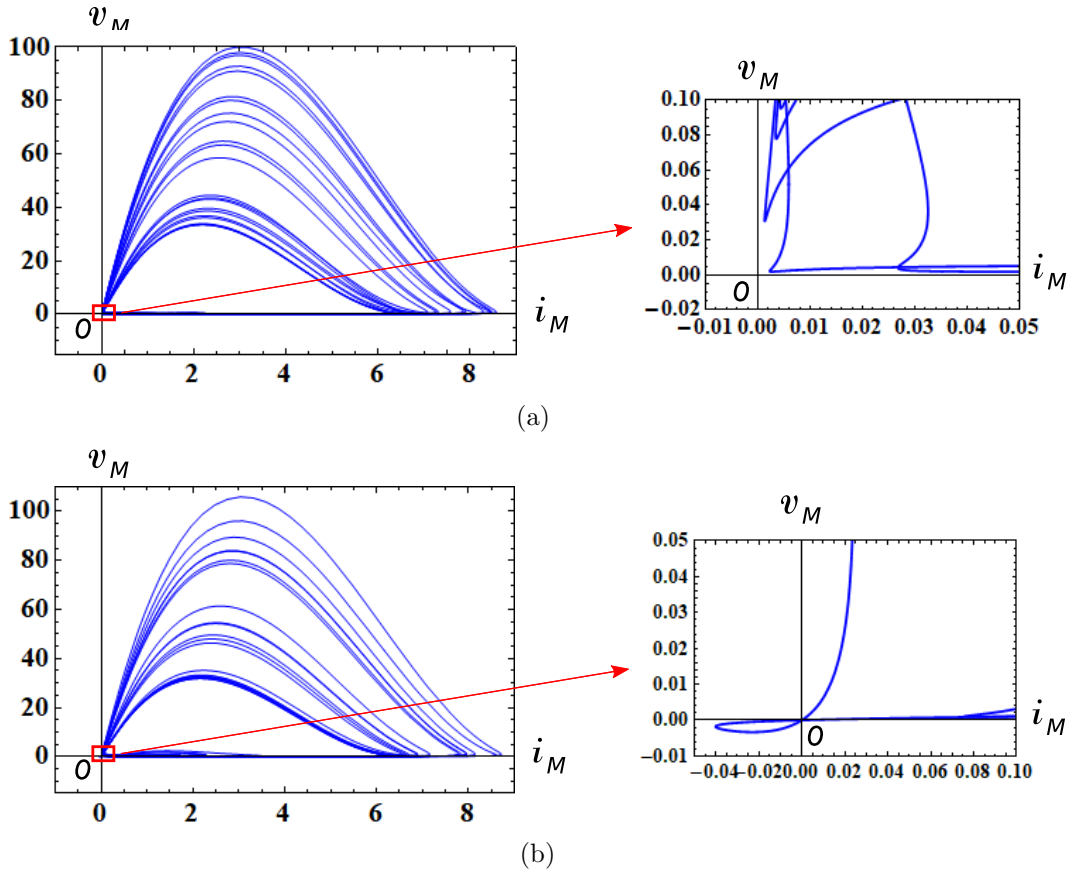

Figure 19: The $i_M - v_M$ loci of the forced memristor Tyson-Kauffman equations (39) (left) and partially enlarged views of the $i_M - v_M$ loci (right). Here, v_M and i_M denote the terminal voltage and the terminal current of the current-controlled generic memristor. Observe that the locus in Figure 19(a) moves in the first quadrant, and the locus in Figure 19(b) moves in the first and third quadrants. Thus, they move in the *passive* region. Parameters: (a) $A = 0.5,\ B = 0.00803,\ r = 0.5,\ \omega = 0.5.$ (b) $A = 0.5,\ B = 0.0079,\ r = 0.55,\ \omega = 0.5.$ Initial conditions: $i(0) = 2.1,\ x(0) = 2.1.$

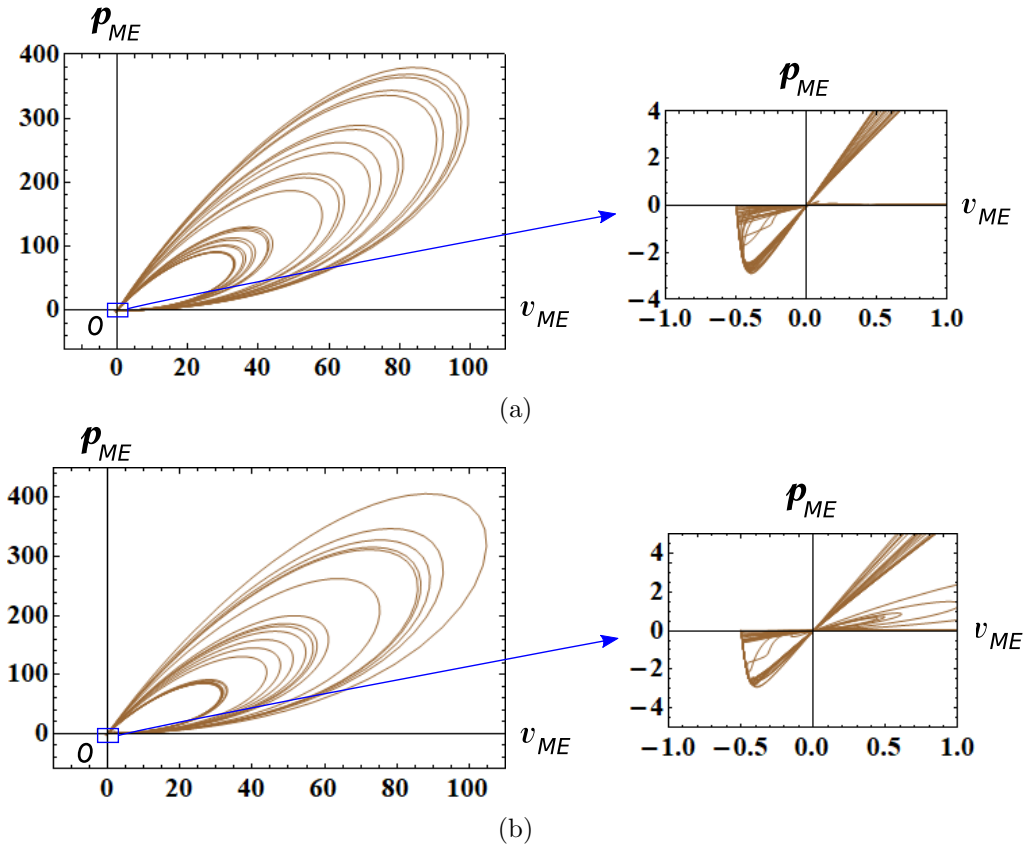

Figure 20: The $v_{ME} - p_{ME}$ loci of the forced memristor Tyson-Kauffman equations (39). Their partially enlarged views are shown on the right side of Figure 20. Here, $v_{ME}(t) = v_M(t) - E$, and $p_{ME}(t)$ is an instantaneous powers defined by $p_{ME}(t) = i_M(t)\, v_{ME}(t)$, v_M and i_M denote the terminal voltage and the terminal current of the current-controlled generic memristor, respectively, and E denotes the voltage of the battery. Observe that the $v_{ME} - p_{ME}$ loci are pinched at the origin, and they lie in the first and the third quadrants. Parameters: (a) $A = 0.5,\ B = 0.00803,\ r = 0.5,\ \omega = 0.5$. (b) $A = 0.5,\ B = 0.0079,\ r = 0.55,\ \omega = 0.5$. Initial conditions: $i(0) = 2.1,\ x(0) = 2.1$.

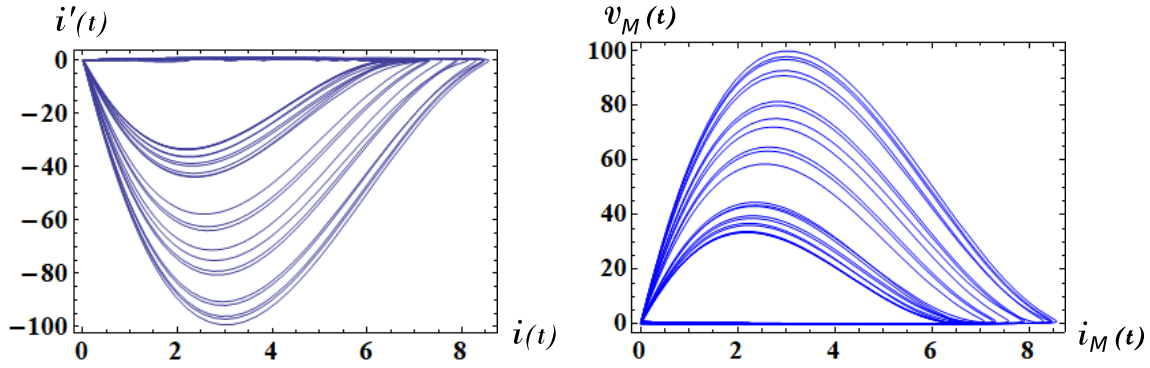

(a) $\big(i(t),\, i'(t)\big)$ reconstruction (b) $\big(i_M(t),\, v_M(t)\big)$ reconstruction

Figure 21: Reconstructed chaotic attractors using $\big(i(t),\, i'(t)\big)$ and $\big(i_M(t),\, v_M(t)\big)$, where v_M and i_M denote the terminal voltage and the terminal current of the current-controlled generic memristor. Parameters: $A = 0.5,\ B = 0.00803,\ r = 0.5,\ \omega = 0.5$. Initial conditions: $i(0) = 2.1,\ x(0) = 2.1$.

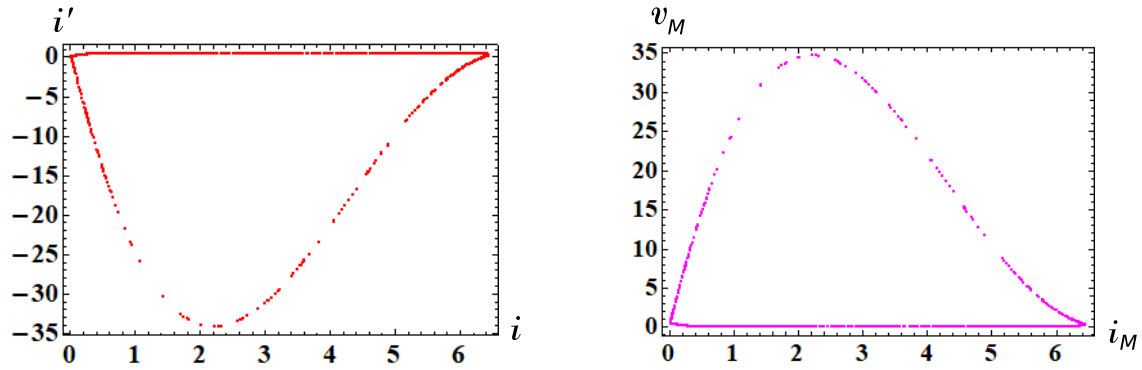

(a) Poincaré map for the attractor in Figure 21(a) (b) Poincaré map for the attractor in Figure 21(b)

Figure 22: Poincaré maps for the reconstructed chaotic attractors in Figure 21. Observe that these two Poincaré maps are quite similar. Parameters: $A = 0.5,\ B = 0.00803,\ r = 0.5,\ \omega = 0.5$. Initial conditions: $i(0) = 2.1,\ x(0) = 2.1$.

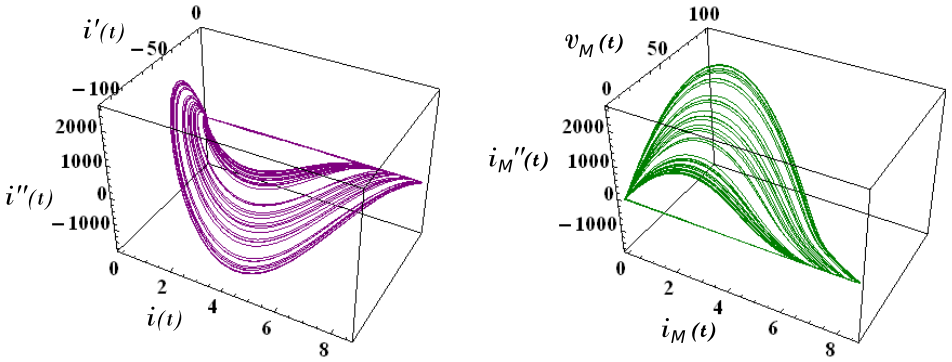

(a) $\big(i(t),\ i'(t),\ i''(t)\big)$ reconstruction (b) $\big(i_M(t),\ v_M(t),\ i_M{}''(t)\big)$ reconstruction

Figure 23: Reconstructed chaotic attractor using $\big(i(t),\ i'(t)\ i''(t)\big)$ and $\big(i_M(t),\ v_M(t),\ i_M{}''(t)\big)$, where v_M and i_M denote the terminal voltage and the terminal current of the current-controlled generic memristor. Parameters: $A = 0.5,\ B = 0.00803,\ r = 0.5,\ \omega = 0.5$. Initial conditions: $i(0) = 2.1,\ x(0) = 2.1$.

2.4 Lotka-Volterra equations

Consider Hamilton's Equations defined by

Hamilton's equations

$$\begin{aligned} \frac{dq}{dt} &= \frac{\partial \mathcal{H}(q,\, p)}{\partial p}, \\ \frac{dp}{dt} &= -\frac{\partial \mathcal{H}(q,\, p)}{\partial q}, \end{aligned} \tag{48}$$

where q and p denote the coordinate and the momentum and $\mathcal{H}(q,\, p)$ is the Hamiltonian.

Let us define the Hamiltonian:

Hamiltonian

$$\mathcal{H}(q,\, p) = -b\, p + a \ln p - c\, q + d \ln q, \tag{49}$$

where $a,\ b,\ c,\ d$ are constants.

From Eq. (48), we obtain

$$\begin{aligned} \frac{dq}{dt} &= \frac{\partial \mathcal{H}}{\partial p} = -b + \frac{a}{p}, \\ \frac{dp}{dt} &= -\frac{\partial \mathcal{H}}{\partial q} = c - \frac{d}{q}. \end{aligned} \tag{50}$$

After time scaling by $d\tau = pq\, dt$, we obtain the associated Pfaff's equation [10]

$$\begin{aligned} \frac{dq}{d\tau} &= \left(-b + \frac{a}{p}\right) pq, \\ \frac{dp}{d\tau} &= \left(c - \frac{d}{q}\right) pq. \end{aligned} \tag{51}$$

Equation (51) can be recast into the Lotka-Volterra equations [14]

Lotka-Volterra equations

$$\begin{aligned} \frac{dq}{d\tau} &= (a - b\, p)\, q, \\ \frac{dp}{d\tau} &= (c\, q - d)\, p, \end{aligned} \tag{52}$$

where $a,\ b,\ c,\ d$ are constants.

Equation (52) has the Hamiltonian (49) as its integral invariant, that is,

$$\frac{d\mathcal{H}(q,\, p)}{d\tau} = 0. \tag{53}$$

Consider next the three-element memristor circuit in Figure 1. The dynamics of this circuit given by Eq. (3). Assume that Eq. (3) satisfies

$$\begin{aligned} E &= 0, \\ \hat{R}(x,i) &= -(c\,x - d), \\ \tilde{f}_1(x,\,i) &= (a - b\,i)x. \end{aligned} \tag{54}$$

Then we obtain

Memristor Lotka-Volterra equations

$$\begin{aligned} \frac{di}{d\tau} &= (c\,x - d)\,i, \\ \frac{dx}{d\tau} &= (a - b\,i)\,x, \end{aligned} \tag{55}$$

where $a,\ b,\ c,\ d$ are constants.

Equations (52) and (55) are equivalent if we change the variables

$$i = p,\ x = q. \tag{56}$$

In this case, the extended memristor in Figure 1 is replaced by the *generic* memristor (see Appendix A). That is,

$$\hat{R}(x,i) = \tilde{R}(x) = -(cx - d). \tag{57}$$

Thus, the terminal voltage v_M and the terminal current i_M of the current-controlled generic memristor are given by

V-I characteristics of the generic memristors

$$\begin{aligned} v_M &= \tilde{R}(x)\,i_M = -(c\,x - d)\,i_M, \\ \frac{dx}{dt} &= (a - b\,i_M)x, \end{aligned} \tag{58}$$

where $\hat{R}(x) = -(cx - d)$.

It follows that the Lotka-Volterra equations (55) can be realized by the three-element memristor circuit in Figure 1.

The Lotka-Volterra equations (55) can exhibit a periodic orbit (one-dimensional curve), since they have

Integral

$$\mathcal{H}(x,\,i) = -b\,i + a\ln i - c\,x + d\ln x, \tag{59}$$

as its integral invariant. When an external source is added as shown in Figure 2, the forced Lotka-Volterra equations can exhibit a quasi-periodic or a non-periodic response,[3] which depends on initial conditions. The dynamics of the circuit is given by

[3]In this paper, we use the terminology "non-periodic response" in order to describe "chaotic-like but non-attracting response".

Forced memristor Lotka-Volterra equations

$$\begin{aligned} \frac{di}{d\tau} &= (cx - d)\, i + r \sin(\omega\tau), \\ \frac{dx}{d\tau} &= (a - b\, i)\, x, \end{aligned} \tag{60}$$

where r and ω are constants.

We show their non-periodic and quasi-periodic responses, Poincaré maps, and $i_M - v_M$ loci in Figures 24, 25(a), and 26, respectively. The following parameters are used in our computer simulations:

$$\begin{aligned} &a = 2/3,\ b = 4/3,\ c = 1,\ d = 1, \\ &r = 0.04,\ \omega = 1,\ \text{or } 1.01. \end{aligned} \tag{61}$$

The $i_M - v_M$ loci in Figure 26 lie in the first and the fourth quadrants. Thus, the generic memristor defined by Eq. (58) is an active element. Let us next show the $v_M - p_M$ locus in Figure 27, where $p_M(t)$ is an instantaneous power defined by $p_M(t) = i_M(t)v_M(t)$. Observe that the $v_M - p_M$ locus is pinched at the origin, and the locus lies in the first and the third quadrants. Thus, when $v_M > 0$, the instantaneous power delivered from the forced signal and the inductor is dissipated in the generic memristor. However, when $v_M < 0$, the instantaneous power delivered from the forced signal and the inductor is not dissipated in the generic memristor. Hence, the memristor switches between passive and active modes of operation, depending on its terminal voltage. We conclude as follow:

Switching behavior of the memristor

Assume that Eq. (60) exhibits non-periodic response. Then the generic memristor defined by Eq. (58) can switch between "passive" and "active" modes of operation, depending on its terminal voltage.

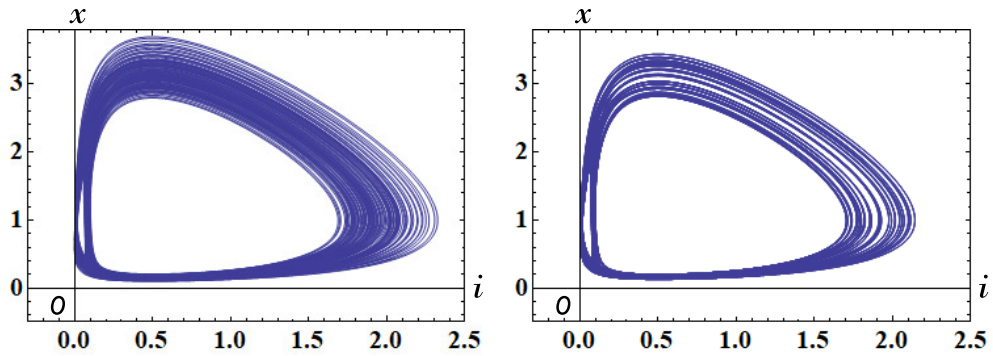

(a) non-periodic ($\omega = 1$) (b) quasi-periodic ($\omega = 1.01$)

Figure 24: Non-periodic and quasi-periodic responses of the forced memristor Lotka-Volterra equations (60). Parameters: (a) $a = 2/3,\ b = 4/3,\ c = 1,\ d = 1,\ r = 0.04,\ \omega = 1$. (b) $a = 2/3,\ b = 4/3,\ c = 1,\ d = 1,\ r = 0.04,\ \omega = 1.01$. Initial conditions: $i(0) = 0.19,\ x(0) = 0.18$.

In order to generate the non-periodic Poincaré map in Figure 25(a), we have to choose the initial conditions and parameters carefully, and the maximum step size h of the numerical integration must be sufficiently small ($h = 0.002$).[4] Compare the three Poincaré maps in Figure 25. In order to view these Poincaré maps

[4]We used "NDSolve" in Mathematica to solve differential equations numerically. Numerical integration tool, like NDSolve, can specify the maximum size of a single step used in generating a result. For most differential equations, the results given by NDSolve are quite accurate.

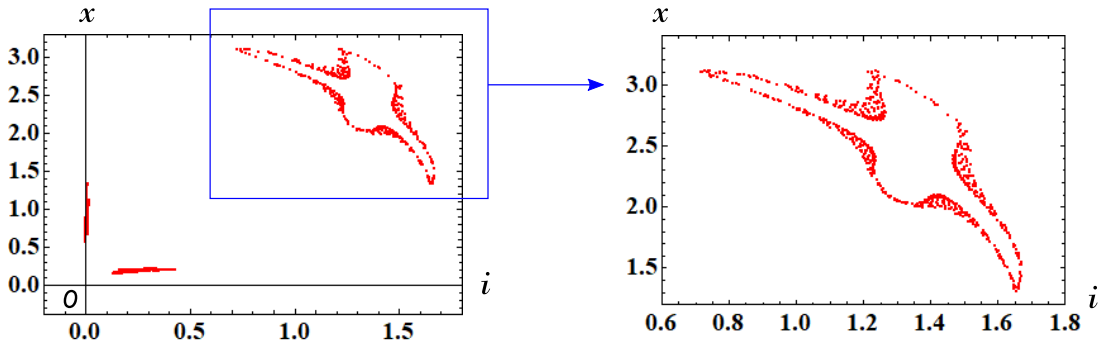

(a) Poincaré map for a non-periodic response. $i(0) = 0.19,\ \ x(0) = 0.18,\ \ r = 0.04,\ \ \omega = 1.$

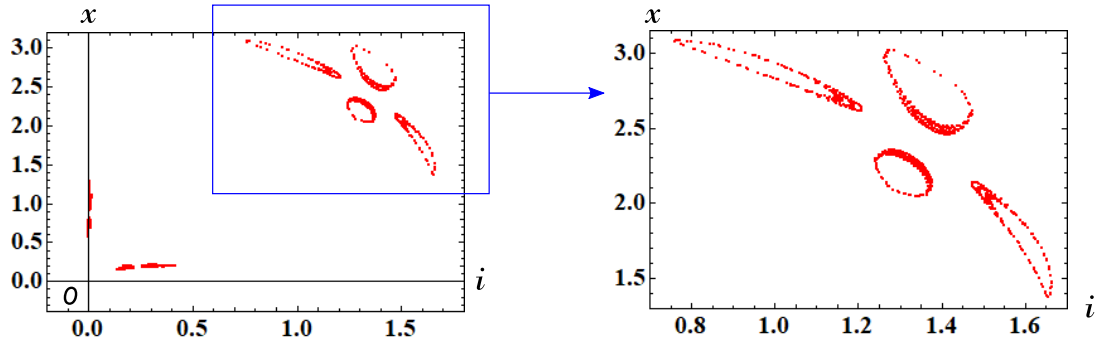

(b) Poincaré map for a quasi-periodic response. $i(0) = 0.185,\ \ x(0) = 0.185,\ \ r = 0.04,\ \ \omega = 1.$

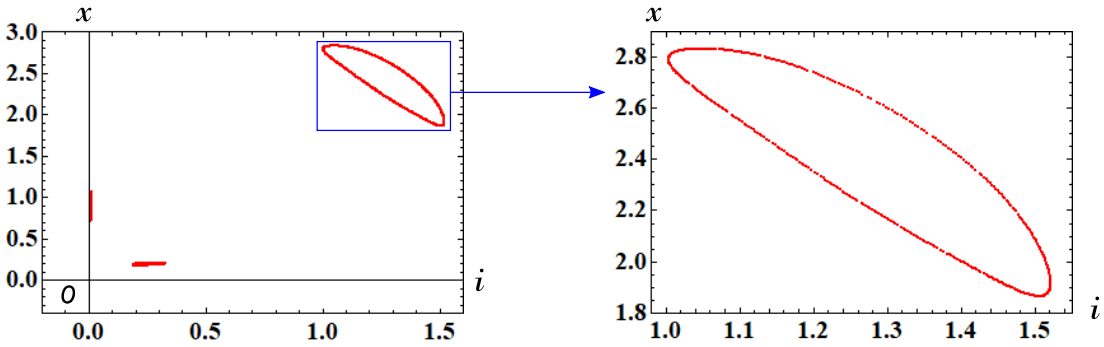

(c) Poincaré map for a quasi-periodic response. $i(0) = 0.19,\ \ x(0) = 0.18,\ \ r = 0.04,\ \ \omega = 1.01.$

Figure 25: Poincaré maps of the forced memristor Lotka-Volterra equations (60). Compare the three Poincaré maps in Figure 25. In order to generate the non-periodic Poincaré map in Figure 25(a), we have to choose the initial conditions and parameters carefully. Parameters: $a = 2/3,\ b = 4/3,\ c = 1,\ d = 1,\ r = 0.04,\ \omega =$ 1 or 1.01.

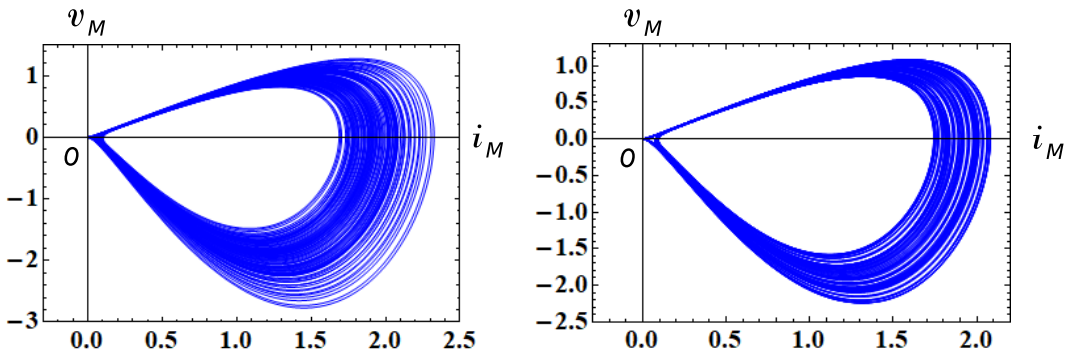

(a) non-periodic ($\omega = 1$) (b) quasi-periodic ($\omega = 1.01$)

Figure 26: The $i_M - v_M$ loci of the forced memristor Lotka-Volterra equations (60). Here, v_M and i_M denote the terminal voltage and the terminal current of the current-controlled generic memristor. Parameters: (a) $a = 2/3,\ b = 4/3,\ c = 1,\ d = 1,\ r = 0.04,\ \omega = 1$. (b) $a = 2/3,\ b = 4/3,\ c = 1,\ d = 1,\ r = 0.04,\ \omega = 1.01$. Initial conditions: $i(0) = 0.19,\ x(0) = 0.18$.

from a different perspective, let us project the trajectories into the $(\xi,\, \eta,\, \zeta)$-space via the transformation

$$\begin{aligned} \xi(\tau) &= (i(\tau) + 5)\cos(\omega\tau), \\ \eta(\tau) &= (i(\tau) + 5)\sin(\omega\tau), \\ \zeta(\tau) &= x(\tau). \end{aligned} \tag{62}$$

Then the trajectory on the $(i,\, x)$-plane is transformed into the trajectory in the three-dimensional $(\xi,\, \eta,\, \zeta)$-space, as shown in Figure 28.[5, 6] Observe the difference among the three trajectories.

Note that the maximum step size limitation for h is important for numerical stability, otherwise an overflow (outside the range of data) is likely to occur. We show its example in Figure 29. Observe that if $h = 0.002$, then the trajectory rapidly grows for $t \geq 1148$, and an overflow occurs as shown in Figure 29(a). However, if $h = 0.001$, then the trajectory stays in a finite region of the first-quadrant of the $(i,\ x)$-plane as shown in Figure 29(b). The above numerical instability in long-time simulations is partially caused by the fact that if $i(\tau)$ takes sufficiently small *negative* values at some time τ_0 by the low-accuracy computation, then we obtain

$$\frac{dx(\tau)}{d\tau} = \big(a - b\, i(\tau)\big)x(\tau)\ > 0, \tag{63}$$

for $\tau \approx \tau_0$ and $0 < -b\, i(\tau) \ll 1$, where $b > 0$. Thus, $x(\tau)$ is approximated by

$$x(\tau) \approx x(\tau_0)e^{a\tau}, \tag{64}$$

and it grows rapidly, where $a > 0$. Consequently, $x(\tau)$ would overflow. Thus, noise may considerably affect the behavior of the above memristor circuit.

As stated in Sec. 2.1, we can reconstruct the non-periodic trajectory into two dimensional plane by using

$$(i(t),\ i'(t)), \tag{65}$$

or

$$\Big(i_M(t),\, v_M(t)\Big) \equiv \Big(i(t),\ -i'(t) + r\sin(\omega t)\Big), \tag{66}$$

[5]For example, if $(i(t),\, x(t))$ moves on the unit circle, that is, $(i(t),\, x(t)) = (\cos(3t),\, \sin(3t))$, then the projected trajectory $(\xi(t),\, \eta(t),\, \zeta(t))$ moves on a torus (for more details on the transformation (62), see Appendix in [15]).

[6]If we plot the intersection of the points with the plane defined by $\{(\xi,\, \eta,\, \zeta) \in \mathbb{R}^3 \,|\, \eta = 0,\, \xi \geq 0\}$, we obtain similar Poincaré maps (see Appendix in [15]).

where $i_M(t) = i(t)$. Their trajectories and Poincaré maps are shown in Figures 30 and 31, respectively. We can also reconstruct the non-periodic trajectory into the three-dimensional Euclidean space by using

$$(i(t),\ i'(t),\ i''(t)), \tag{67}$$

or

$$\Big(i_M(t),\, v_M(t),\, i''_M(t)\Big) \equiv \Big(i(t),\ -i'(t) + r\sin(\omega t),\, i''(t)\Big). \tag{68}$$

These reconstructed trajectories are shown in three-dimensional space in Figure 32.

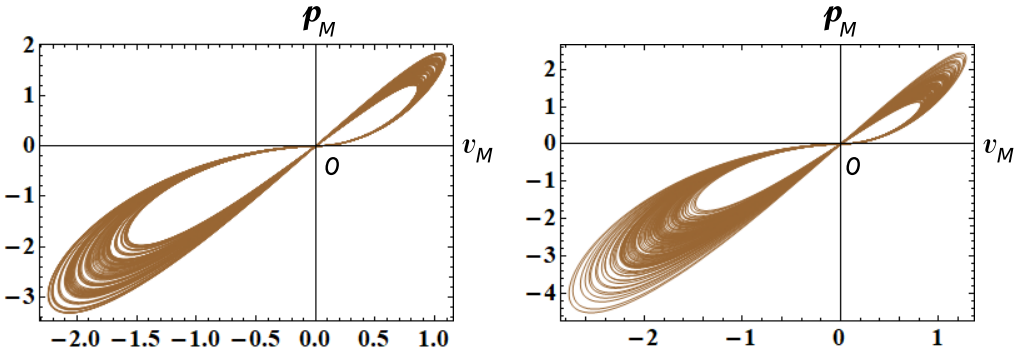

(a) non-periodic ($\omega = 1$) (b) quasi-periodic ($\omega = 1.01$)

Figure 27: The $v_M - p_M$ loci of the forced memristor Lotka-Volterra equations (60). Here, $p_M(t)$ is an instantaneous power defined by $p_M(t) = i_M(t)v_M(t)$, and $v_M(t)$ and $i_M(t)$ denote the terminal voltage and the terminal current of the current-controlled generic memristor. Observe that the $v_M - p_M$ locus is pinched at the origin, and the locus lies in the first and the third quadrants. The memristor switches between passive and active modes of operation, depending on its terminal voltage $v_M(t)$. Parameters: (a) $a = 2/3,\ b = 4/3,\ c = 1,\ d = 1,\ r = 0.04,\ \omega = 1$. (b) $a = 2/3,\ b = 4/3,\ c = 1,\ d = 1,\ r = 0.04,\ \omega = 1.01$. Initial conditions: $i(0) = 0.19,\ x(0) = 0.18$.

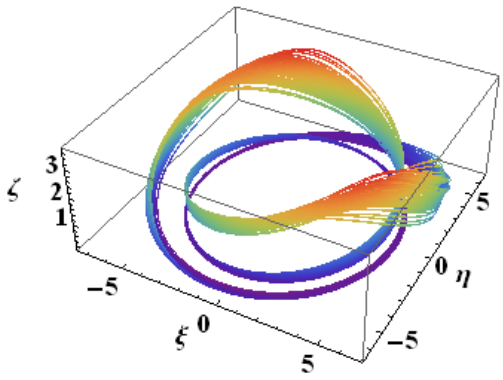

(a) A non-periodic response with $i(0) = 0.19,\ \ x(0) = 0.18,\ \ r = 0.04$, and $\omega = 1$.

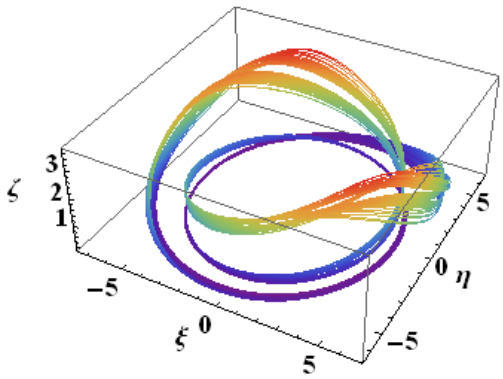

(b) A quasi-periodic response with $i(0) = 0.185,\ \ x(0) = 0.185,\ \ r = 0.04$, and $\omega = 1$.

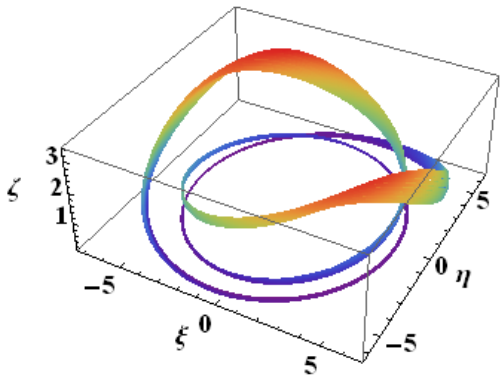

(c) A quasi-periodic response with $i(0) = 0.19,\ \ x(0) = 0.18,\ \ r = 0.04$, and $\omega = 1.01$.

Figure 28: Three trajectories of the forced memristor Lotka-Volterra equations (60), which are projected into the (ξ, η, ζ)-space via the coordinate transformation (62). Compare these three trajectories in Figure 28 with the three Poincaré maps in Figure 25. The trajectories are colored with the *Rainbow* color code in Mathematica, that is, the color evolves through violet, indigo, blue, green, yellow, orange and red, as ζ varies from its minimum to its maximum value. Parameters: $a = 2/3,\ b = 4/3,\ c = 1,\ d = 1,\ r = 0.04,\ \omega = 1$ or 1.01.

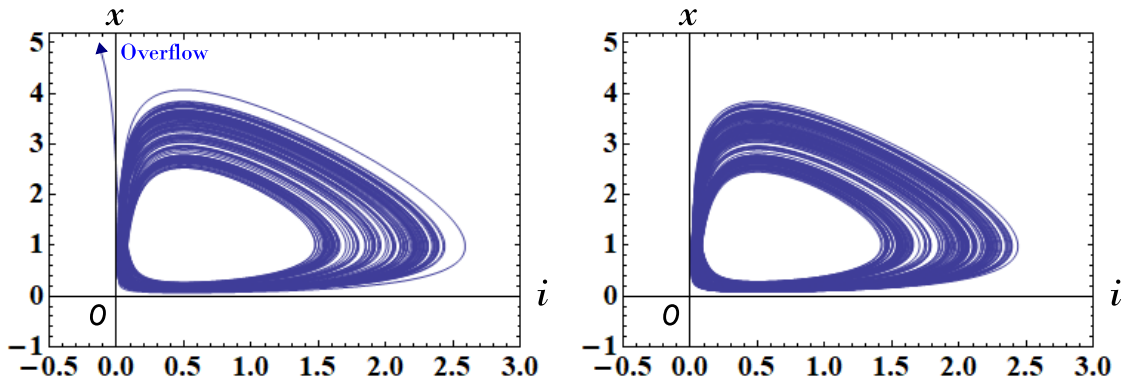

(a) $h = 0.002$ (b) $h = 0.001$

Figure 29: Behavior of the forced memristor Lotka-Volterra equations (60). If $h = 0.002$, then the trajectory rapidly grows for $t \geq 1148$, and an overflow occurs as shown in Figure 29(a). However, if $h = 0.001$, then the trajectory stays in a finite region of the first-quadrant of the $(i,\ x)$-plane as shown in Figure 29(b). Here, h denotes the maximum step size of the numerical integration. Parameters: $a = 2/3,\ b = 4/3,\ c = 1,\ d = 1,\ r = 0.04,\ \omega = 1.056$. Initial conditions: $i(0) = 0.18,\ x(0) = 0.18$.

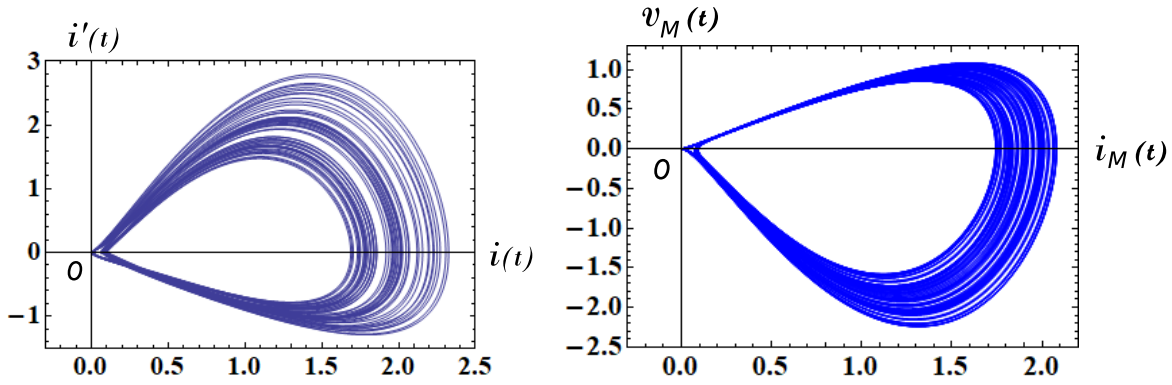

(a) $\big(i(t),\, i'(t)\big)$ reconstruction (b) $\big(i_M(t),\ v_M(t)\big)$ reconstruction

Figure 30: Reconstructed non-periodic trajectories using $\big(i(t),\, i'(t)\big)$ and $\big(i_M(t),\ v_M(t)\big)$, where v_M and i_M denote the terminal voltage and the terminal current of the current-controlled generic memristor. Parameters: $a = 2/3,\ b = 4/3,\ c = 1,\ d = 1,\ r = 0.04,\ \omega = 1$. Initial conditions: $i(0) = 0.19,\ x(0) = 0.18$.

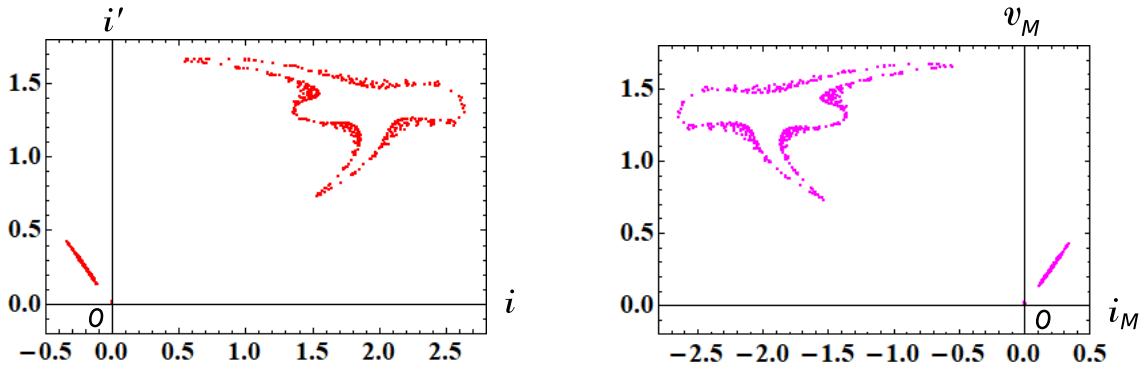

(a) Poincaré map for the attractor in Figure 30(a) (b) Poincaré map for the attractor in Figure 30(b)

Figure 31: Poincaré maps for the reconstructed non-periodic trajectories in Figure 30 . Observe that these two Poincaré maps are quite similar. Parameters: $a = 2/3,\ b = 4/3,\ c = 1,\ d = 1,\ r = 0.04,\ \omega = 1$. Initial conditions: $i(0) = 0.19,\ x(0) = 0.18$.

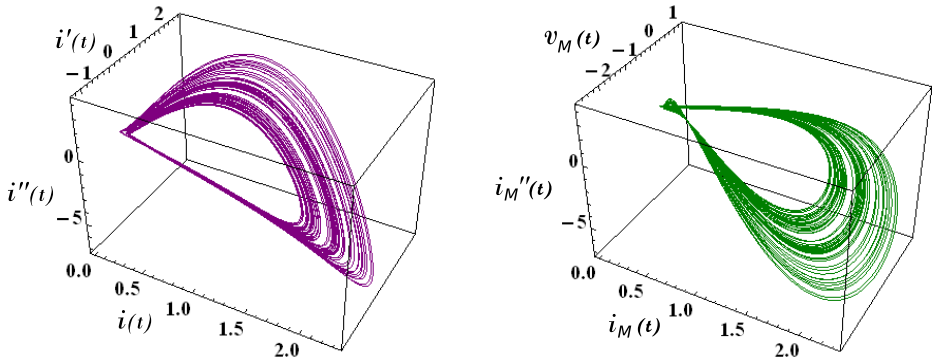

(a) $\big(i(t),\ i'(t),\ i''(t)\big)$ reconstruction (b) $\big(i_M(t),\ v_M(t),\ {i_M}''(t)\big)$ reconstruction

Figure 32: Reconstructed non-periodic trajectory using $\big(i(t),\ i'(t)\ i''(t)\big)$ and $\big(i_M(t),\ v_M(t),\ {i_M}''(t)\big)$, where v_M and i_M denote the terminal voltage and the terminal current of the current-controlled generic memristor. Parameters: $a = 2/3,\ b = 4/3,\ c = 1,\ d = 1,\ r = 0.04,\ \omega = 1$. Initial conditions: $i(0) = 0.19,\ x(0) = 0.18$.

2.5 Rössler system

The dynamics of the *Rössler system* [16, 17] is defined by

Rössler system

$$\left.\begin{aligned} \frac{dx_1}{dt} &= -x_2 - x_3, \\ \frac{dx_2}{dt} &= x_1 + a\,x_2, \\ \frac{dx_3}{dt} &= b + x_3\,(x_1 - c), \end{aligned}\right\} \tag{69}$$

where $a = 0.2$, $b = 0.2$, and $c = 5.7$.

The behavior of Eq. (69) is chaotic for certain ranges of the three parameters, a, b and c.

Consider the three-element memristor circuit in Figure 1. The dynamics of this circuit given by Eq. (2). Assume that Eq. (2) satisfies

$$\begin{aligned} E = b, \qquad & L = 1, \\ \hat{R}(x_1,\, x_2,\, i) &= -(x_1 - c), \\ \tilde{f}_1(x_1,\, x_2,\, i) &= -x_2 - i, \\ \tilde{f}_2(x_1,\, x_2,\, i) &= x_1 + a\,x_2. \end{aligned} \tag{70}$$

Then we obtain

Memristor Rössler system

$$\left.\begin{aligned} \frac{di}{dt} &= E + (x_1 - c)\,i, \\ \frac{dx_1}{dt} &= -x_2 - i, \\ \frac{dx_2}{dt} &= x_1 + a\,x_2, \end{aligned}\right\} \tag{71}$$

where $a = 0.2$, $E = b = 0.2$, $c = 5.7$.

Equations (69) and (71) are equivalent if we change the variables and the parameter

$$i = x_3, \quad E = b. \tag{72}$$

In this case, the extended memristor in Figure 1 is replaced by the *generic* memristor (see Appendix A). That is,

$$\hat{R}(x_1,\, x_2,\, i) = \tilde{R}(x_1,\, x_2) = -(x_1 - c). \tag{73}$$

The terminal voltage v_M and the terminal current i_M of the current-controlled generic memristor are described by

V-I characteristics of the generic memristor

$$\begin{aligned} v_M &= \tilde{R}(x_1,\, x_2)\, i_M = -(x_1 - c)\, i_M, \\ \frac{dx_1}{dt} &= -x_2 - i_M, \\ \frac{dx_2}{dt} &= x_1 + a\, x_2, \end{aligned} \tag{74}$$

where $\tilde{R}(x_1,\, x_2) = -(x_1 - c)$.

It follows that the Rössler system (69) can be realized by the three-element memristor circuit in Figure 1. The memristor Rössler equations (71) also exhibit chaotic oscillation. Thus, an external periodic forcing is unnecessary to generate chaotic or non-periodic oscillation. We show their chaotic attractor, Poincaré map, and $i_M - v_M$ locus Figures 33, 34, and 35, respectively. The following parameters are used in our computer simulations:

$$a = 0.2,\ b = E = 0.2,\ c = 5.7. \tag{75}$$

Observe that a chaotic attractor is a simple stretched and folded ribbon (see Figures 33 and 34). The $i_M - v_M$ locus in Figure 35 lies in the first and the fourth quadrants. Thus, the extended memristor defined by Eq. (74) is an active element. Let us show the $v_M - p_M$ locus in Figure 36, where $p_M(t)$ is an instantaneous power defined by $p_M(t) = i_M(t)v_M(t)$. Observe that the $v_M - p_M$ locus is pinched at the origin, and the locus lies in the first and the third quadrants. Thus, when $v_M > 0$, the instantaneous power is dissipated in the memristor. However, when $v_M < 0$, the instantaneous power is not dissipated in the memristor. Hence, the memristor switches between passive and active modes of operation, depending on its terminal voltage. We conclude as follow:

Switching behavior of the memristor

Assume that Eq. (71) exhibits chaotic oscillation. Then the generic memristor defined by Eq. (74) can switch between "passive" and "active" modes of operation, depending on its terminal voltage.

Finally, we reconstruct a chaotic attractor by using the current $i(t)$ (see [6]), that is,

$$\Big(i(t),\ i'(t),\ i''(t)\Big), \tag{76}$$

and by using the i_M and v_M, that is,

$$\Big(i_M(t),\ v_M(t),\ i''_M(t)\Big) \equiv \Big(i(t),\ -i'(t) + E,\ i''(t)\Big), \tag{77}$$

where $i_M(t) = i(t)$. We show the reconstructed attractors in Figure 37.

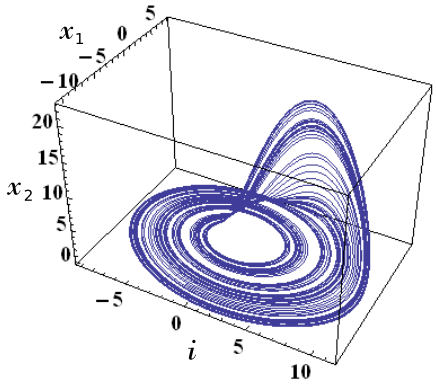

Figure 33: Chaotic attractor of the memristor Rössler equations (71). Parameters: $a = 0.2,\ b = E = 0.2,\ c = 5.7$. Initial conditions: $i(0) = 0.1,\ x_1(0) = 0.1,\ x_2(0) = 0.1$.

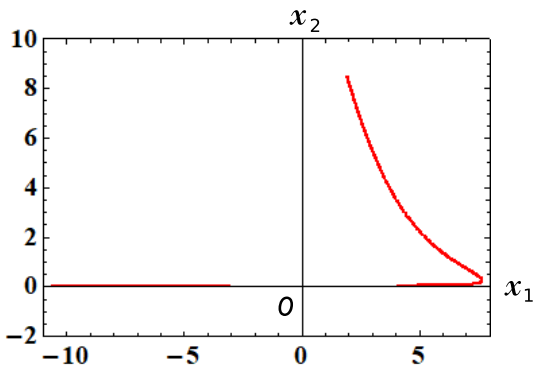

Figure 34: Poincaré map of the memristor Rössler equations (71). Its Poincaré cross-section (plane) is defined by $\{(i,\ x_1,\ x_2) \in R^3 \mid i = 0\}$. The trajectory of Eq. (71) crosses the above Poincaré cross-section (plane) many times. From Figures 33 and 34, we can observe that a chaotic attractor is a simple stretched and folded ribbon. Parameters: $a = 0.2,\ b = E = 0.2,\ c = 5.7$. Initial conditions: $i(0) = 0.1,\ x_1(0) = 0.1,\ x_2(0) = 0.1$.

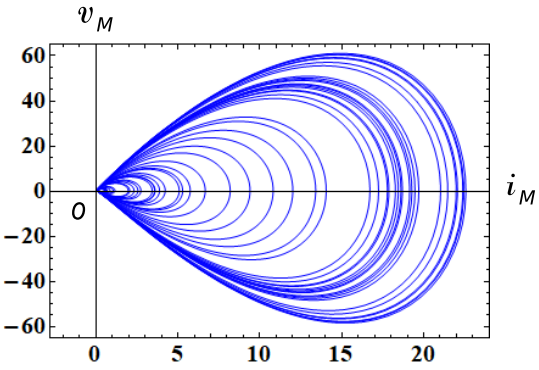

Figure 35: The $i_M - v_M$ locus of the memristor Rössler equations (71). Here, v_M and i_M denote the terminal voltage and the terminal current of the current-controlled generic memristor. Parameters: $a = 0.2,\ b = E = 0.2,\ c = 5.7$. Initial conditions: $i(0) = 0.1,\ x_1(0) = 0.1,\ x_2(0) = 0.1$.

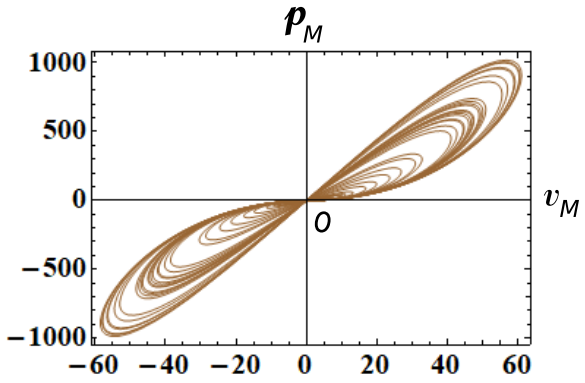

Figure 36: The $v_M - p_M$ locus of the Rössler equations (71). Here, $p_M(t)$ is an instantaneous power defined by $p_M(t) = i_M(t)v_M(t)$, and $v_M(t)$ and $i_M(t)$ denote the terminal voltage and the terminal current of the current-controlled generic memristor. Observe that the $v_M - p_M$ locus is pinched at the origin, and the locus lies in the first and the third quadrants. The memristor switches between passive and active modes of operation, depending on its terminal voltage $v_M(t)$. Parameters: $a = 0.2,\ b = E = 0.2,\ c = 5.7$. Initial conditions: $i(0) = 0.1,\ x_1(0) = 0.1,\ x_2(0) = 0.1$.

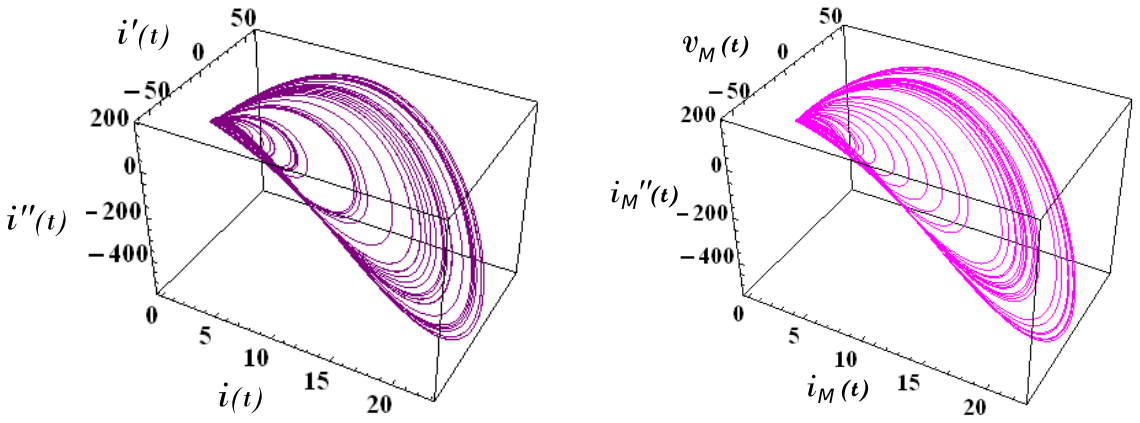

(a) $\Big(i(t),\ i'(t),\ i''(t)\Big)$ reconstruction

(b) $\Big(i_M(t),\ v_M(t),\ {i_M}''(t)\Big)$ reconstruction

Figure 37: Two reconstructed chaotic attractors using $\Big(i(t),\ i'(t),\ i''(t)\Big)$ and $\Big(i_M(t),\ v_M(t),\ {i_M}''(t)\Big)$. Parameters: $a = 0.2,\ b = E = 0.2,\ c = 5.7$. Initial conditions: $i(0) = 0.1,\ x_1(0) = 0.1,\ x_2(0) = 0.1$.

2.6 CO_2 laser model

The dynamics of the CO_2 laser model is given by [18]

CO_2 laser model equations

$$\left.\begin{aligned}
\frac{dX_1}{dt} &= k_0 X_1 \left\{X_2 - 1 - k_1 \sin^2 X_6\right\}, \\
\frac{dX_2}{dt} &= -\Gamma_1 X_2 - 2k_0 X_1 X_2 + \gamma X_3 + X_4 + P_0, \\
\frac{dX_3}{dt} &= -\Gamma_1 X_3 + X_5 + \gamma X_2 + P_0, \\
\frac{dX_4}{dt} &= -\Gamma_2 X_4 + \gamma X_5 + z X_2 + z P_0, \\
\frac{dX_5}{dt} &= -\Gamma_2 X_5 + z X_3 + \gamma X_4 + z P_0, \\
\frac{dX_6}{dt} &= -b X_6 + b B_0 - \frac{bRX_1}{1 + aX_1}.
\end{aligned}\right\} \tag{78}$$

Here, X_1 is the photon number proportional to the laser intensity, X_2 is proportional to the laser inversion, X_3 is proportional to the sum of the populations of the laser resonant levels, X_4 and X_5 are, respectively, proportional to the difference and sum of the populations of the rotational manifolds coupled to the resonant levels, and X_6 is a term proportional to the feedback voltage which acts on the cavity loss [18]. The parameters are chosen as follows:

$$\left.\begin{aligned}
&k_0 = 28.5714, \quad k_1 = 4.5556, \quad \gamma = 0.05, \\
&P_0 = 0.016, \quad a = 32.8767, \quad b = 0.4286, \\
&G_1 = 10.0643, \quad G_2 = 1.0643, \quad z = 10.0, \\
&B_0 = 0.1026, \quad R = 159,\, 160.
\end{aligned}\right\} \tag{79}$$

Let us consider the three-element memristor circuit in Figure 1. The dynamics of this circuit is given by Eq. (2). Assume that Eq. (2) satisfies

$$\left.\begin{aligned}
&E = 0, \qquad L = 1, \\
\hat{R}(\boldsymbol{x},\, i) &= -k_0 \left\{x_1 - 1 - k_1 \sin^2 x_5\right\}, \\
\tilde{f}_1(\boldsymbol{x},\, i) &= -\Gamma_1 x_1 - 2k_0 x_1 x_1 + \gamma x_2 + x_3 + P_0, \\
\tilde{f}_2(\boldsymbol{x},\, i) &= -\Gamma_1 x_2 + x_4 + \gamma x_1 + P_0, \\
\tilde{f}_3(\boldsymbol{x},\, i) &= -\Gamma_2 x_3 + \gamma x_4 + z x_1 + z P_0, \\
\tilde{f}_4(\boldsymbol{x},\, i) &= -\Gamma_2 x_4 + z x_2 + \gamma x_3 + z P_0, \\
\tilde{f}_5(\boldsymbol{x},\, i) &= -b x_5 + b B_0 - \frac{bR\, i}{1 + a\, i}.
\end{aligned}\right\} \tag{80}$$

Then we obtain

Memristor CO_2 laser model equations

$$\left.\begin{aligned}
\frac{di}{dt} &= k_0\left\{x_1 - 1 - k_1\sin^2 x_5\right\} i, \\
\frac{dx_1}{dt} &= -\Gamma_1 x_1 - 2k_0 x_1 x_1 + \gamma x_2 + x_3 + P_0, \\
\frac{dx_2}{dt} &= -\Gamma_1 x_2 + x_4 + \gamma x_1 + P_0, \\
\frac{dx_3}{dt} &= -\Gamma_2 x_3 + \gamma x_4 + z x_1 + z P_0, \\
\frac{dx_4}{dt} &= -\Gamma_2 x_4 + z x_2 + \gamma x_3 + z P_0, \\
\frac{dx_5}{dt} &= -b x_5 + bB_0 - \frac{bR\, i}{1 + a\, i},
\end{aligned}\right\} \tag{81}$$

where

$$\left.\begin{aligned}
&X_1 = i, \quad X_2 = x_1, \quad X_3 = x_2, \\
&X_4 = x_3, \quad X_5 = x_4, \quad X_6 = x_5.
\end{aligned}\right\} \tag{82}$$

In this case, the extended memristor in Figure 1 is replaced by the *generic* memristor. That is,

$$\hat{R}(\boldsymbol{x},\, i) = \tilde{R}(\boldsymbol{x}) = -k_0\left\{x_1 - 1 - k_1\sin^2 x_5\right\}. \tag{83}$$

The terminal voltage v_M and the terminal current i_M of the generic memristor are described by

V-I characteristics of the generic memristor

$$\left.\begin{aligned}
v_M &= \tilde{R}(\boldsymbol{x})\, i_M = -k_0\left\{x_1 - 1 - k_1\sin^2 x_5\right\} i_M, \\
\frac{dx_1}{dt} &= -\Gamma_1 x_1 - 2k_0 x_1 x_1 + \gamma x_2 + x_3 + P_0, \\
\frac{dx_2}{dt} &= -\Gamma_1 x_2 + x_4 + \gamma x_1 + P_0, \\
\frac{dx_3}{dt} &= -\Gamma_2 x_3 + \gamma x_4 + z x_1 + z P_0, \\
\frac{dx_4}{dt} &= -\Gamma_2 x_4 + z x_2 + \gamma x_3 + z P_0, \\
\frac{dx_5}{dt} &= -b x_5 + bB_0 - \frac{bR\, i}{1 + a\, i},
\end{aligned}\right\} \tag{84}$$

where $\tilde{R}(\boldsymbol{x}) = -k_0\left\{x_1 - 1 - k_1\sin^2 x_5\right\}$.

Thus, the CO_2 laser model (78) can be realized by the three-element memristor circuit in Figure 1. Equations (78) and (81) can exhibit chaotic oscillation [18]. Thus, an external periodic forcing is unnecessary to generate chaotic or non-periodic oscillation.

We next show the chaotic attractors and $i_M - v_M$ loci in Figures 38 and 39, respectively. The $i_M - v_M$ locus in Figure 39 lies in the first and the fourth quadrants. Thus, the generic memristor defined by Eq. (84) is an active element. Let us show the $v_M - p_M$ locus in Figure 40, where $p_M(t)$ is an instantaneous

power defined by $p_M(t) = i_M(t)v_M(t)$. Observe that the $v_M - p_M$ locus is pinched at the origin, and the locus lies in the first and the third quadrants. Thus, when $v_M > 0$, the instantaneous power is dissipated in the memristor. However, when $v_M < 0$, the instantaneous power is not dissipated in the memristor. Hence, the memristor switches between passive and active modes of operation, depending on its terminal voltage. In order to obtain these figures, we have to choose the parameters and the initial conditions carefully and the maximum step size h of the numerical integration must be sufficiently small ($h = 0.005$). It is due to the fact that a stable limit cycle (drawn in red) also coexists with a chaotic attractor (drawn in blue) as shown in Figure 41. We conclude as follow:

Switching behavior of the memristor

Assume that Eq. (81) exhibits chaotic oscillation. Then the generic memristor defined by Eq. (84) can switch between "passive" and "active" modes of operation, depending on its terminal voltage.

We next show the Lorenz maps[7] in Figure 42, instead of Poincaré maps, since Eq.(81) is the high-dimensional differential equations. The Lorenz map in Figure 42(b) represents a repeated folding and stretching of the space on which it is defined. In order to view the above folding action from a different perspective, let us plot the point (x_2, x_3) when $x_6 = K$ (K is a constant). This is the simplified version of Poincaré map. We show the above plot in Figure 43. Observe that Figure 43(b) exhibits the repeated folding and stretching action.

Finally, we reconstruct the chaotic attractors by using the time-delayed current signal (For more details, see [6]), that is,

$$\Big(i(t),\ i(t-1)\Big). \tag{85}$$

The reconstructed chaotic attractors are shown in Figure 44. Observe that the chaotic attractors in Figure 44 are similar to those in Figure 38. As stated in Sec. 2.1, the $i_M - v_M$ locus in Figure 39 is considered to be the reconstruction of the chaotic attractor on the two-dimensional plane.

[7]The Lorenz map is defined as follow: Consider a chaotic solution $i(t)$ of the memristor CO_2 laser model equations (81). Extract the local maxima in $i(t)$ and label the nth local maximum i_n. Plot of the maximum i_{n+1} versus the maximum i_n. The above constructed map is called Lorenz map, and it gives a well-defined relation between successive peaks, that is, we can estimate the peak knowing the peak. Furthermore, we need only one state variable to construct the Lorenz map.

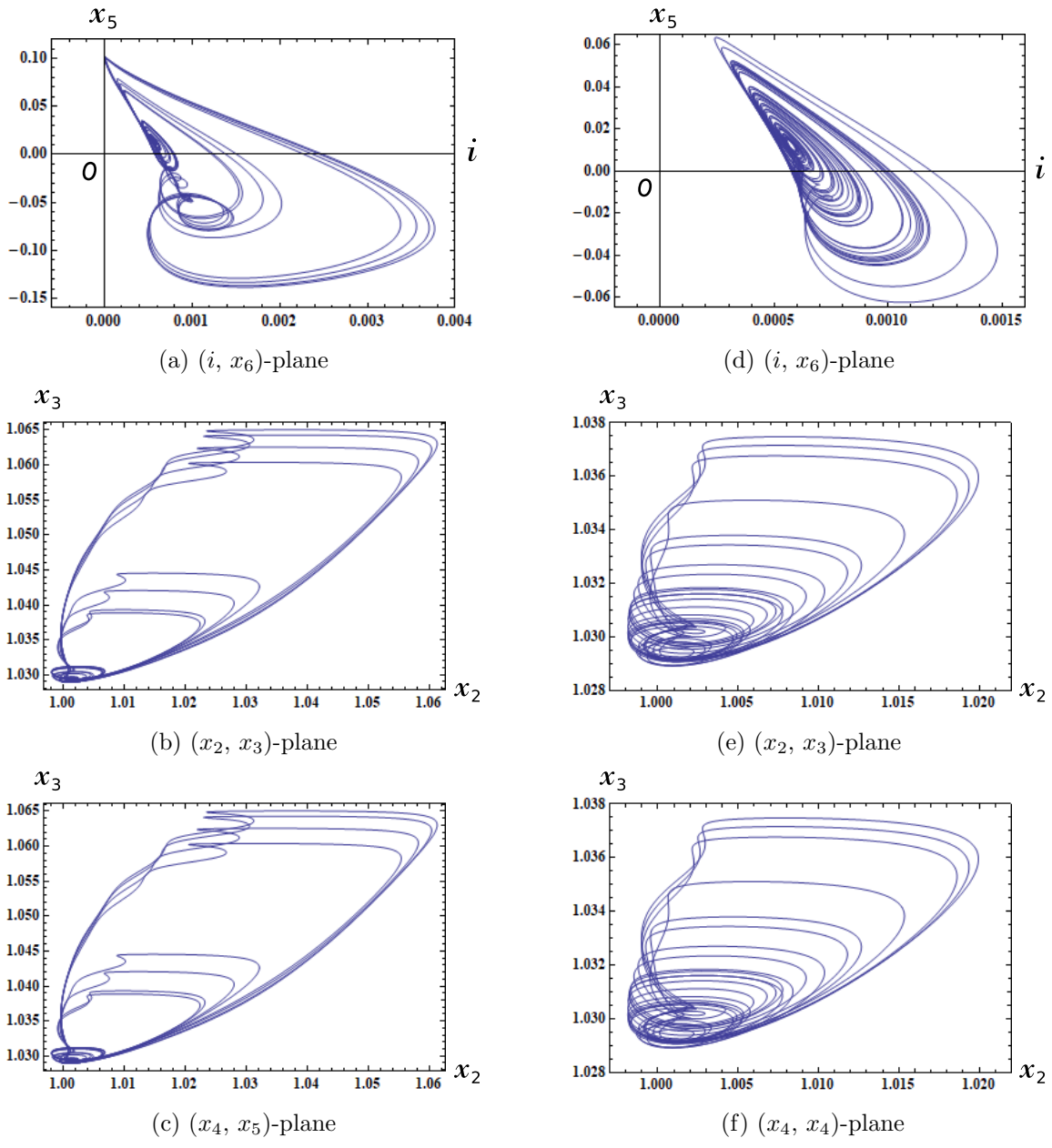

(a) $(i,\, x_6)$-plane

(d) $(i,\, x_6)$-plane

(b) $(x_2,\, x_3)$-plane

(e) $(x_2,\, x_3)$-plane

(c) $(x_4,\, x_5)$-plane

(f) $(x_4,\, x_4)$-plane

Figure 38: Chaotic attractors of the memristor CO2 laser model equations (81). All parameters except for R are given in Eq. (79). Parameters: (a)-(c) $R = 159$, (d)-(f) $R = 160$. Initial conditions: $i(0) = x_1(0) = x_2(0) = x_3(0) = x_4(0) = x_5(0) = 0.1$.

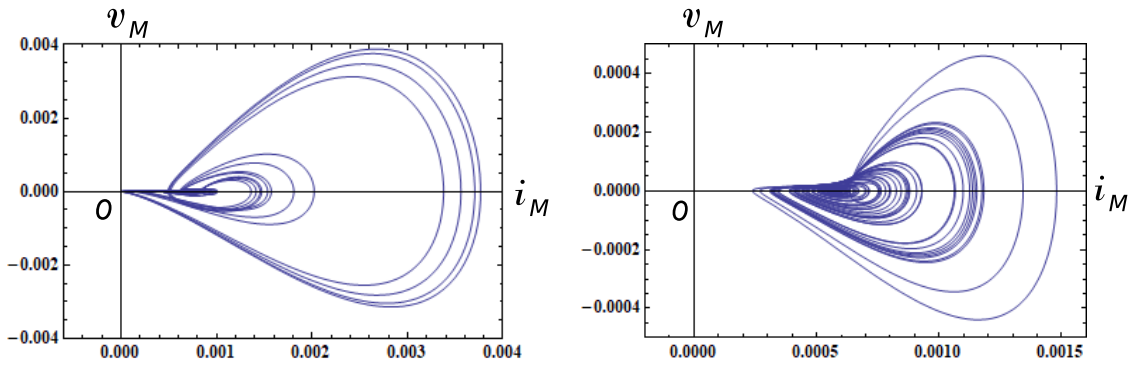

(a) $R = 159$ (b) $R = 160$

Figure 39: The $i_M - v_M$ locus of the memristor CO2 laser model equations (81). Here, v_M and i_M denote the terminal voltage and the terminal current of the current-controlled generic memristor. All parameters except for R are given in Eq. (79). Initial conditions: $i(0) = x_1(0) = x_2(0) = x_3(0) = x_4(0) = x_5(0) = 0.1$.

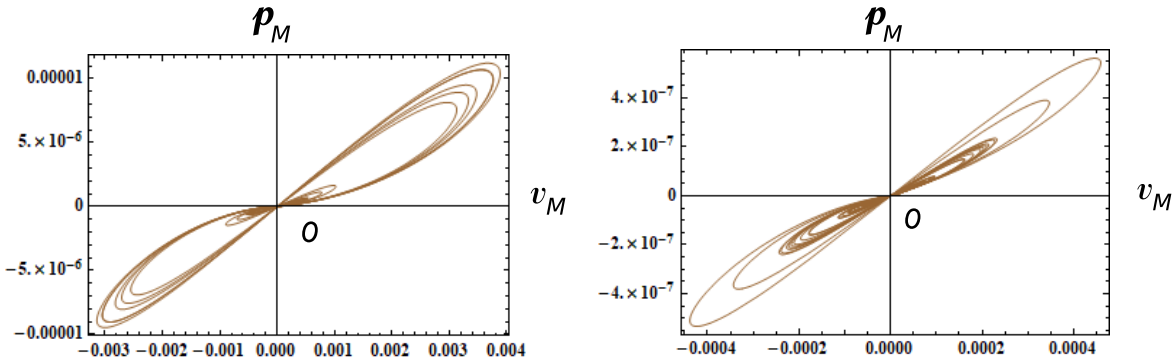

(a) $R = 159$ (b) $R = 160$

Figure 40: The $v_M - p_M$ locus of the memristor CO2 laser model equations (81). Here, $p_M(t)$ is an instantaneous power defined by $p_M(t) = i_M(t)v_M(t)$, and $v_M(t)$ and $i_M(t)$ denote the terminal voltage and the terminal current of the current-controlled generic memristor. Observe that the $v_M - p_M$ locus is pinched at the origin, and the locus lies in the first and the third quadrants. The memristor switches between passive and active modes of operation, depending on its terminal voltage $v_M(t)$. All parameters except for R are given in Eq. (79). Initial conditions: $i(0) = x_1(0) = x_2(0) = x_3(0) = x_4(0) = x_5(0) = 0.1$.

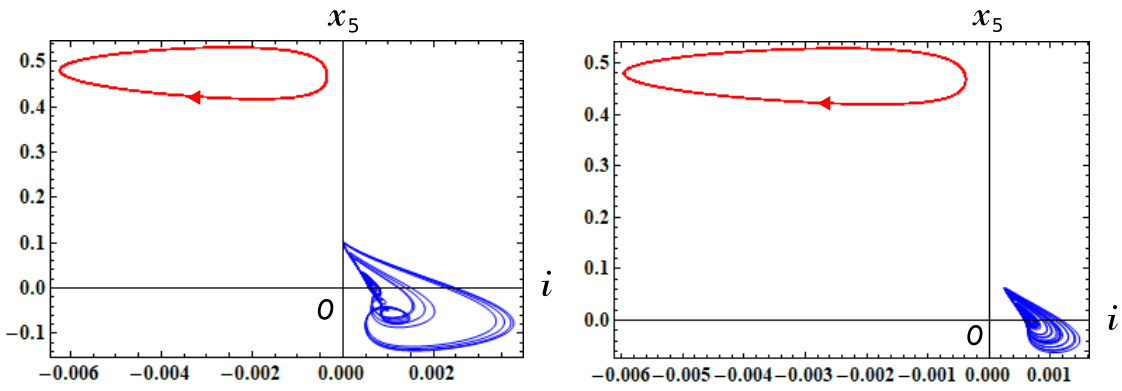

(a) $R = 159$ (b) $R = 160$

Figure 41: A stable limit cycle (red) coexists with a chaotic attractor (blue). All parameters except for R are given in Eq. (79). Initial conditions for chaotic attractors: $i(0) = x_1(0) = x_2(0) = x_3(0) = x_4(0) = x_5(0) = 0.1$. Initial conditions for a limit cycles: $i(0) = x_1(0) = x_2(0) = x_3(0) = x_4(0) = 0.1$, $x_5(0) = 5.1$.

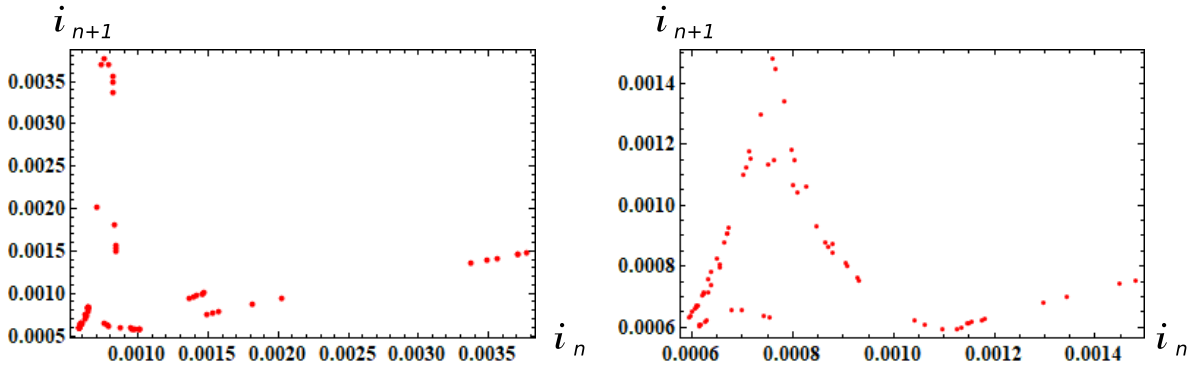

(a) $R = 159$ (b) $R = 160$

Figure 42: Lorenz maps of the memristor CO_2 laser model equations (81). All parameters except for R are given in Eq. (79). Initial conditions: $i(0) = x_1(0) = x_2(0) = x_3(0) = x_4(0) = x_5(0) = 0.1$.

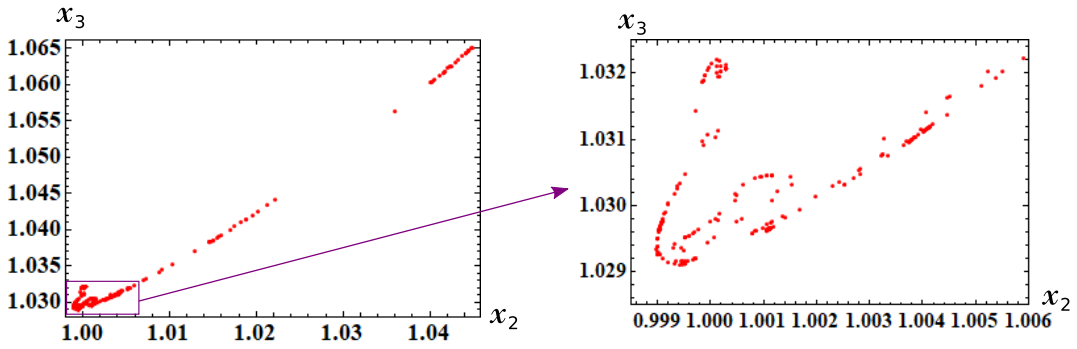

(a) Poincaré map for $x_6 = 0.01$ and $R = 159$.

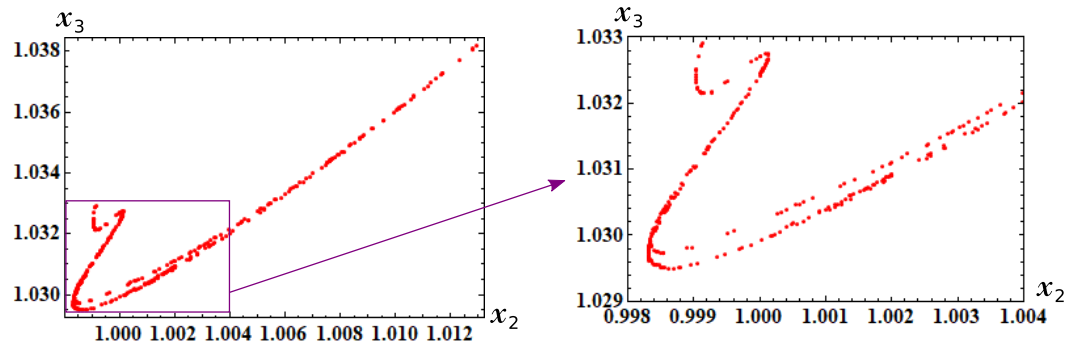

(b) Poincaré map for $x_6 = 0$ and $R = 160$.

Figure 43: Two-dimensional plot of the memristor CO2 laser model equations (81). (a) The point (x_2, x_3) is plotted when $x_6 = 0.01$. (b) The point (x_2, x_3) is plotted when $x_6 = 0$. Observe that Figure 43(b) exhibits the repeated folding and stretching action, and Figure 43(a) exhibits the distorted folding action. All parameters except for R are given in Eq. (79). Initial conditions: $i(0) = x_1(0) = x_2(0) = x_3(0) = x_4(0) = x_5(0) = 0.1$.

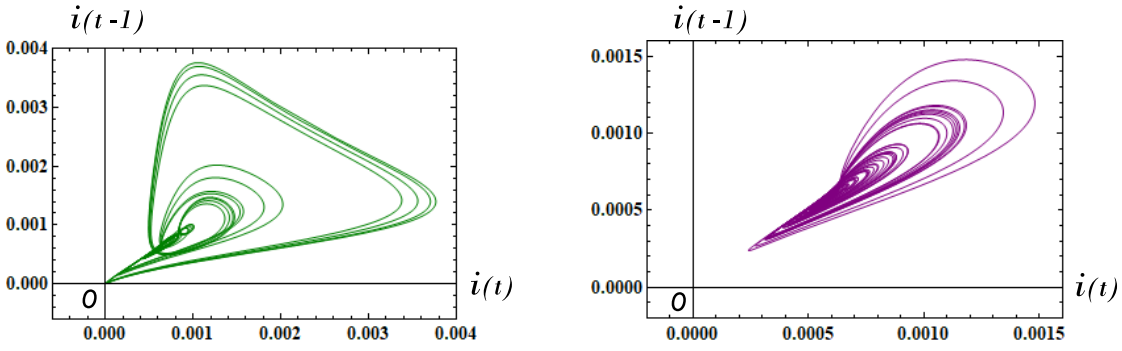

(a) $R = 159$ (b) $R = 160$

Figure 44: Reconstructed chaotic attractors using $\Big(i(t),\ i(t-1)\Big)$. Observe that the chaotic attractors in Figure 44 are similar to those in Figure 38. All parameters except for R are given in Eq. (79). Initial conditions: $i(0) = x_1(0) = x_2(0) = x_3(0) = x_4(0) = x_5(0) = 0.1$.

3 $2N$-element memristor circuit

Let us consider the $2N$-element memristor circuit shown in Figure 45. It consists of N inductors with the inductance L_n $(n = 1,\ 2, \cdots\ N)$ and N extended memristors described by

V-I characteristics of the extended memristors

$$\begin{aligned} v_n &= \hat{R}(\boldsymbol{x},\ i_n)\, i_n, \\ \frac{d\boldsymbol{x}}{dt} &= \tilde{\boldsymbol{f}}(\boldsymbol{x},\ \boldsymbol{i}). \end{aligned} \tag{86}$$

Here, $\boldsymbol{x} = (x_1, x_2, \cdots, x_N) \in \mathbb{R}^N$, $\boldsymbol{i} = (i_1, i_2, \cdots, i_N) \in \mathbb{R}^N$, $\hat{R}(\boldsymbol{x},\ i_n)$ is a continuous scalar-valued function, and $\tilde{\boldsymbol{f}} = (\tilde{f}_1, \tilde{f}_2, \cdots, \tilde{f}_N) : \mathbb{R}^N \to \mathbb{R}^N$. Even though the extended memristors in Figure 45 appear to be disconnected, their dynamics are coupled via the memristance equation involving the same state variables $\boldsymbol{x} = (x_1,\ x_2,\ \cdots,\ x_N)$ and $\boldsymbol{i} = (i_1, i_2, \cdots, i_N)$. Note the memristor defined by Eq. (86) is considered to be a special case of the *extended memristor* defined in Appendix A. That is, we modified the current i of Eq. (241) into the vector form $\boldsymbol{i} = (i_1, i_2, \cdots, i_N)$.

The dynamics of the above $2N$-element memristor circuit is given by

$2N$-element memristor circuit equations

$$\begin{aligned} L_n \frac{di_n}{dt} &= -v_n = -\hat{R}(\boldsymbol{x},\ i_n)\, i_n, \\ \frac{d\boldsymbol{x}}{dt} &= \tilde{\boldsymbol{f}}(\boldsymbol{x},\ \boldsymbol{i}), \end{aligned} \tag{87}$$

where $n = 1,\ 2, \cdots,\ N$ and we usually assume $L_n = 1$.

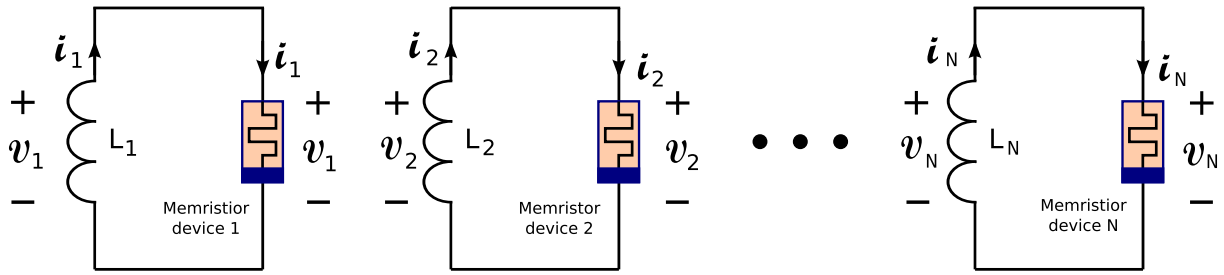

Figure 45: A $2N$-element extended memristor circuit, which consists of N inductors with the inductance L_k $(k = 1,\ 2, \cdots N)$ and N memristor devices described by $v_k = \hat{R}_k(\boldsymbol{x}, i_k)\ i_k$ $(k = 1,\ 2, \cdots N)$. $\frac{d\boldsymbol{x}}{dt} = \tilde{\boldsymbol{f}}(\boldsymbol{x},\ \boldsymbol{i})$, Here, $\hat{R}_k(\boldsymbol{x}, i_k)$ denotes the memristance of the kth extended memristor device, $\boldsymbol{x} = (x_1, x_2, \cdots, x_N) \in \mathbb{R}^n$, $\boldsymbol{i} = (i_1, i_2, \cdots, i_N) \in \mathbb{R}^N$, and $\tilde{\boldsymbol{f}} = (\tilde{f}_1, \tilde{f}_2, \cdots, \tilde{f}_N) : \mathbb{R}^N \to \mathbb{R}^N$. Even though the extended memristor devices appear to be disconnected, their dynamics are coupled via the memristance equation involving the same state variables $\boldsymbol{x} = (x_1,\ x_2,\ \cdots,\ x_N)$ and $\boldsymbol{i} = (i_1,\ i_2,\ \cdots,\ i_N)$.

3.1 Toda lattice equations

Consider the Hamiltonian for a chain of particles with nearest neighbor exponential interaction [19, 20]

$$\mathcal{H} = \sum_n \frac{1}{2}\, {p_n}^2 + \sum_n e^{-(\,q_{n+1} - q_n\,)}, \tag{88}$$

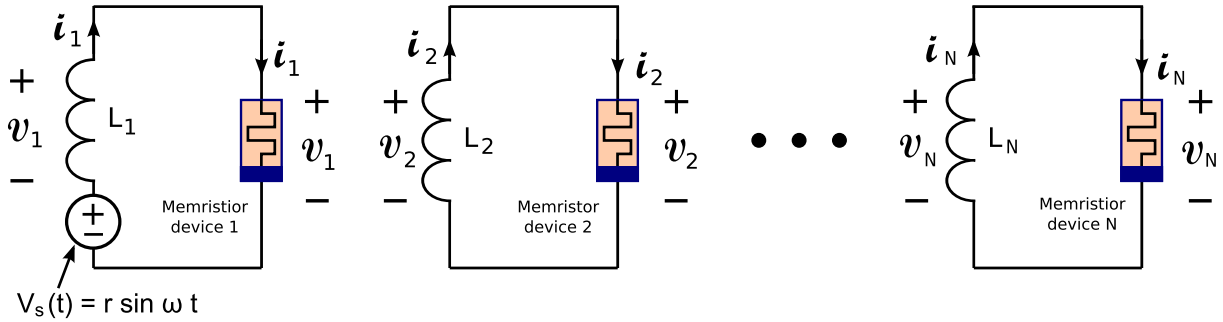

Figure 46: A $2N$-element extended memristor circuit driven by a periodic voltage source $v_s(t) = r\sin(\omega t)$, where r and ω are constants.

where q_n is the displacement of the n-th particle from its equilibrium position, and p_n is its momentum (mass $m = 1$). Then, the Hamilton's Equations are given by

Toda lattice equations A

$$\begin{aligned} \frac{dq_n}{dt} &= p_n, \\ \frac{dp_n}{dt} &= e^{-(q_n - q_{n-1})} - e^{-(q_{n+1} - q_n)}, \end{aligned} \tag{89}$$

where $n = 1,\ 2, \cdots,\ N$ and we consider the case of a periodic lattice of the length N: $q_n = q_{n+N}$.

3.1.1 Toda lattice equations B

Let us define a new variable

$$X_n = e^{-(q_{n+1} - q_n)}. \tag{90}$$

Then, Eq. (89) can be recast into the form [21]

Toda lattice equations B

$$\begin{aligned} \frac{dX_n}{dt} &= (p_n - p_{n+1})X_n, \\ \frac{dp_n}{dt} &= X_{n-1} - X_n, \end{aligned} \tag{91}$$

where $n = 1,\ 2, \cdots,\ N$ and we consider the case of a periodic lattice of the length N: $p_n = p_{n+N}$, $X_n = X_{n+N}$.

Consider the $2N$-element memristor circuit in Figure 45. The dynamics of this circuit given by Eq. (87). Assume that Eq. (87) satisfies

$$\begin{aligned} L_n &= 1, \\ \hat{R}(\boldsymbol{x},\ i_n) &= -(x_n - x_{n+1}) \\ \tilde{f}_n(\boldsymbol{x}, \boldsymbol{i}) &= i_{n-1} - i_n. \end{aligned} \tag{92}$$

Then we obtain

Memristor Toda lattice equations B

$$\begin{aligned} \frac{di_n}{dt} &= (x_n - x_{n+1})\, i_n, \\ \frac{dx_n}{dt} &= i_{n-1} - i_n, \end{aligned} \tag{93}$$

where $n = 1,\ 2, \cdots,\ N$ and we consider the case of a periodic lattice of the length N: $x_n = x_{n+N}$, $i_n = i_{n+N}$.

Equations (91) and (93) are equivalent if we change the variables

$$i_n = X_n,\ x_n = p_n. \tag{94}$$

In this case, the extended memristors in Figure 45 are replaced by the *generic* memristors, that is,

$$\hat{R}_n(\boldsymbol{x},\ i_n) = \tilde{R}_n(\boldsymbol{x}) = -(x_n - x_{n+1}), \tag{95}$$

though the current i of Eq. (240) is modified into the vector form $\boldsymbol{i} = (i_1,\ i_2,\ \cdots,\ i_n)$. Thus, their terminal voltage v_n and the terminal current i_n are described by

V-I characteristics of the generic memristors

$$\begin{aligned} v_n &= \tilde{R}_n(x_n,\ x_{n+1})\ i_n = -(x_n - x_{n+1}) i_n, \\ \frac{dx_n}{dt} &= \tilde{f}_n(i_{n-1},\ i_n) = i_{n-1} - i_n, \end{aligned} \tag{96}$$

where $x_n = x_{n+N}$, $i_n = i_{n+N}$, and $n = 1,\ 2, \cdots,\ N$.

It follows that Eq. (91) can be realized by the $2N$-element memristor circuit in Figure 45.

For $N = 3$, Eq. (91) is given by

Toda lattice equations B with $N = 3$

$$\left.\begin{aligned} \frac{dX_1}{dt} &= (p_1 - p_2)X_1, \\ \frac{dp_1}{dt} &= X_3 - X_1, \\ \frac{dX_2}{dt} &= (p_2 - p_3)X_2, \\ \frac{dp_2}{dt} &= X_1 - X_2, \\ \frac{dX_3}{dt} &= (p_3 - p_1)X_3, \\ \frac{dp_3}{dt} &= X_2 - X_3. \end{aligned}\right\} \tag{97}$$

Equation (97) has the three integrals [21, 20], since the solution satisfies

Integrals

$$\frac{d}{dt}\big(p_1+p_2+p_3\big)=0,$$
$$\frac{d}{dt}\Big\{p_1p_2+p_1p_2+p_3p_1-X_1-X_2-X_3\Big\}=0,$$
$$\frac{d}{dt}\Big(p_1p_2p_3-p_1X_2-p_2X_3-p_3X_1\Big)=0. \tag{98}$$

The corresponding memristor circuit equations for Eq. (97) are given by

Memristor Toda lattice equations B with $N=3$

$$\left.\begin{aligned}
\frac{di_1}{dt} &= (x_1-x_2)i_1,\\
\frac{dx_1}{dt} &= i_3-i_1,\\
\frac{di_2}{dt} &= (x_2-x_3)i_2,\\
\frac{dx_2}{dt} &= i_1-i_2,\\
\frac{di_3}{dt} &= (x_3-x_1)i_3,\\
\frac{dx_3}{dt} &= i_2-i_3,
\end{aligned}\right\} \tag{99}$$

where i_1, i_2, and i_3 denote the current through the generic memristor.

The terminal voltage v_n and the terminal current i_n of the generic memristors are described by

V-I characteristics of the 3 generic memristors

$$\left.\begin{aligned}
v_1 &= \tilde{R}_1(x_1,\,x_2)\;i_1=-(x_1-x_2)i_1,\\
\frac{dx_1}{dt} &= \tilde{f}_1(i_3,\,i_1)=i_3-i_1,
\end{aligned}\right\}$$
$$\left.\begin{aligned}
v_2 &= \tilde{R}_2(x_2,\,x_3)\;i_2=-(x_2-x_3)i_2,\\
\frac{dx_1}{dt} &= \tilde{f}_2(i_1,\,i_2)=i_1-i_2,
\end{aligned}\right\}$$
$$\left.\begin{aligned}
v_3 &= \tilde{R}_3(x_3,\,x_1)\;i_3=-(x_3-x_1)i_3,\\
\frac{dx_1}{dt} &= \tilde{f}_3(i_2,\,i_3)=i_2-i_3,
\end{aligned}\right\} \tag{100}$$

where $x_4=x_1$, $i_0=i_3$.

Equation (99) can exhibit periodic behavior. If an external source is added to the memristor circuit as shown

in Figure 46, then the forced memristor circuit can exhibit a non-periodic response. The dynamics of this circuit is given by

Forced memristor Toda lattice equations B with $N = 3$

$$\left.\begin{aligned}
\frac{di_1}{dt} &= (x_1 - x_2)i_1 + r\sin(\omega t),\\
\frac{dx_1}{dt} &= i_3 - i_1,\\
\frac{di_2}{dt} &= (x_2 - x_3)i_2,\\
\frac{dx_2}{dt} &= i_1 - i_2,\\
\frac{di_3}{dt} &= (x_3 - x_1)i_3,\\
\frac{dx_3}{dt} &= i_2 - i_3,
\end{aligned}\right\} \qquad (101)$$

where r and ω are constants.

We show their non-periodic and quasi-periodic responses, Poincaré maps, and $i_j - v_j$ loci in Figures 47, 48, and 49, respectively ($j = 1, 2, 3$). In order to obtain these figures, we have to choose the parameters and the initial conditions carefully and the maximum step size h of the numerical integration must be sufficiently small ($h = 0.006$). The following parameters are used in our computer simulations:

$$r = 0.25,\ \omega = 0.925. \qquad (102)$$

The $i_j - v_j$ loci in Figure 49 lie in the first and the fourth quadrants. Thus, the three generic memristors are active element. Let us show the $v_j - p_j$ locus in Figure 50, where $p_j(t)$ is an instantaneous power defined by $p_j(t) = i_j(t)v_j(t)$ ($j = 1, 2, 3$). Observe that the $v_j - p_j$ loci are pinched at the origin, and the loci lie in the first and the third quadrants. Thus, when $v_j > 0$, the instantaneous power $p_j(t)$ delivered from the forced signal and the inductor is dissipated in the memristor. However, when $v_j < 0$, the instantaneous power $p_j(t)$ is *not* dissipated in the memristor. Hence, the memristors switch between passive and active modes of operation, depending on its terminal voltage. Thus, we conclude as follow:

Switching behavior of the memristor

Assume that Eq. (101) exhibits non-periodic or quasi-periodic oscillation. Then the generic memristors defined by Eq. (100) can switch between "passive" and "active" modes of operation, depending on its terminal voltage.

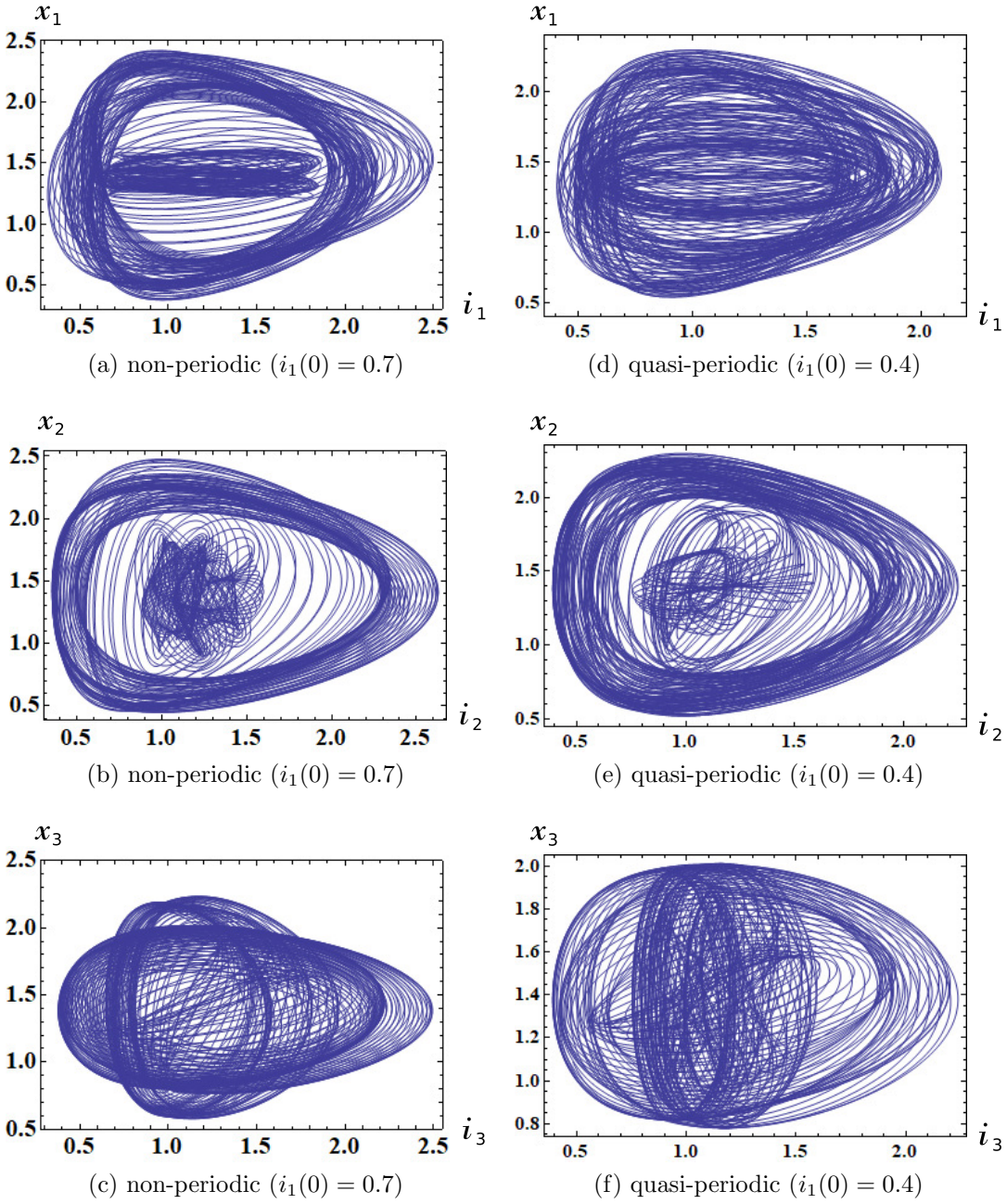

(a) non-periodic ($i_1(0) = 0.7$) (d) quasi-periodic ($i_1(0) = 0.4$)

(b) non-periodic ($i_1(0) = 0.7$) (e) quasi-periodic ($i_1(0) = 0.4$)

(c) non-periodic ($i_1(0) = 0.7$) (f) quasi-periodic ($i_1(0) = 0.4$)

Figure 47: Non-periodic and quasi-periodic responses of the forced memristor Toda lattice equations B, which are defined by Eq. (101). Here, i_j and x_j denote the terminal current and the internal state of the j-th generic memristor, respectively ($j = 1, 2, 3$). Parameters: $r = 0.25$, $\omega = 0.925$. Initial conditions: (a) $i_1(0) = 0.7$, $x_1(0) = 1.2$, $i_2(0) = 1.3$, $x_2(0) = 1.4$, $i_3(0) = 1.5$, $x_3(0) = 1.6$. (b) $i_1(0) = 0.4$, $x_1(0) = 1.2$, $i_2(0) = 1.3$, $x_2(0) = 1.4$, $i_3(0) = 1.5$, $x_3(0) = 1.6$.

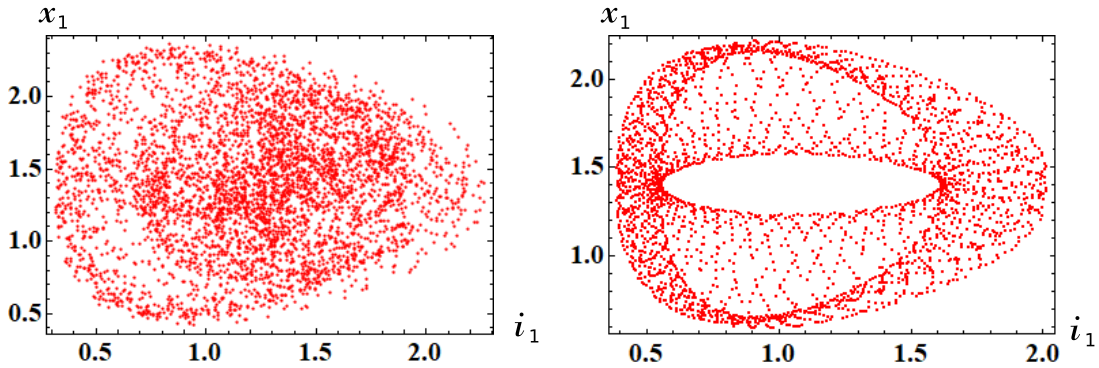

(a) non-periodic ($i_1(0) = 0.7$)

(d) quasi-periodic ($i_1(0) = 0.4$)

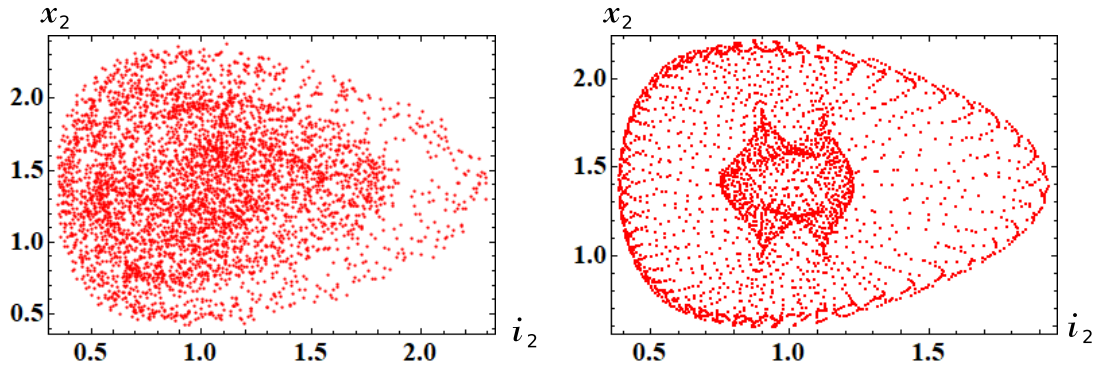

(b) non-periodic ($i_1(0) = 0.7$)

(e) quasi-periodic ($i_1(0) = 0.4$)

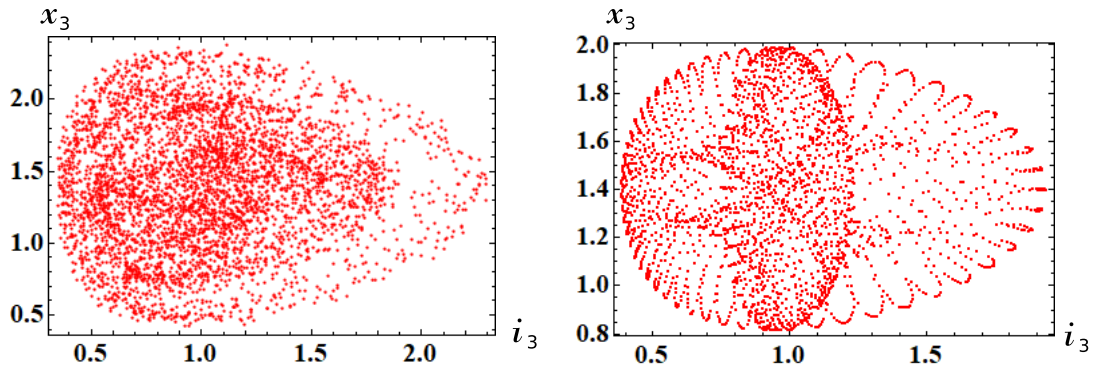

(c) non-periodic ($i_1(0) = 0.7$)

(f) quasi-periodic ($i_1(0) = 0.4$)

Figure 48: Poincaré maps of the forced memristor Toda lattice equations B, which are defined by Eq. (101). Here, i_j and x_j denote the terminal current and the internal state of the j-th generic memristor, respectively ($j = 1, 2, 3$). Parameters: $r = 0.25$, $\omega = 0.925$. Initial conditions: (a) $i_1(0) = 0.7$, $x_1(0) = 1.2$, $i_2(0) = 1.3$, $x_2(0) = 1.4$, $i_3(0) = 1.5$, $x_3(0) = 1.6$. (b) $i_1(0) = 0.4$, $x_1(0) = 1.2$, $i_2(0) = 1.3$, $x_2(0) = 1.4$, $i_3(0) = 1.5$, $x_3(0) = 1.6$.

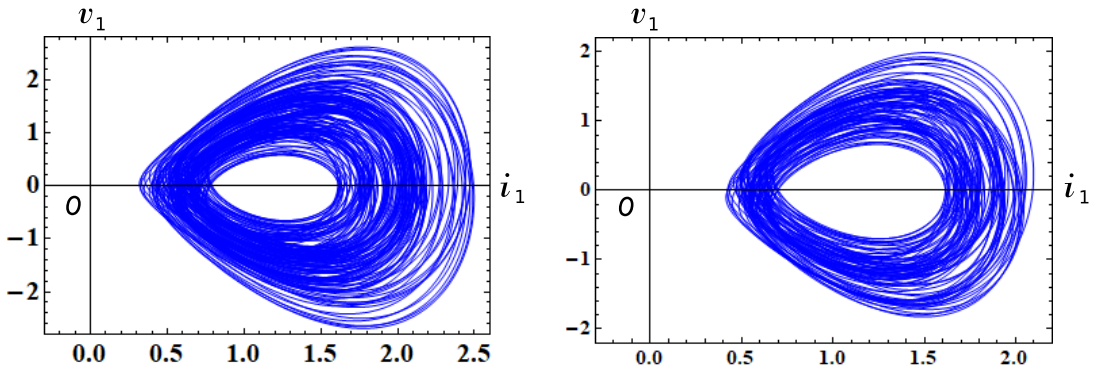

(a) non-periodic ($i_1(0) = 0.7$)

(d) quasi-periodic ($i_1(0) = 0.4$)

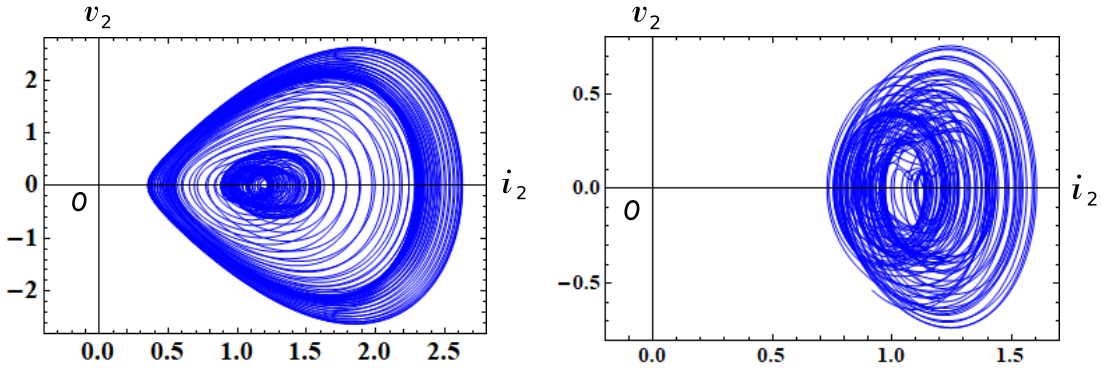

(b) non-periodic ($i_1(0) = 0.7$)

(e) quasi-periodic ($i_1(0) = 0.4$)

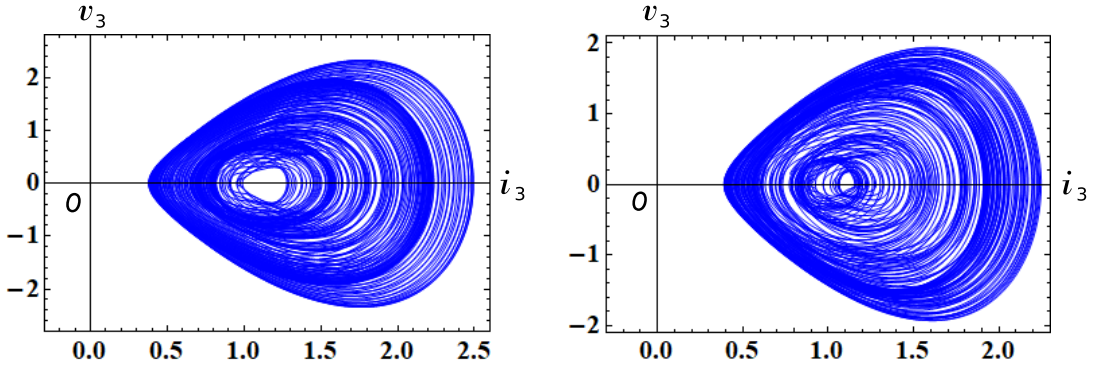

(c) non-periodic ($i_1(0) = 0.7$)

(f) quasi-periodic ($i_1(0) = 0.4$)

Figure 49: The $i_j - v_j$ loci of the forced memristor Toda lattice equations B, which are defined by Eq. (101). Here, i_j and v_j denote the terminal current and the voltage of the j-th generic memristor, respectively ($j = 1, 2, 3$). Parameters: $r = 0.25$, $\omega = 0.925$. Initial conditions: (a)-(c) $i_1(0) = 0.7$, $x_1(0) = 1.2$, $i_2(0) = 1.3$, $x_2(0) = 1.4$, $i_3(0) = 1.5$, $x_3(0) = 1.6$. (d)-(f) $i_1(0) = 0.4$, $x_1(0) = 1.2$, $i_2(0) = 1.3$, $x_2(0) = 1.4$, $i_3(0) = 1.5$, $x_3(0) = 1.6$.

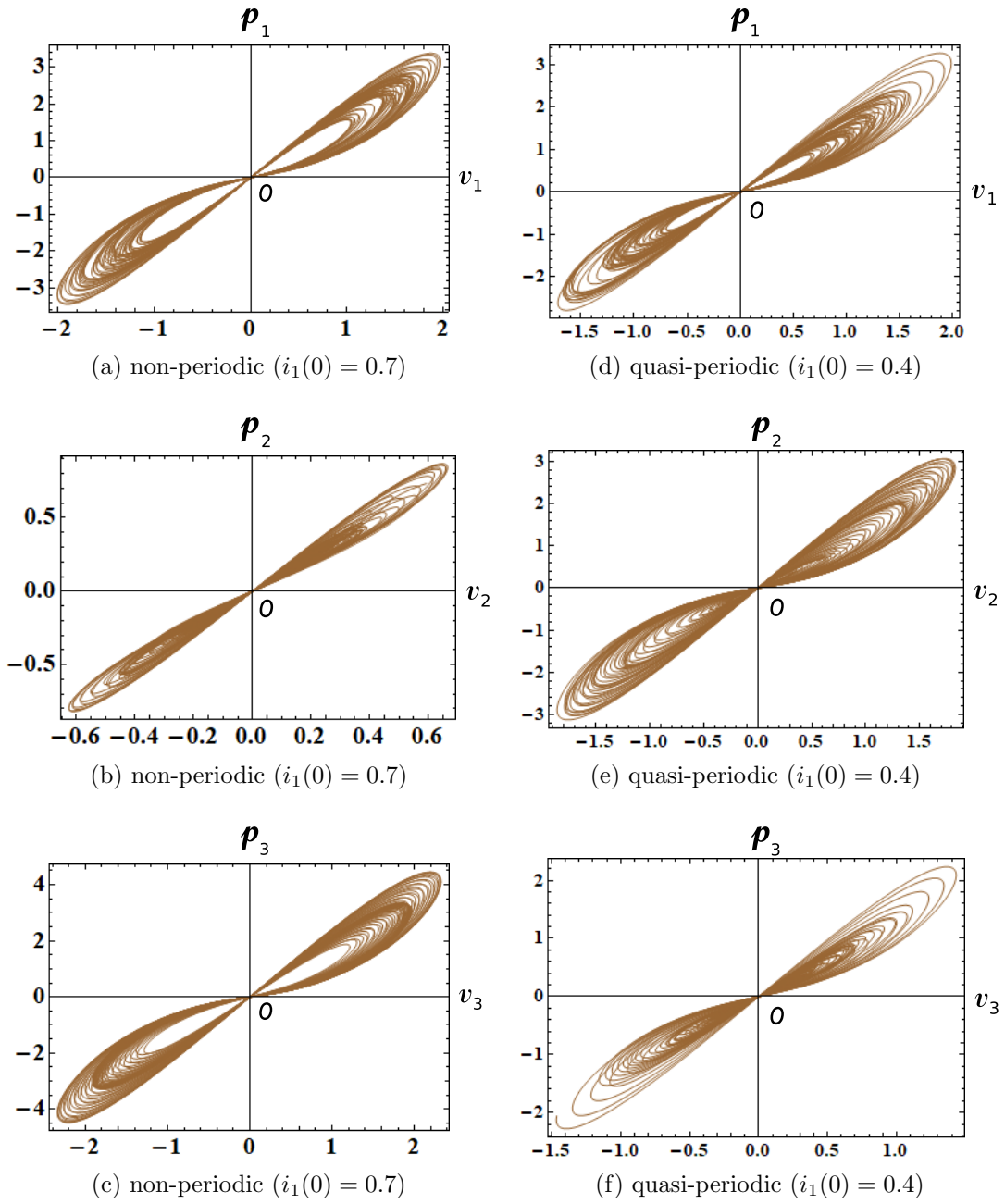

(a) non-periodic ($i_1(0) = 0.7$)

(d) quasi-periodic ($i_1(0) = 0.4$)

(b) non-periodic ($i_1(0) = 0.7$)

(e) quasi-periodic ($i_1(0) = 0.4$)

(c) non-periodic ($i_1(0) = 0.7$)

(f) quasi-periodic ($i_1(0) = 0.4$)

Figure 50: The $v_j - p_j$ loci of the forced memristor Toda lattice equations B, which are defined by Eq. (101). Here, $p_j(t)$ is an instantaneous power defined by $p_j(t) = i_j(t)v_j(t)$, and $v_j(t)$ and $i_j(t)$ denote the terminal voltage and the terminal current of the j-th generic memristor, respectively ($j = 1, 2, 3$). Observe that the $v_j - p_j$ locus is pinched at the origin, and the locus lies in the first and the third quadrants. The memristor switches between passive and active modes of operation, depending on its terminal voltage $v_j(t)$. Parameters: $r = 0.25$, $\omega = 0.925$. Initial conditions: (a)-(c) $i_1(0) = 0.7$, $x_1(0) = 1.2$, $i_2(0) = 1.3$, $x_2(0) = 1.4$, $i_3(0) = 1.5$, $x_3(0) = 1.6$. (d)-(f) $i_1(0) = 0.4$, $x_1(0) = 1.2$, $i_2(0) = 1.3$, $x_2(0) = 1.4$, $i_3(0) = 1.5$, $x_3(0) = 1.6$.

3.1.2 Toda lattice equations C

Consider Eq.(89) and define new variables

$$\begin{aligned} a_n &= \frac{1}{2}e^{-(q_{n+1}-q_n)/2}, \\ b_n &= \frac{1}{2}p_n, \end{aligned} \tag{103}$$

where $n = 1,\ 2, \cdots,\ N$. Then Eq.(89) can be recast into the form [20, 24]

Toda lattice equations C

$$\begin{aligned} \frac{da_n}{dt} &= (b_n - b_{n+1})a_n, \\ \frac{db_n}{dt} &= 2({a_{n-1}}^2 - {a_n}^2), \end{aligned} \tag{104}$$

where $n = 1,\ 2, \cdots,\ N$ and we consider the case of a periodic lattice of the length N: $a_n = a_{n+N}$, $b_n = b_{n+N}$.

Consider the $2N$-element memristor circuit in Figure 45. The dynamics of this circuit given by Eq. (87). Assume that Eq. (87) satisfies

$$\begin{aligned} L_n &= 1, \\ \hat{R}(\boldsymbol{x},\ i_n) &= -(x_n - x_{n+1}) \\ \tilde{f}_n(\boldsymbol{x}, \boldsymbol{i}) &= 2({i_{n-1}}^2 - {i_n}^2). \end{aligned} \tag{105}$$

Then we obtain

Memristor Toda lattice equations C

$$\begin{aligned} \frac{di_n}{dt} &= (x_n - x_{n+1})i_n, \\ \frac{dx_n}{dt} &= 2({i_{n-1}}^2 - {i_n}^2), \end{aligned} \tag{106}$$

where $n = 1,\ 2, \cdots,\ N$ and we consider the case of a periodic lattice of the length N: $i_n = i_{n+N}$, $x_n = x_{n+N}$.

Equations (104) and (106) are equivalent if we change the variables

$$i_n = a_n,\ x_n = b_n. \tag{107}$$

In this case, the extended memristors in Figure 45 are replaced by the *generic* memristors, that is,

$$\hat{R}(\boldsymbol{x},\ i_n) = \tilde{R}_n(\boldsymbol{x}) = -(x_n - x_{n+1}), \tag{108}$$

though the current i of Eq. (240) is modified into the vector form $\boldsymbol{i} = (i_1,\ i_2,\ \cdots,\ i_n)$. Thus, their terminal voltage v_n and the terminal current i_n of the current-controlled memristor are described by

V-I characteristics of the generic memristors

$$\begin{aligned} v_n &= \tilde{R}_n(\boldsymbol{x}) = \tilde{R}_n(x_n,\, x_{n+1})\; i_n \\ &= -(x_n - x_{n+1}) i_n, \\ \frac{dx_n}{dt} &= \tilde{f}_n(\boldsymbol{x}, \boldsymbol{i}) = \tilde{f}(i_{n-1},\, i_n) \\ &= 2({i_{n-1}}^2 - {i_n}^2), \end{aligned} \tag{109}$$

where $i_n = i_{n+N}$, $x_n = x_{n+N}$, and $n = 1,\ 2, \cdots,\ N$.

It follows that Eq. (104) can be realized by the $2N$-element memristor circuit in Figure 45.

For $n = 3$, Eq. (104) is given by

Toda lattice equations C with N = 3

$$\left.\begin{aligned} \frac{da_1}{dt} &= (b_1 - b_2)a_1, \\ \frac{db_1}{dt} &= 2({a_3}^2 - {a_1}^2), \\ \frac{da_2}{dt} &= (b_2 - b_3)a_2, \\ \frac{db_2}{dt} &= 2({a_1}^2 - {a_2}^2), \\ \frac{da_3}{dt} &= (b_3 - b_1)a_3, \\ \frac{db_3}{dt} &= 2({a_2}^2 - {a_3}^2), \end{aligned}\right\} \tag{110}$$

Equation (110) has the three integrals [21, 20], since the solution satisfies

Integrals

$$\begin{aligned} &\frac{d}{dt}\big(b_1 + b_2 + b_3\big) = 0, \\ &\frac{d}{dt}\Big\{{b_1}^2 + {b_2}^2 + {b_3}^2 + 2\,({a_1}^2 + {a_2}^2 + {a_3}^2)\Big\} = 0, \\ &\frac{d}{dt}\Big(b_1 b_2 b_3 - b_1 {a_2}^2 - b_2 {a_3}^2 - b_3 {a_1}^2 + 2a_1 a_2 a_3\Big) = 0, \end{aligned} \tag{111}$$

where $2a_1 a_2 a_3 = \dfrac{1}{4}$.

The corresponding memristor circuit equations for Eq. (110) are given by

Memristor Toda lattice equations C with N = 3

$$\left.\begin{aligned}
\frac{di_1}{dt} &= (x_1 - x_2)i_1, \\
\frac{dx_1}{dt} &= 2({i_3}^2 - {i_1}^2), \\
\frac{di_2}{dt} &= (x_2 - x_3)i_2, \\
\frac{dx_2}{dt} &= 2({i_1}^2 - {i_2}^2), \\
\frac{di_3}{dt} &= (x_3 - x_1)i_3, \\
\frac{dx_3}{dt} &= 2({i_2}^2 - {i_3}^2).
\end{aligned}\right\} \tag{112}$$

The terminal voltage v_n and the terminal current i_n of the three generic memristors are described by

V-I characteristics of the 3 generic memristors

$$\left.\begin{aligned}
v_1 &= \tilde{R}_1(x_1, x_2)\ i_1 = -(x_1 - x_2)i_1, \\
\frac{dx_1}{dt} &= \tilde{f}_1(i_3, i_1) = 2({i_3}^2 - {i_1}^2),
\end{aligned}\right\}$$

$$\left.\begin{aligned}
v_2 &= \tilde{R}_2(x_2, x_3)\ i_2 = -(x_2 - x_3)i_2, \\
\frac{dx_1}{dt} &= \tilde{f}_2(i_1, i_2) = 2({i_1}^2 - {i_2}^2),
\end{aligned}\right\}$$

$$\left.\begin{aligned}
v_3 &= \tilde{R}_3(x_3, x_1)\ i_3 = -(x_3 - x_1)i_3, \\
\frac{dx_1}{dt} &= \tilde{f}_3(i_2, i_3) = 2({i_2}^2 - {i_3}^2).
\end{aligned}\right\} \tag{113}$$

where $x_4 = x_1$, $i_0 = i_3$.

Equations (112) can exhibit periodic behavior. If an external source is added as shown in Figure 46, then the forced memristor circuit can exhibit non-periodic response. The dynamics of this circuit is given by

Forced memristor Toda lattice equations C with N = 3

$$\left.\begin{aligned}
\frac{di_1}{dt} &= (x_1 - x_2)i_1 + r\sin(\omega t),\\
\frac{dx_1}{dt} &= 2({i_3}^2 - {i_1}^2),\\
\frac{di_2}{dt} &= (x_2 - x_3)i_2,\\
\frac{dx_2}{dt} &= 2({i_1}^2 - {i_2}^2),\\
\frac{di_3}{dt} &= (x_3 - x_1)i_3,\\
\frac{dx_3}{dt} &= 2({i_2}^2 - {i_3}^2),
\end{aligned}\right\} \qquad (114)$$

where r and ω are constants.

We show their non-periodic and quasi-periodic responses, Poincaré maps, and $i_j - v_j$ loci in Figures 51, 52, and 53, respectively ($j = 1, 2, 3$). In order to obtain these figures, we have to choose the parameters and the initial conditions carefully, and the maximum step size h of the numerical integration must be sufficiently small ($h = 0.006$). The following parameters are used in our computer simulations:

$$r = 0.12,\ \omega = 1. \qquad (115)$$

3.1.3 Complexity order

Consider the case where Eq. (114) exhibits the quasi-periodic response. Then, the $i_j - v_j$ loci lie in the first and the fourth quadrants as shown in Figure 53(d)-(f). We show next the $v_j - p_j$ locus in Figure 54(d)-(f), where $p_j(t)$ is an instantaneous power defined by $p_j(t) = i_j(t)v_j(t)$ ($j = 1, 2, 3$). Observe that the $v_j - p_j$ loci are pinched at the origin, and the loci lie in the first and the third quadrants. Thus, when $v_j > 0$, the instantaneous power $p_j(t)$ delivered from the forced signal and the inductor is dissipated in the memristor. However, when $v_j < 0$, the instantaneous power $p_j(t)$ is *not* dissipated in the memristor. Hence, the memristors switch between passive and active modes of operation, depending on its terminal voltage. They switches between two modes of operation:

$$(v_j,\, p_j) = (+,\, +),\ (-,\, -),\quad (j = 1,\, 2,\, 3). \qquad (116)$$

Here, $(v_j,\, p_j) = (+,\, +)$ is read as $v_1 > 0$ and $p_1 > 0$, $(v_j,\, p_j) = (-,\, -)$ is read as $v_1 < 0$ and $p_1 < 0$, and we excluded the special case where $(v_1,\, p_1) = (0,\, 0)$. Thus, we conclude as follow:

Switching behavior of the memristor

Assume that Eq. (114) exhibits the *quasi-periodic* response. Then the generic memristors defined by Eq. (113) can switch between "passive" and "active" modes of operation, depending on its terminal voltage.

In the case of *non-periodic* response, the above property does not hold as shown in Figure 53(a) and Figure 54(a). The generic memristor connected across the periodic source exhibits more complicated behavior. It switches between four modes of operation:

$$(v_1,\, p_1) = (+,\, +),\ (+,\, -),\ (-,\, +),\ (-,\, -). \qquad (117)$$

Here, v_1 and p_1 denote the terminal voltage and the instantaneous power of the generic memristor connected across the periodic source. That is, $p_1(t)$ is defined by $p_1(t) = i_1(t)v_1(t)$, and $(v_1,\, p_1) = (+,\, -)$ is read as $v_1 > 0$ and $p_1 < 0$. Here, we exclude the special case where $(v_1,\, p_1) = (0,\, 0)$. Note that the other two memristors switch between passive and active modes of operation, depending on its terminal voltage, as shown in Figures Figure 53(b)-(c) and Figure 54(b)-(c). That is, they switch between two modes of operation:

$$(v_1,\, p_1) = (+,\, +),\ (-,\, -), \tag{118}$$

and

$$(v_2,\, p_2) = (+,\, +),\ (-,\, -). \tag{119}$$

Thus, the memristor's operation modes (117) can be coded by two bits:

$$(0,\, 0),\ (0,\, 1),\ (1,\, 0),\ (1,\, 1), \tag{120}$$

where $+$ is coded to a binary number 0 and $-$ to 1. The operation modes (116), (118), and (119) are coded by one bit:

$$(0),\ (1), \tag{121}$$

which are equivalent to $(0,\, 0),\ (1,\, 1)$, respectively. Hence, we can measure the *complexity order* of the memristor's operation modes, by using the above binary coding. Thus, the memristor's operation have the higher complexity when Eq. (114) exhibits *non-periodic* response. We conclude as follow:

Switching behavior of the memristor

1. Assume that Eq. (114) exhibits *non-periodic* response. Then the generic memristor defined by Eq. (113) switches randomly between four modes of operation, that is,

   $$(v_1,\, p_1) = (+,\, +),\ (+,\, -),\ (-,\, +),\ (-,\, -).$$

   They can be coded by two bits:

   $$(0,\, 0),\ (0,\, 1),\ (1,\, 0),\ (1,\, 1),$$

   where $+$ is coded to a binary number 0 and $-$ to 1.

2. Assume that Eq. (114) exhibits *quasi-periodic* response. Then the generic memristor defined by Eq. (113) switches randomly between two modes of operation, that is,

   $$(v_1,\, p_1) = (+,\, +), (-,\, -).$$

   They can be coded by

   $$(0,\, 0),\ (1,\, 1),$$

   respectively, which are equivalent to the one-bit coding $(0),\ (1)$.

Note that if the forced memristor circuits have different kinds of elements, for example, capacitors, then more complicated modes may appear.

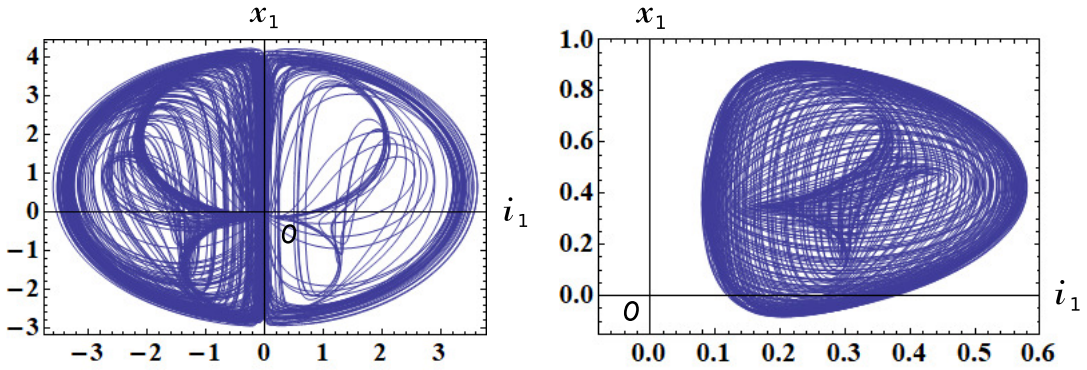

(a) non-periodic ($r = 0.12,\ \omega = 1$) (d) quasi-periodic ($r = 0.001,\ \omega = 1$)

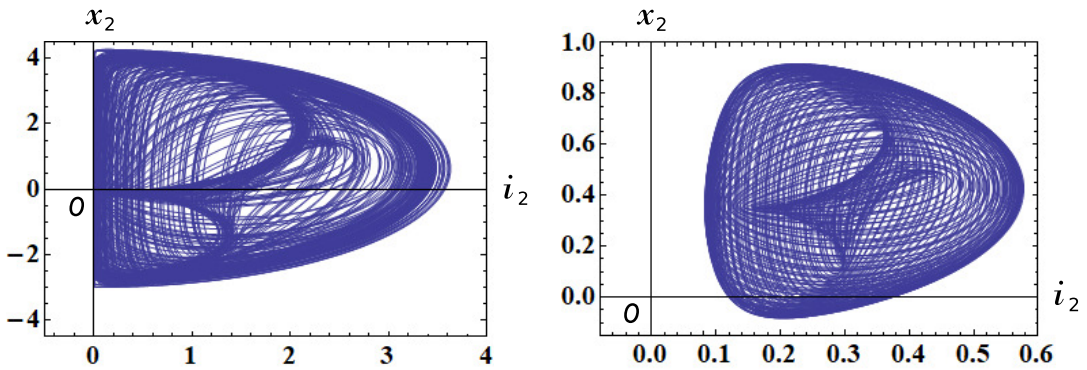

(b) non-periodic ($r = 0.12,\ \omega = 1$) (e) quasi-periodic ($r = 0.001,\ \omega = 1$)

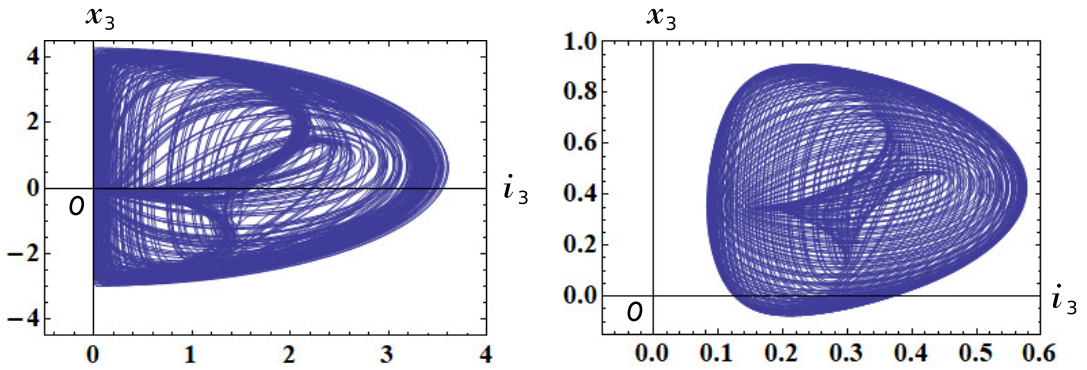

(c) non-periodic ($r = 0.12,\ \omega = 1$) (f) quasi-periodic ($r = 0.001,\ \omega = 1$)

Figure 51: Non-periodic and quasi-periodic responses of the forced memristor Toda lattice equations C, which are defined by Eq. (114). Here, i_j and x_j denote the terminal current and the internal state of the j-th generic memristor, respectively ($j = 1, 2, 3$). Parameters: (a)-(c) $r = 0.12$, $\omega = 1$. (b)-(c) $r = 0.001$, $\omega = 1$. Initial conditions: $i_1(0) = 0.1$, $x_1(0) = 0.2$, $i_2(0) = 0.3$, $x_2(0) = 0.4$, $i_3(0) = 0.5$, $x_3(0) = 0.6$.

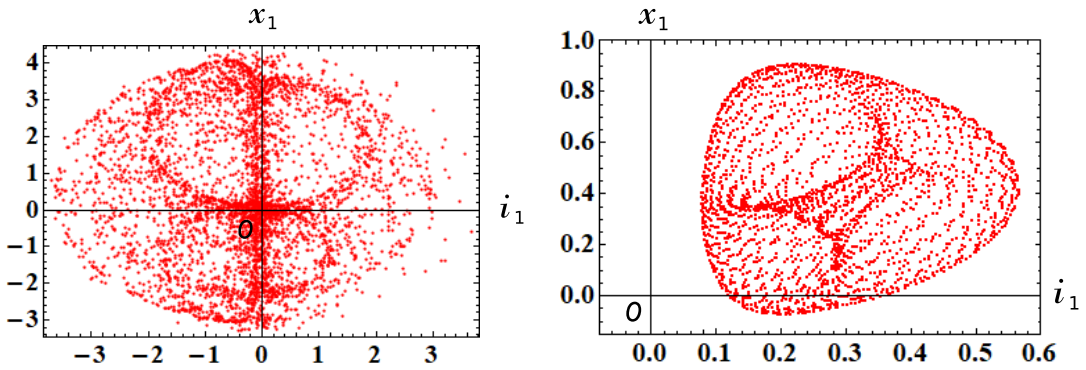

(a) non-periodic ($r = 0.12,\ \omega = 1$)

(d) quasi-periodic ($r = 0.001,\ \omega = 1$)

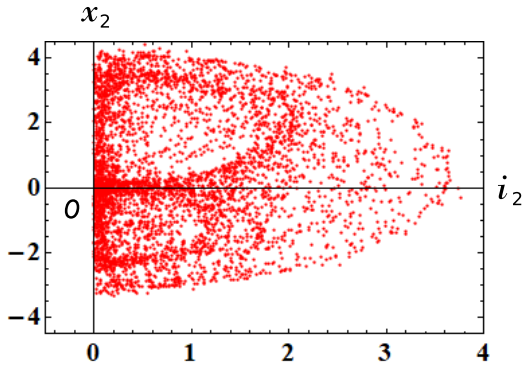

(b) non-periodic ($r = 0.12,\ \omega = 1$)

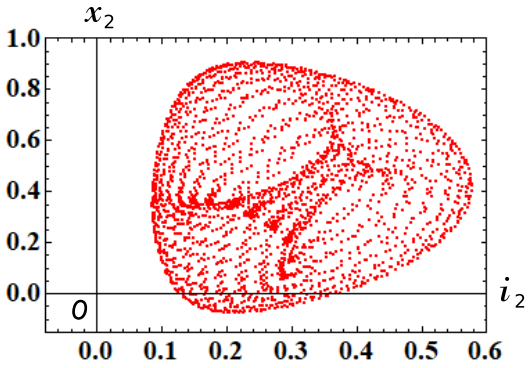

(e) quasi-periodic ($r = 0.001,\ \omega = 1$)

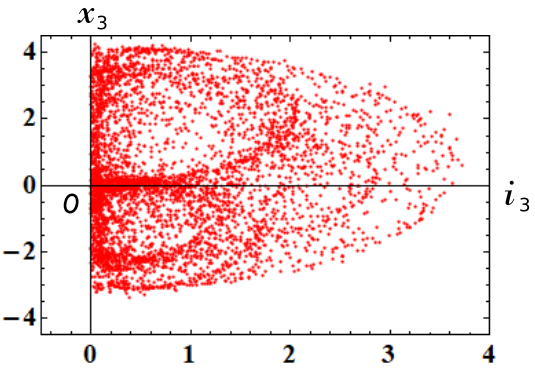

(c) non-periodic ($r = 0.12,\ \omega = 1$)

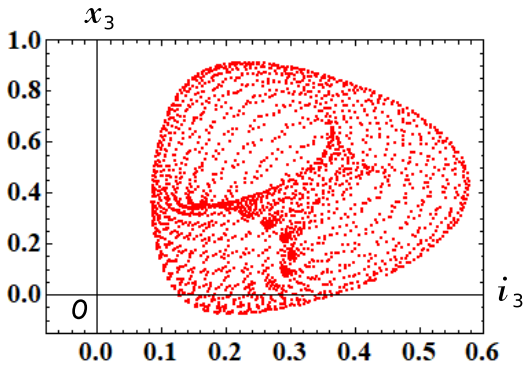

(f) quasi-periodic ($r = 0.001,\ \omega = 1$)

Figure 52: Poincaré maps of the forced memristor Toda lattice equations C, which are defined by Eq. (114). Here, i_j and x_j denote the terminal current and the internal state of the j-th generic memristor, respectively ($j = 1, 2, 3$). Parameters: (a)-(c) $r = 0.12,\ \omega = 1$. (b)-(c) $r = 0.001,\ \omega = 1$. Initial conditions: $i_1(0) = 0.1$, $x_1(0) = 0.2$, $i_2(0) = 0.3$, $x_2(0) = 0.4$, $i_3(0) = 0.5$, $x_3(0) = 0.6$.

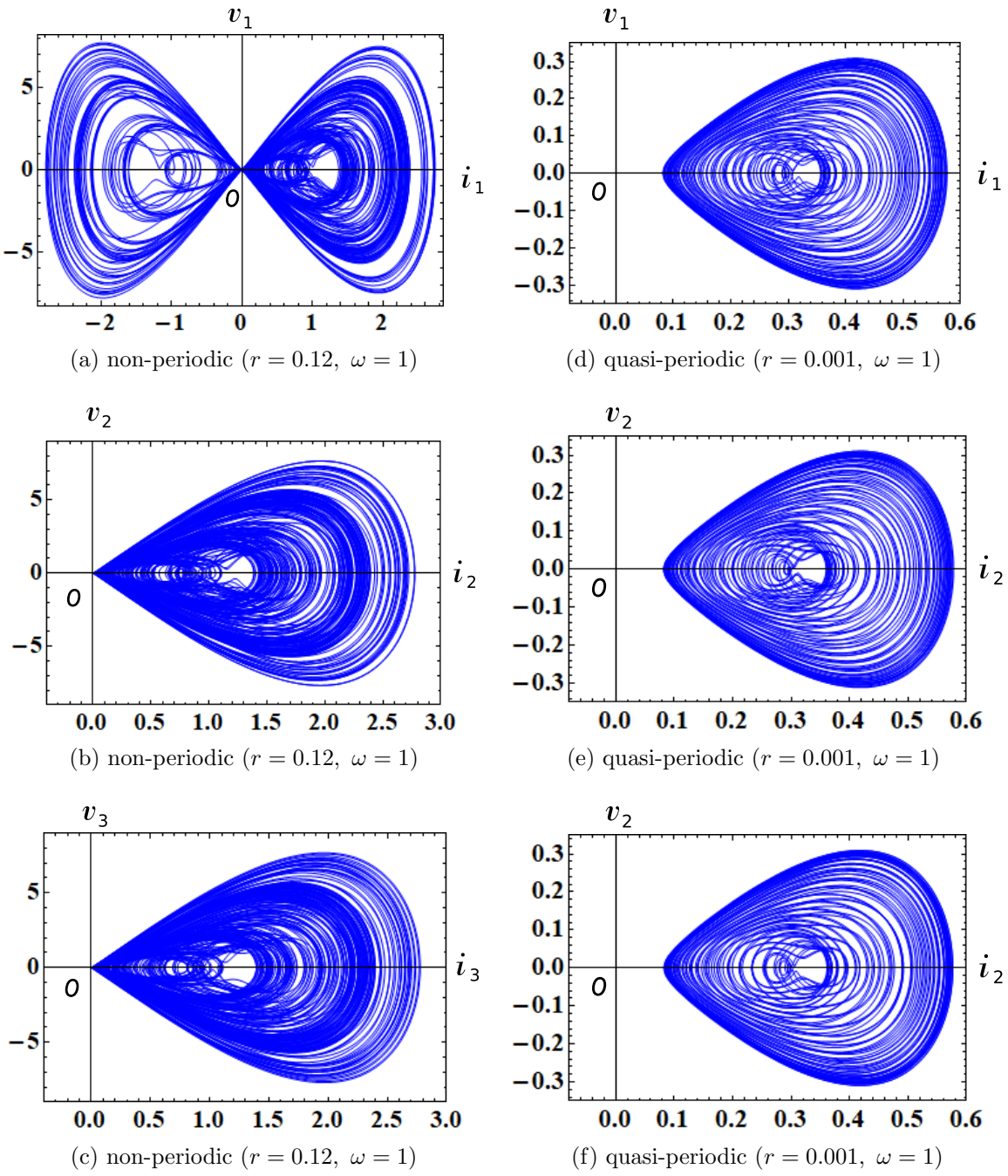

(a) non-periodic ($r = 0.12,\ \omega = 1$)

(d) quasi-periodic ($r = 0.001,\ \omega = 1$)

(b) non-periodic ($r = 0.12,\ \omega = 1$)

(e) quasi-periodic ($r = 0.001,\ \omega = 1$)

(c) non-periodic ($r = 0.12,\ \omega = 1$)

(f) quasi-periodic ($r = 0.001,\ \omega = 1$)

Figure 53: The $i_j - v_j$ loci of the forced memristor Toda lattice equations C, which are defined by Eq. (114). Here, i_j and v_j denote the terminal current and the voltage of the j-th generic memristor, respectively ($j = 1, 2, 3$). Parameters: (a)-(c) $r = 0.12,\ \omega = 1$. (d)-(f) $r = 0.001,\ \omega = 1$. Initial conditions: $i_1(0) = 0.1$, $x_1(0) = 0.2$, $i_2(0) = 0.3$, $x_2(0) = 0.4$, $i_3(0) = 0.5$, $x_3(0) = 0.6$.

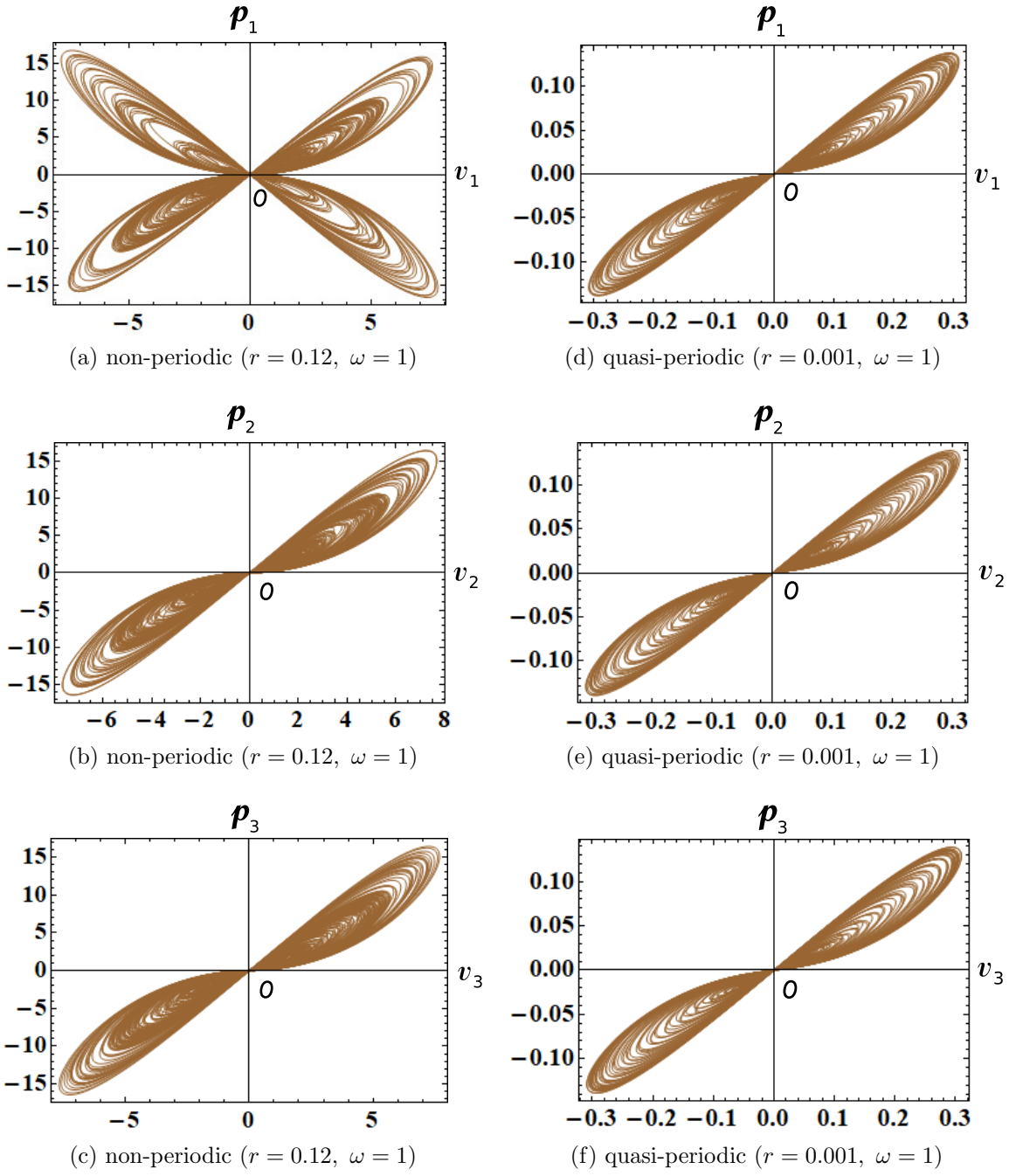

(a) non-periodic ($r = 0.12,\ \omega = 1$)

(d) quasi-periodic ($r = 0.001,\ \omega = 1$)

(b) non-periodic ($r = 0.12,\ \omega = 1$)

(e) quasi-periodic ($r = 0.001,\ \omega = 1$)

(c) non-periodic ($r = 0.12,\ \omega = 1$)

(f) quasi-periodic ($r = 0.001,\ \omega = 1$)

Figure 54: The $v_j - p_j$ loci of the forced memristor Toda lattice equations C, which are defined by Eq. (114). Here, $p_j(t)$ is an instantaneous power defined by $p_j(t) = i_j(t)v_j(t)$, and $v_j(t)$ and $i_j(t)$ denote the terminal voltage and the terminal current of the j-th generic memristor, respectively ($j = 1, 2, 3$). Observe that the loci except for Figure 54(a) are pinched at the origin, and their loci lie in the first and the third quadrants. These memristors switch between passive and active modes of operation, depending on its terminal voltage $v_j(t)$. However, the $v_1 - p_1$ locus in Figure 54(a) does not satisfy this behavior. Parameters: (a)-(c) $r = 0.12,\ \omega = 1$. (d)-(f) $r = 0.001,\ \omega = 1$. Initial conditions: $i_1(0) = 0.1$, $x_1(0) = 0.2$, $i_2(0) = 0.3$, $x_2(0) = 0.4$, $i_3(0) = 0.5$, $x_3(0) = 0.6$.

3.2 N-dimensional Lotka-Volterra equations

Consider the Hamiltonian defined by [25]

$$\mathcal{H} = -\sum_{j=1}^{N} e^{\left(P_j + \frac{1}{2}\sum_{k=1}^{N} a_{jk}\, Q_k \right)}, \tag{122}$$

where a_{jk} is skew-symmetric ($a_{jk} = -a_{kj}$). Let us define the Hamiltonian form

$$\begin{aligned} \frac{dQ_i}{dt} &= -\frac{\partial \mathcal{H}}{\partial P_i}, \\ \frac{dP_i}{dt} &= \frac{\partial \mathcal{H}}{\partial Q_i}. \end{aligned} \tag{123}$$

Remark the reversed sign of the Hamiltonian form of Eq. (123) [25].

From Eq. (48), we obtain

$$\begin{aligned} \frac{dQ_i}{dt} &= -\frac{\partial \mathcal{H}}{\partial P_i} = e^{\left(P_i + \frac{1}{2}\sum_{k=1}^{N} a_{ik}\, Q_k \right)}, \\ \frac{dP_i}{dt} &= \frac{\partial \mathcal{H}}{\partial Q_i} = -\sum_{j=1}^{N} \frac{a_{ji}}{2}\, e^{\left(P_j + \frac{1}{2}\sum_{k=1}^{N} a_{jk}\, Q_k \right)}. \end{aligned} \tag{124}$$

It can be recast into the form [25]

$$\ddot{Q}_i = \sum_{k=1}^{N} a_{ik}\, \dot{Q}_i \dot{Q}_k, \tag{125}$$

where $\dot{Q}_i = \frac{dQ_i}{dt}$ and $\ddot{Q}_i = \frac{d^2 Q_i}{dt^2}$. If we set $X_i = \dot{Q}_i$, we obtain

$$\frac{dX_i}{dt} = \sum_{k=1}^{N} a_{ik} X_i X_k. \tag{126}$$

As a special case of Eq. (126), we can define the following N-dimensional Lotka-Volterra equations [20].

The dynamics of the N-dimensional Lotka-Volterra equations is given by

N-dimensional Lotka-Volterra equations

$$\frac{dX_n}{dt} = (X_{n-1} - X_{n+1}) X_n, \tag{127}$$

where $n = 1,\ 2, \cdots,\ N$ and we consider the case of a periodic lattice of the length N: $X_n = X_{n+N}$.

For example, if $n = 3$, Eq. (127) is written as

3-*dimensional Lotka-Volterra equations*

$$\left.\begin{aligned} \frac{dX_1}{dt} &= (X_3 - X_2)X_1, \\ \frac{dX_2}{dt} &= (X_1 - X_3)X_2, \\ \frac{dX_3}{dt} &= (X_2 - X_1)X_3. \end{aligned}\right\} \tag{128}$$

Equation (128) has the two integrals [26], since the solution satisfies

Integrals

$$\begin{aligned} &\frac{d}{dt}\big(X_1 + X_2 + X_3\big) = 0, \\ &\frac{d}{dt}\big(X_1 X_2 X_3\big) = 0. \end{aligned} \tag{129}$$

3.2.1 Three-element memristor circuit realization

Consider first the three-element memristor circuit in Figure 1. The dynamics of this circuit given by Eq. (2). Assume that Eq. (2) satisfies

$$\left.\begin{aligned} E = 0, \qquad & L = 1, \\ \hat{R}(x_1,\, x_2,\, i) \quad &= -(x_2 - x_1), \\ \tilde{f}_1(x_1,\, x_2,\, i) \quad &= (i - x_2)x_1, \\ \tilde{f}_2(x_1,\, x_2,\, i) \quad &= (x_1 - i)x_2. \end{aligned}\right\} \tag{130}$$

Then, we obtain the following 3-dimensional memristor Lotka-Volterra equations

3-*dimensional memristor Lotka-Volterra equations*

$$\left.\begin{aligned} \frac{di}{dt} &= (x_2 - x_1)i, \\ \frac{dx_1}{dt} &= (i - x_2)x_1, \\ \frac{dx_2}{dt} &= (x_1 - i)x_2. \end{aligned}\right\} \tag{131}$$

Equations (128) and (131) are equivalent if we change the variables

$$X_1 = i,\ X_2 = x_1,\ X_3 = x_2. \tag{132}$$

In this case, the extended memristor in Figure 1 is replaced by the *generic* memristor (see Appendix A). Thus,

$$\hat{R}(x_1,\, x_2,\, i) = \tilde{R}(x_1,\, x_2) = -(x_2 - x_1). \tag{133}$$

The terminal voltage v_M and the terminal current i_M of the current-controlled generic memristor are given by

V-I characteristics of the generic memristor

$$\begin{aligned} v_M &= \tilde{R}(x_1, x_2)\, i_M = -(x_2 - x_1)\, i_M, \\ \frac{dx_1}{dt} &= (i_M - x_2)x_1, \\ \frac{dx_2}{dt} &= (x_1 - i_M)x_2, \end{aligned} \tag{134}$$

where $\tilde{R}(x_1, x_2) = -(x_2 - x_1)$.

It follows that the 3-dimensional memristor Lotka-Volterra equations (131) can be realized by the three-element memristor circuit in Figure 1. This circuit can exhibit periodic behavior. If an external source is added as shown in Figure 2, then the forced memristor circuit can exhibit a non-periodic response. The dynamics of this circuit is given by

Forced 3-dimensional memristor Lotka-Volterra equations

$$\left.\begin{aligned} \frac{di}{dt} &= (x_2 - x_1)i + r\sin(\omega t), \\ \frac{dx_1}{dt} &= (i - x_2)x_1, \\ \frac{dx_2}{dt} &= (x_1 - i)x_2, \end{aligned}\right\} \tag{135}$$

where r and ω are constants.

The solution of Eq. (135) satisfies

$$i(t) + x_1(t) + x_2(t) + \frac{r}{\omega}\cos(\omega t) = K, \tag{136}$$

where K is a constant. Thus, by eliminating x_2 from Eq. (135), we obtain the second-order non-autonomous differential equations:

$$\left.\begin{aligned} \frac{di}{dt} &= \left\{-\frac{r}{\omega}\cos(\omega t) + K - i - 2x_1\right\}i + r\sin(\omega t), \\ \frac{dx_1}{dt} &= \left\{2i + \frac{r}{\omega}\cos(\omega t) - K + x_1)\right\}x_1. \end{aligned}\right\} \tag{137}$$

Equations (135) and (137) can exhibit non-periodic behavior. We show the non-periodic and quasi-periodic responses, Poincaré maps, and $i_M - v_M$ loci of Eq. (135) in Figures 55, 56, and 57, respectively. The $i_M - v_M$ loci in Figure 57 lie in the first and the fourth quadrants. Thus, the generic memristor defined by Eq. (134) is an active element. We show the $v_M - p_M$ locus in Figure 58, where $p_M(t)$ is an instantaneous power defined by $p_M(t) = i_M(t)v_M(t)$. Observe that the $v_M - p_M$ locus is pinched at the origin, and the locus lies in the first and the third quadrants. Thus, the memristor switches between passive and active modes of operation, depending on its terminal voltage. We conclude as follow:

Switching behavior of the memristor

Assume that Eq. (135) exhibits non-periodic or quasi-periodic oscillation. Then the generic memristor defined by Eq. (134) can switch between "passive" and "active" modes of operation, depending on its terminal voltage.

The following parameters are used in our computer simulations:

$$r = 0.5,\ \omega = 1.1. \tag{138}$$

We also show Poincaré maps of Eq. (137) in Figure 59. Compare the Poincaré maps in Figure 56(a) and Figure 59(a). The rightmost part in these figures is not identical, since the small differences due to rounding errors in numerical computation result in differences in a later state.

In order to view the Poincaré maps in Figure 56 from a different perspective, let us project the trajectory into the $(\xi,\ \eta,\ \zeta)$-space via the transformation

$$\begin{aligned} \xi(\tau) &= (i(\tau)+5)\cos(\omega\tau), \\ \eta(\tau) &= (i(\tau)+5)\sin(\omega\tau), \\ \zeta(\tau) &= x_1(\tau). \end{aligned} \tag{139}$$

Then the trajectory on the $(i,\ x)$-plane is transformed into the trajectory in the three-dimensional $(\xi,\ \eta,\ \zeta)$-space, as shown in Figure 60. Observe that the trajectory in Figure 60(b) is less dense than Figure 60(a).

Note that in order to generate a non-periodic response, we have to choose the initial conditions and the maximum step size h carefully. In our computer simulations, we choose $h = 0.002$. It is important for numerical stability, otherwise an overflow (outside the range of data) is likely to occur. That is, the numerical instability in long-time simulations is likely to occur. We show its example in Figure 61. Suppose that Eq. (137) has the following parameters and initial conditions:

$$\begin{aligned} &\text{Parameters: } r = 0.5,\ \ \omega = 1.1, \\ &\text{Initial conditions: } i(0) = 1.12,\ x_1(0) = 1.21. \end{aligned} \tag{140}$$

If we choose $h = 0.005$, then $i(t)$ rapidly decreases for $t \geq 6848$, and an overflow (outside the range of data) occurs as shown in Figure 61(a). However, if we choose $h = 0.002$, then the trajectory stays in the first-quadrant of the $(i,\ x_1)$-plane as shown in Figure 61(b). The maximum step size of the numerical integration greatly affects the behavior of Eq. (137). Thus, noise may considerably affect the behavior in the physical memristor circuits.

Similarly, the 4-dimensional Lotka-Volterra equations are given by

4-dimensional Lotka-Volterra equations

$$\left.\begin{aligned} \frac{dX_1}{dt} &= (X_4 - X_2)X_1, \\ \frac{dX_2}{dt} &= (X_1 - X_3)X_2, \\ \frac{dX_3}{dt} &= (X_2 - X_4)X_3, \\ \frac{dX_4}{dt} &= (X_3 - X_1)X_4. \end{aligned}\right\} \tag{141}$$

Equation (141) can be realized by the circuit in Figure 1. The dynamics of this circuit is given by

4-dimensional memristor Lotka-Volterra equations

$$\left.\begin{aligned} \frac{di}{dt} &= (x_3 - x_1)i, \\ \frac{dx_1}{dt} &= (i - x_2)x_1, \\ \frac{dx_2}{dt} &= (x_1 - x_3)x_2, \\ \frac{dx_3}{dt} &= (x_2 - i)x_3. \end{aligned}\right\} \tag{142}$$

The terminal voltage v_M and the terminal current i_M of the generic memristor are given by

V-I characteristics of the generic memristor

$$\begin{aligned} v_M &= \tilde{R}(x_1,\, x_3)\, i_M = -(x_3 - x_1)\, i_M, \\ \frac{dx_1}{dt} &= (i_M - x_2)x_1, \\ \frac{dx_2}{dt} &= (x_1 - x_3)x_2, \\ \frac{dx_3}{dt} &= (x_3 - i_M)x_3, \end{aligned} \tag{143}$$

where $\tilde{R}(x_1,\, x_3) = -(x_3 - x_1)$.

The memristor circuit equations (142) exhibit periodic behavior. If an external source is added as shown in Figure 2, then the forced memristor Lotka-Volterra equations can exhibit a non-periodic response. The dynamics of this circuit is given by

Forced 4-dimensional memristor Lotka-Volterra equations

$$\left.\begin{aligned} \frac{di}{dt} &= (x_3 - x_1)i + r\sin(\omega t), \\ \frac{dx_1}{dt} &= (i - x_2)x_1, \\ \frac{dx_2}{dt} &= (x_1 - x_3)x_2, \\ \frac{dx_3}{dt} &= (x_2 - i)x_3, \end{aligned}\right\} \tag{144}$$

where r and ω are constants.

The solution of Eq. (144) satisfies

$$i(t) + x_1(t) + x_2(t) + x_3(t) + \frac{r}{\omega}\cos(\omega t) = K, \tag{145}$$

where K is a constant. Thus, by eliminating x_3 from Eq. (144), Eq. (144) can be recast into the third-order

non-autonomous differential equations

$$\left.\begin{aligned}\frac{di}{dt} &= \Big\{K - i - 2x_1 - x_2 - \frac{r}{\omega}\cos(\omega t)\Big\} i \\ &\quad + r\sin(\omega t), \\ \frac{dx_1}{dt} &= (i - x_2)x_1, \\ \frac{dx_2}{dt} &= \Big\{2x_1 - K + i + x_2 + \frac{r}{\omega}\cos(\omega t))\Big\} x_2.\end{aligned}\right\} \tag{146}$$

We show the non-periodic response, quasi-periodic response, Poincaré maps, and $i_M - v_M$ loci of Eq. (144) in Figures 62, 63, 64, and 66, respectively. The $i_M - v_M$ loci in Figure 66 lie in the first and the fourth quadrants. Thus, the extended memristor defined by Eq. (143) is an active element. We show next the $v_M - p_M$ locus in Figure 67, where $p_M(t)$ is an instantaneous power defined by $p_M(t) = i_M(t)v_M(t)$. Observe that the $v_M - p_M$ locus is pinched at the origin, and the locus lies in the first and the third quadrants. Thus, the memristor switches between passive and active modes of operation, depending on its terminal voltage. We conclude as follow:

Switching behavior of the memristor

Assume that Eq. (144) exhibits non-periodic or quasi-periodic oscillation. Then the generic memristor defined by Eq. (143) can switch between "passive" and "active" modes of operation, depending on its terminal voltage.

We also show Poincaré maps of Eq. (146) in Figure 65. In order to view the Poincaré maps from a different perspective, let us project the trajectory of Eq. (144) into the (ξ, η, ζ)-space via the transformation

$$\begin{aligned}\xi(\tau) &= (i(\tau) + 5)\cos(\omega\tau), \\ \eta(\tau) &= (i(\tau) + 5)\sin(\omega\tau), \\ \zeta(\tau) &= x_1(\tau).\end{aligned} \tag{147}$$

Observe that the trajectory in Figure 68(a) is less dense than Figure 68(b). The following parameters are used in our computer simulations:

$$r = 0.1,\ \omega = 2. \tag{148}$$

Note that in order to generate a non-periodic response in Figure 68(a), we have to choose the initial conditions and the maximum step size h, carefully. In our computer simulations, we choose $h = 0.0015$. Furthermore, an overflow (outside the range of data) is likely to occur due to the numerical instability in long-time simulations. We show its example in Figure 69. Suppose that Eq. (144) has the following parameters and initial conditions:

$$\begin{aligned}&\text{Parameters:} && r = 0.107,\ \ \omega = 2, \\ &\text{Initial conditions:} && i(0) = 0.608,\ x_1(0) = 1.2, \\ & && x_2(0) = 1.3,\ x_3(0) = 1.3.\end{aligned} \tag{149}$$

If we choose $h = 0.0015$, then the trajectory rapidly grows for $t \geq 1443$, and an overflow (outside the range of data) occurs as shown in Figure 69(a). However, if we choose $h = 0.001$, then the trajectory stays in a finite region of the (r_1, r_2)-plane as shown in Figure 69(b). The maximum step size of the numerical integration greatly affects the behavior of Eq. (144). Therefore, noise may considerably affect the behavior of the physical memristor circuits.

3.2.2 $2N$-element memristor circuit realization

In order to realize Eq. (127) by the $2N$-element memristor circuit in Figure 45, let us group with odd or even indexes in Eq. (127) separately, namely,

$2N$-dimensional Lotka-Volterra equations

$$\begin{aligned} \frac{dX_{2n-1}}{dt} &= (X_{2n-2} - X_{2n})X_{2n-1}, \\ \frac{dX_{2n}}{dt} &= (X_{2n-1} - X_{2n+1})X_{2n}, \end{aligned} \tag{150}$$

where $n = 1,\ 2, \cdots,\ N$.

We assume a periodic lattice of the length $2N$: $X_n = X_{n+2N}$, that is,

$$X_{2N+1} = X_1,\ X_{2N+2} = X_2. \tag{151}$$

Consider next the $2N$-element memristor circuit in Figure 45. The dynamics of this circuit, which is given by Eq. (87). Assume that Eq. (87) satisfies

$$\begin{aligned} L_n &= 1, \\ \hat{R}(\boldsymbol{x},\ i_n) &= \tilde{R}_n(\boldsymbol{x}) = \tilde{R}_n(x_{n-1},\, x_n) = -(x_n - x_{n+1}) \\ \tilde{f}_n(\boldsymbol{x}, \boldsymbol{i}) &= \tilde{f}_n(x_n,\, i_n,\, i_{n+1}) = (i_n - i_{n+1})x_n. \end{aligned} \tag{152}$$

Then we obtain

$2N$-dimensional memristor Lotka-Volterra equations

$$\begin{aligned} \frac{di_n}{dt} &= (x_{n-1} - x_n)i_n, \\ \frac{dx_n}{dt} &= (i_n - i_{n+1})x_n, \end{aligned} \tag{153}$$

Equations (150) and (153) are equivalent if we change the variables

$$i_n = X_{2n-1},\ x_n = X_{2n}. \tag{154}$$

In this case, the extended memristors in Figure 45 are replaced by the *generic* memristors, though the current i of Eq. (240) is modified into the vector form $\boldsymbol{i} = (i_1,\, i_2,\, \cdots,\, i_n)$. Their terminal voltage v_n and the terminal current i_n of the current-controlled generic memristor are described by

V-I characteristics of the generic memristors

$$\begin{aligned} v_n &= \tilde{R}_n(x_{n-1},\, x_n)\, i_n = -(x_{n-1} - x_n)i_n, \\ \frac{dx_n}{dt} &= \tilde{f}_n(x_n,\, i_n,\, i_{n+1}) = (i_n - i_{n+1})x_n. \end{aligned} \tag{155}$$

For $N = 2$, Eq. (153) can be written as

4-dimensional memristor Lotka-Volterra equations

$$\left.\begin{aligned} \frac{di_1}{dt} &= (x_2 - x_1)\, i_1, \\ \frac{dx_1}{dt} &= (i_1 - i_2)\, x_1, \\ \frac{di_2}{dt} &= (x_1 - x_2)\, i_2, \\ \frac{dx_2}{dt} &= (i_2 - i_1)\, x_2. \end{aligned}\right\} \tag{156}$$

Here i_1 and i_2 denote the currents of two generic memristors. The terminal voltage v_n and the terminal current i_n of these memristors are given by

V-I characteristics of the 2 generic memristors

$$\left.\begin{aligned} v_1 &= \tilde{R}_1(x_1,\, x_2)\, i_1 = -(x_2 - x_1)\, i_1, \\ \frac{dx_1}{dt} &= \tilde{f}_1(x_1,\, i_1,\, i_2) = (i_1 - i_2)x_1 \end{aligned}\right\}$$

$$\left.\begin{aligned} v_2 &= \tilde{R}_2(x_1,\, x_2)\, i_2 = -(x_1 - x_2)\, i_2, \\ \frac{dx_2}{dt} &= \tilde{f}_2(x_2,\, i_1,\, i_2) = (i_2 - i_1)x_2. \end{aligned}\right\} \tag{157}$$

Since (141) is equivalent to Eq. (156), Eq. (141) can be realized by the 4-element memristor circuit in Figure 45.

3.3 Ecological predator-prey model

Consider the ecological predator-prey model [22] defined by

Ecological predator-prey model equations

$$\frac{dM_n}{dt} = (M_{n-1} - M_{n+1}){M_n}^2, \tag{158}$$

where $n = 1,\ 2, \cdots,\ N$ and we consider the case of a periodic lattice of the length N: $M_n = M_{n+N}$.

Assume that $n = 3$. Then Eq. (158) is written as

3-dimensional ecological predator-prey model equations

$$\left.\begin{aligned} \frac{dM_1}{dt} &= (M_3 - M_2){M_1}^2, \\ \frac{dM_2}{dt} &= (M_1 - M_3){M_2}^2, \\ \frac{dM_3}{dt} &= (M_2 - M_1){M_3}^2. \end{aligned}\right\} \tag{159}$$

Equation (159) has the two integrals, since the solution satisfies

Integrals

$$\left.\begin{aligned} &\frac{d}{dt}\big(M_1M_2M_3\big) = 0, \\ &\frac{d}{dt}\big(M_1M_2 + M_2M_3 + M_3M_1\big) = 0. \end{aligned}\right\} \tag{160}$$

Thus, Eq. (159) can not exhibit chaotic oscillation nor a quasi-periodic oscillation. Furthermore, it can be recast into Eq. (127) [22] if we set

$$L_n = M_{n+\frac{1}{2}}M_{n-\frac{1}{2}}. \tag{161}$$

Consider first the three-element memristor circuit in Figure 1. The dynamics of this circuit given by Eq. (2). Assume that Eq. (2) satisfies

$$\left.\begin{aligned} E = 0, \qquad & L = 1, \\ \hat{R}(x_1,\, x_2,\, i) &= -(x_2 - x_1)\, i, \\ \tilde{f}_1(x_1,\, x_2,\, i) &= (i - x_2){x_1}^2, \\ \tilde{f}_2(x_1,\, x_2,\, i) &= (x_1 - i){x_2}^2. \end{aligned}\right\} \tag{162}$$

Then we obtain

3-dimensional memristor ecological predator-prey model equations

$$\left.\begin{aligned} \frac{di}{dt} &= (x_2 - x_1)i^2, \\ \frac{dx_1}{dt} &= (i - x_2){x_1}^2, \\ \frac{dx_2}{dt} &= (x_1 - i){x_2}^2. \end{aligned}\right\} \tag{163}$$

Equations (159) and (163) are equivalent if we change the variables

$$M_1 = i,\ M_2 = x_1,\ M_3 = x_2. \tag{164}$$

In this case, the small-signal *memristance* of the extended memristor in Figure 1 is defined by

$$\hat{R}(\boldsymbol{x},\, i) = \hat{R}(x_1,\, x_2,\, i) = -(x_2 - x_1)\, i. \tag{165}$$

where $\boldsymbol{x} = (x_1,\, x_2)$. The terminal voltage v_M and the terminal current i_M of the extended memristor are described by

V-I characteristics of the extended memristor

$$\begin{aligned} v_M &= \hat{R}(x_1,\, x_2,\, i_M)\, i_M = -(x_2 - x_1)\, {i_M}^2, \\ \frac{dx_1}{dt} &= (i_M - x_2){x_1}^2, \\ \frac{dx_2}{dt} &= (x_1 - i_M){x_2}^2, \end{aligned} \tag{166}$$

where $\hat{R}(x_1,\, x_2\, i_M) = -(x_2 - x_1)\, i_M$ and $i_M = i$.

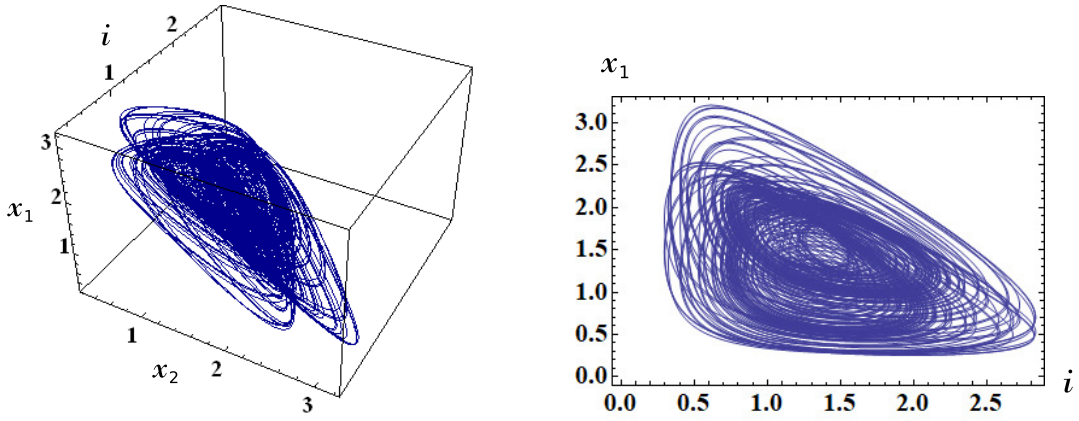

(a) non-periodic

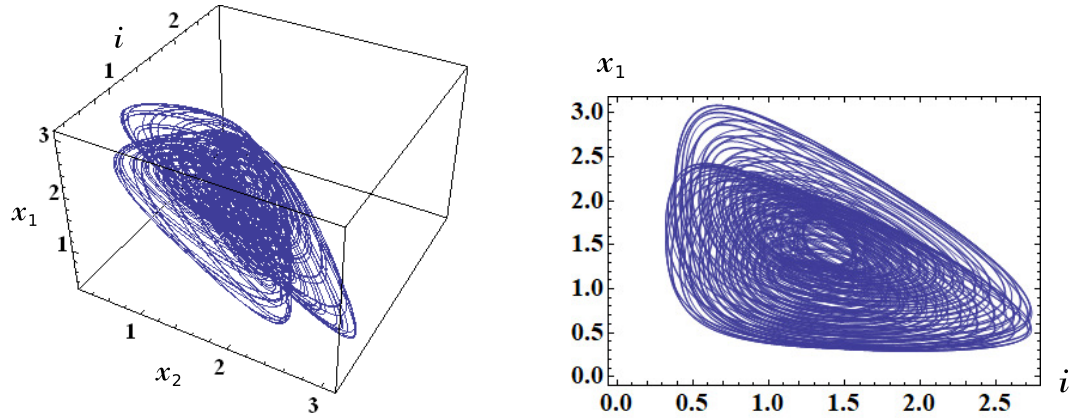

(b) quasi-periodic

Figure 55: Non-periodic and quasi-periodic responses of the forced 3-dimensional memristor Lotka-Volterra equations (135). Parameters: $r = 0.5$, $\omega = 1.1$. Initial conditions: (a) $i(0) = 1.121$, $x_1(0) = 1.2$, $x_2(0) = 1.3$. (b) $i(0) = 1.09$, $x_1(0) = 1.2$, $x_2(0) = 1.3$

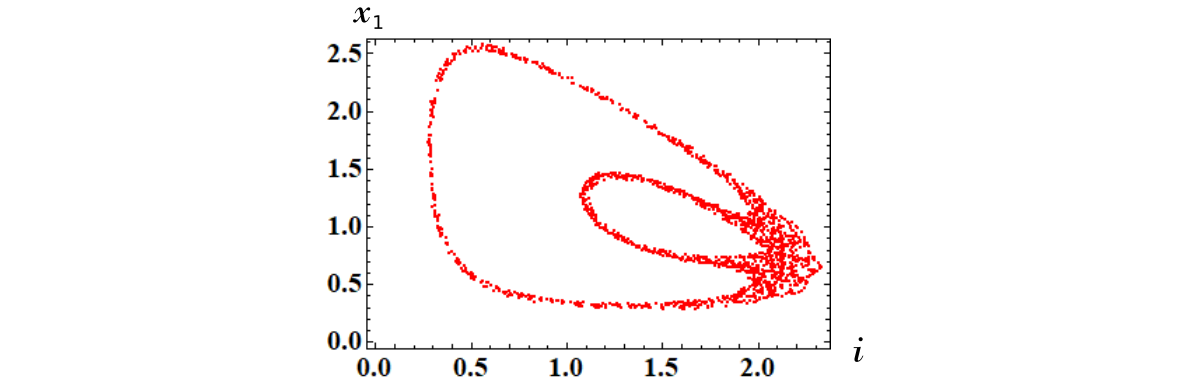

(a) non-periodic

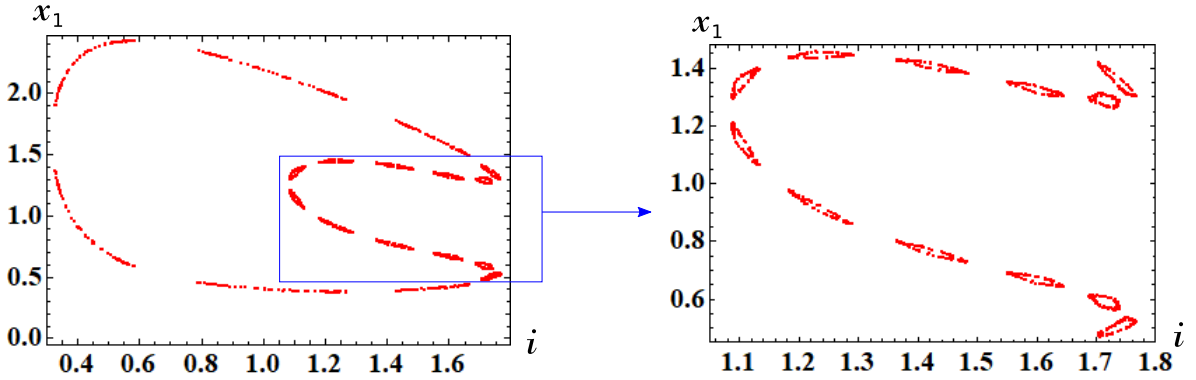

(b) quasi-periodic

Figure 56: Poincaré maps of the forced 3-dimensional memristor Lotka-Volterra equations (135). Observe the islands of tori in Figure 56(b). Parameters: $r = 0.5$, $\omega = 1.1$. Initial conditions: (a) $i(0) = 1.121$, $x_1(0) = 1.2$, $x_2(0) = 1.3$. (b) $i(0) = 1.09$, $x_1(0) = 1.2$, $x_2(0) = 1.3$.

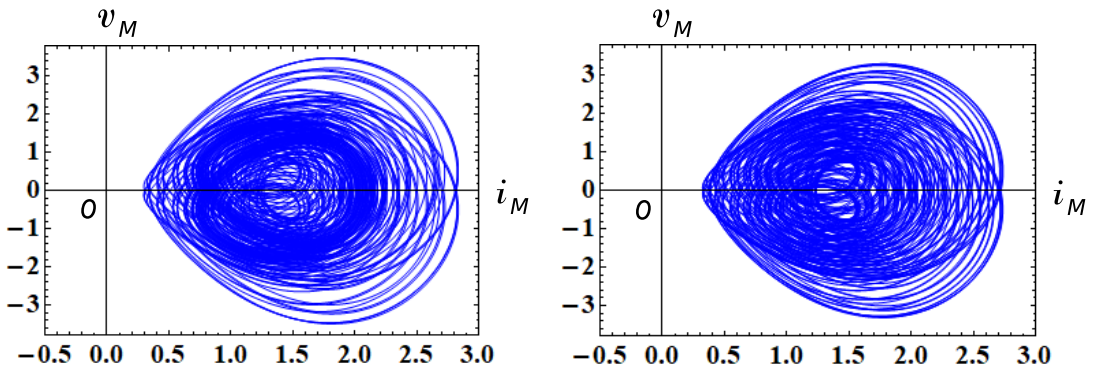

(a) non-periodic (b) quasi-periodic

Figure 57: The $i_M - v_M$ loci of the forced 3-dimensional memristor Lotka-Volterra equations (135). Here, v_M and i_M denote the terminal voltage and the terminal current of the current-controlled generic memristor. Parameters: $r = 0.5$, $\omega = 1.1$. Initial conditions: (a) $i(0) = 1.121$, $x_1(0) = 1.2$, $x_2(0) = 1.3$. (b) $i(0) = 1.09$, $x_1(0) = 1.2$, $x_2(0) = 1.3$.

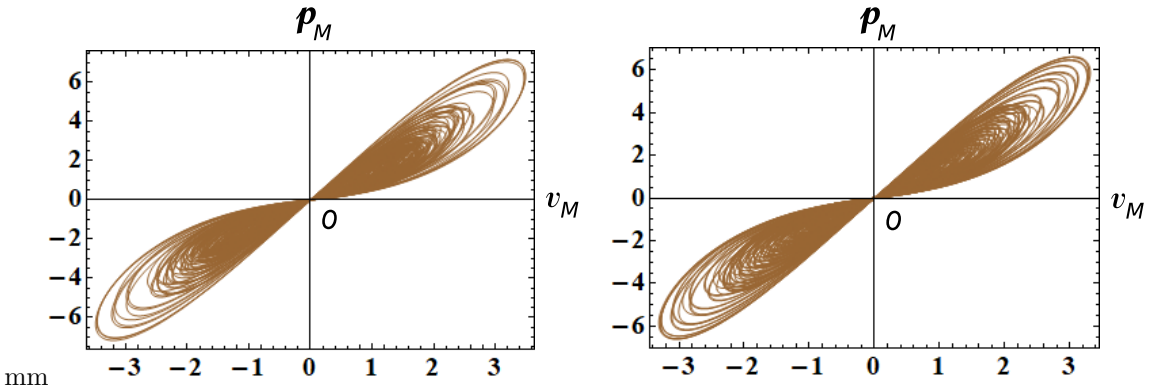

(a) non-periodic (b) quasi-periodic

Figure 58: The $v_M - p_M$ locus of the forced 3-dimensional memristor Lotka-Volterra equations (135). Here, $p_M(t)$ is an instantaneous power defined by $p_M(t) = i_M(t)v_M(t)$, and $v_M(t)$ and $i_M(t)$ denote the terminal voltage and the terminal current of the current-controlled generic memristor. Observe that the $v_M - p_M$ locus is pinched at the origin, and the locus lies in the first and the third quadrants. The memristor switches between passive and active modes of operation, depending on its terminal voltage $v_M(t)$. Parameters: $r = 0.5$, $\omega = 1.1$. Initial conditions: (a) $i(0) = 1.121$, $x_1(0) = 1.2$, $x_2(0) = 1.3$. (b) $i(0) = 1.09$, $x_1(0) = 1.2$, $x_2(0) = 1.3$.

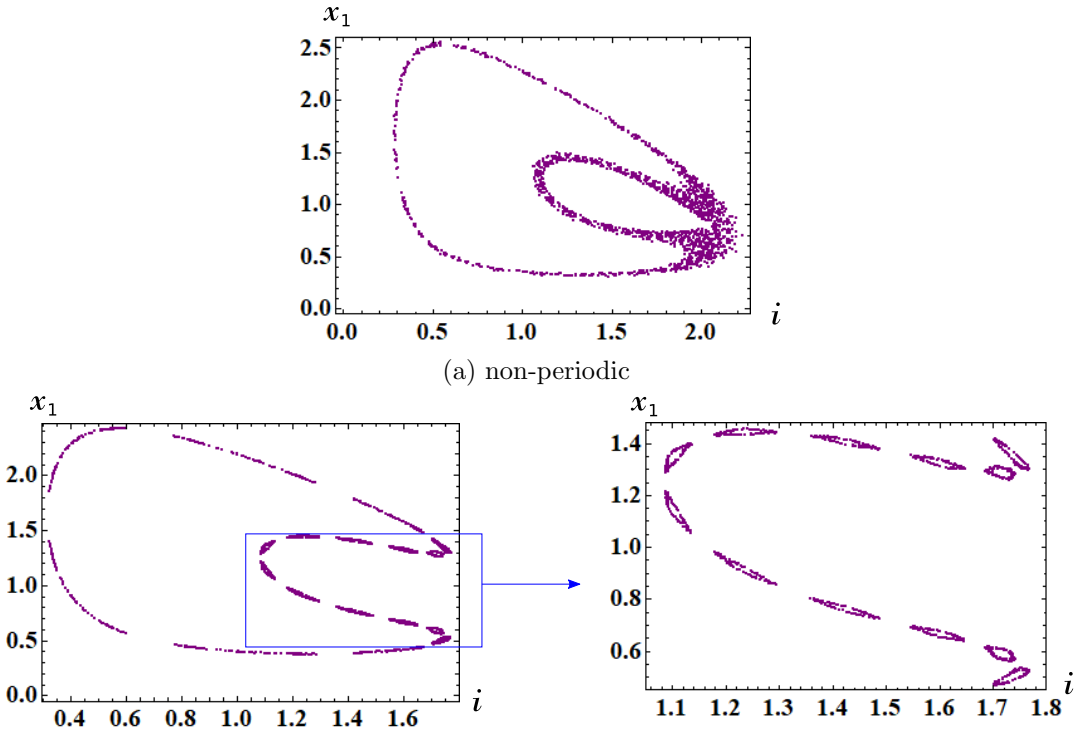

(a) non-periodic

(b) quasi-periodic

Figure 59: Poincaré maps of the non-autonomous equations (137). Observe the islands of tori in Figure 59(b). Parameters: $r = 0.5$, $\omega = 1.1$. Initial conditions: (a) $i(0) = 1.121$, $x_1(0) = 1.2$, $x_2(0) = 1.3$, $k = i(0)+x_1(0)+x_2(0)+r/\omega \approx 4.0756$. (b) $i(0) = 1.09$, $x_1(0) = 1.2$, $x_2(0) = 1.3$, $k = i(0)+x_1(0)+x_2(0)+r/\omega \approx 4.0446$.

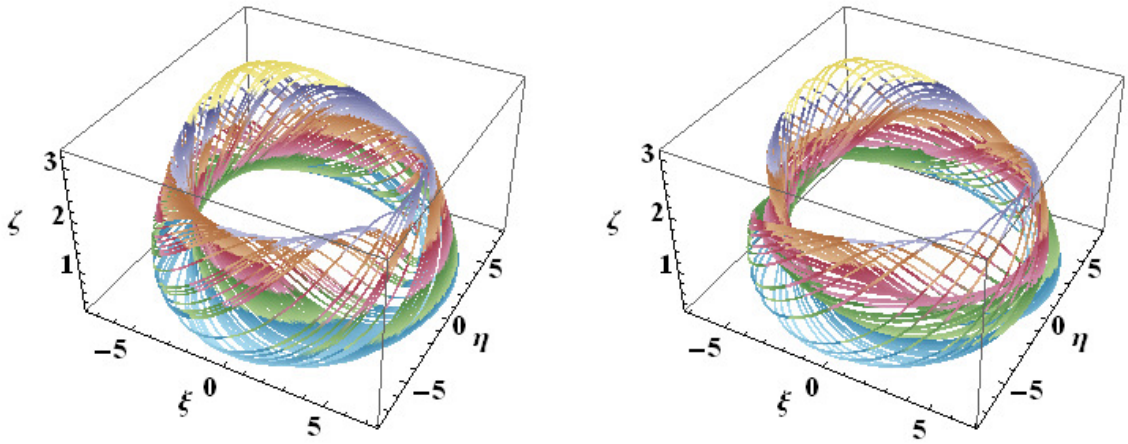

(a) non-periodic (b) quasi-periodic

Figure 60: The two trajectories of the forced 3-dimensional memristor Lotka-Volterra equations (135), which are projected into the (ξ, η, ζ)-space via the coordinate transformation (139). Observe that the trajectory in Figure 60(b) is less dense than that in Figure 60(a). The trajectories are colored with the *DarkBands* color code in Mathematica. Parameters: $r = 0.5$, $\omega = 1.1$. Initial conditions: (a) $i(0) = 1.121$, $x_1(0) = 1.2$, $x_2(0) = 1.3$. (b) $i(0) = 1.09$, $x_1(0) = 1.2$, $x_2(0) = 1.3$.

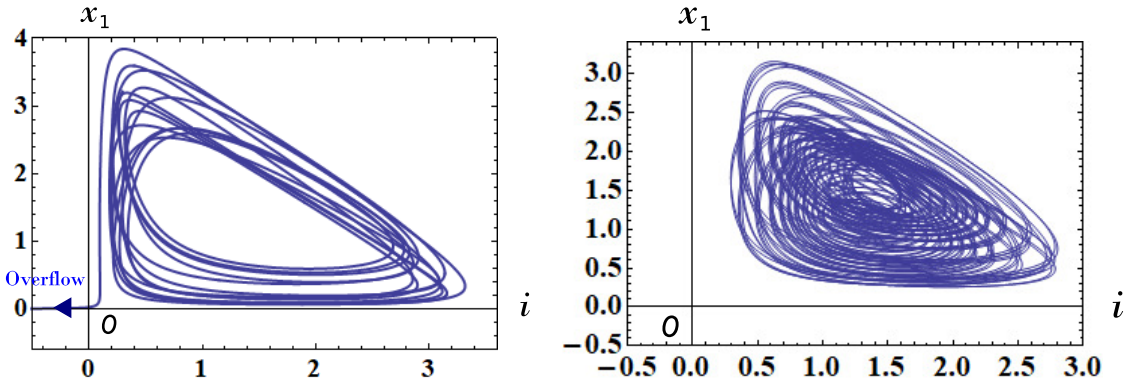

(a) $h = 0.005$ (b) $h = 0.002$

Figure 61: Behavior of the second-order non-autonomous differential equations (137). If we choose $h = 0.005$, then $i(t)$ rapidly decreases for $t \geq 6848$, and an overflow occurs as shown in Figure 69(a). However, if we choose $h = 0.002$, then the trajectory stays in the first-quadrant of the $(i,\ x_1)$-plane as shown in Figure 61(b). Here, h denotes the maximum step size of the numerical integration. Parameters: $r = 0.5$, $\omega = 1.1$. Initial conditions: $i(0) = 1.2$, $x_1(0) = 1.121$.

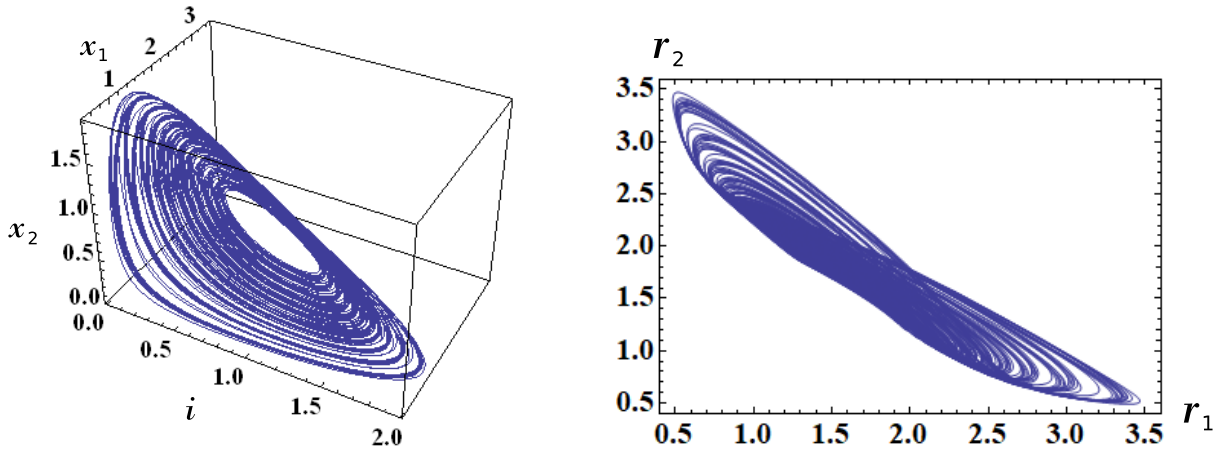

(a) $(i,\ x_1,\ x_2)$-space (b) $(r_1,\ r_2)$-plane

Figure 62: Non-periodic responses of the forced 4-dimensional memristor Lotka-Volterra equations (144), where $r_1 = \sqrt{i^2 + {x_1}^2}$ and $r_2 = \sqrt{{x_2}^2 + {x_3}^2}$ Parameters: $r = 0.1,\ \omega = 2$. Initial conditions: $i(0) = 0.6072$, $x_1(0) = 1.2$, $x_2(0) = 1.3$, $x_3(0) = 1.3$.

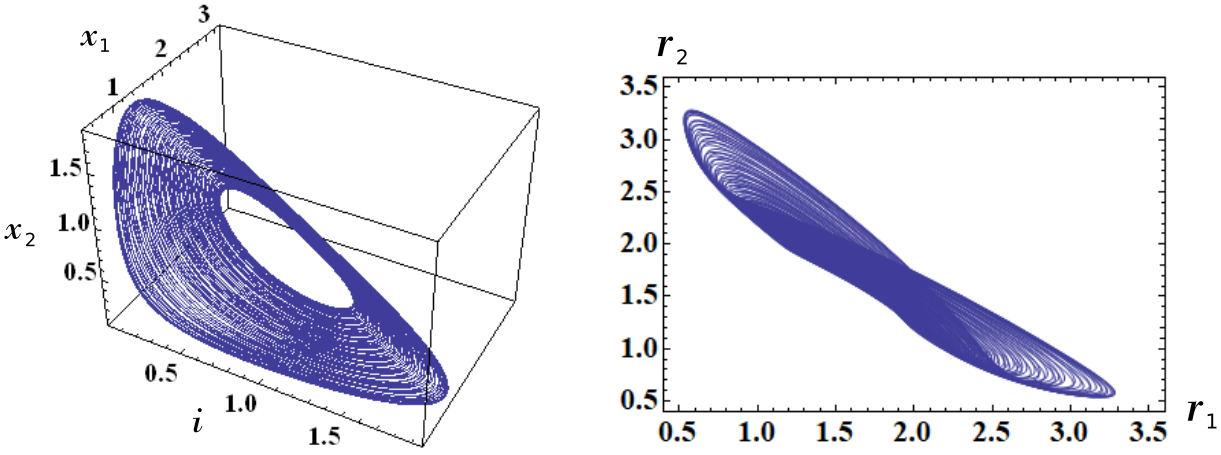

(a) $(i,\ x_1,\ x_2)$-space (b) $(r_1,\ r_2)$-plane

Figure 63: Quasi-periodic responses of the forced 4-dimensional memristor Lotka-Volterra equations (144), where $r_1 = \sqrt{i^2 + {x_1}^2}$ and $r_2 = \sqrt{{x_2}^2 + {x_3}^2}$ Parameters: $r = 0.1,\ \omega = 2$.
Initial conditions: $i(0) = 0.585$, $x_1(0) = 1.2$, $x_2(0) = 1.3$, $x_3(0) = 1.3$.

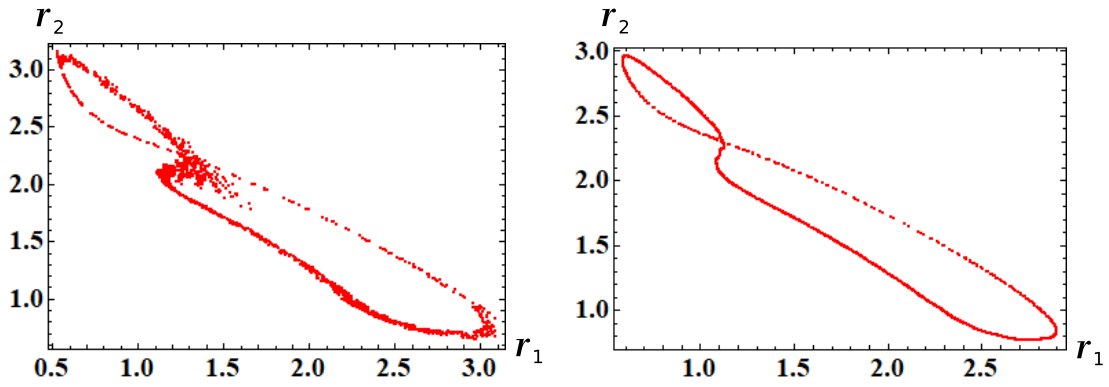

(a) non-periodic (b) quasi-periodic

Figure 64: Poincaré maps of the forced 4-dimensional memristor Lotka-Volterra equations (144), where $r_1 = \sqrt{i^2 + {x_1}^2}$ and $r_2 = \sqrt{{x_2}^2 + {x_3}^2}$. Parameters: $r = 0.1$, $\omega = 2$. Initial conditions: (a) $i(0) = 0.6072$, $x_1(0) = 1.2$, $x_2(0) = 1.3$, $x_3(0) = 1.3$. (b) $i(0) = 0.585$, $x_1(0) = 1.2$, $x_2(0) = 1.3$, $x_3(0) = 1.3$.

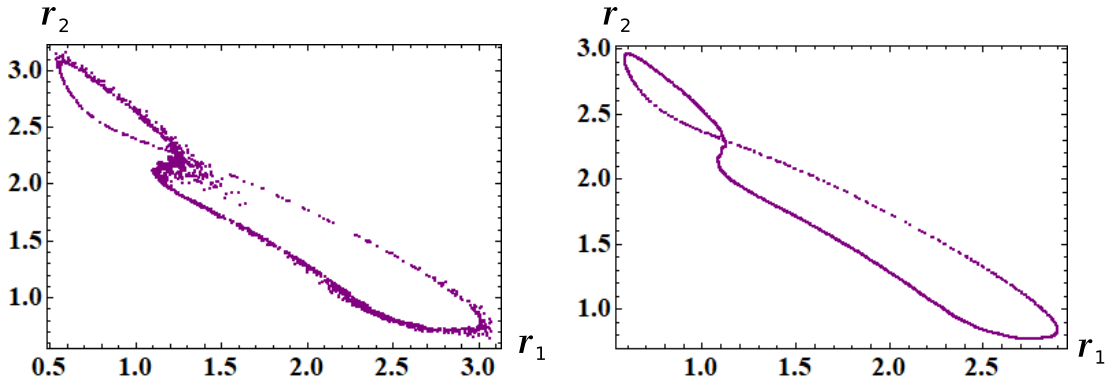

(a) non-periodic (b) quasi-periodic

Figure 65: Poincaré maps of the non-autonomous equations (146), where $r_1 = \sqrt{i^2 + {x_1}^2}$, $r_2 = \sqrt{{x_2}^2 + {x_3}^2}$, and $x_3 = K - i - x_1 - x_2(t) - \frac{r}{\omega}\cos(\omega t)$. Parameters: $r = 0.5$, $\omega = 2$. Initial conditions: (a) $i(0) = 0.6072$, $x_1(0) = 1.2$, $x_2(0) = 1.3$, $x_3(0) = 1.3$, $k = i(0) + x_1(0) + x_2(0) + x_3(0) + r/\omega \approx 4.0756$. (b) $i(0) = 0.585$, $x_1(0) = 1.2$, $x_2(0) = 1.3$, $x_3(0) = 1.3$, $k = i(0) + x_1(0) + x_2(0) + x_3(0) + r/\omega \approx 4.0446$.

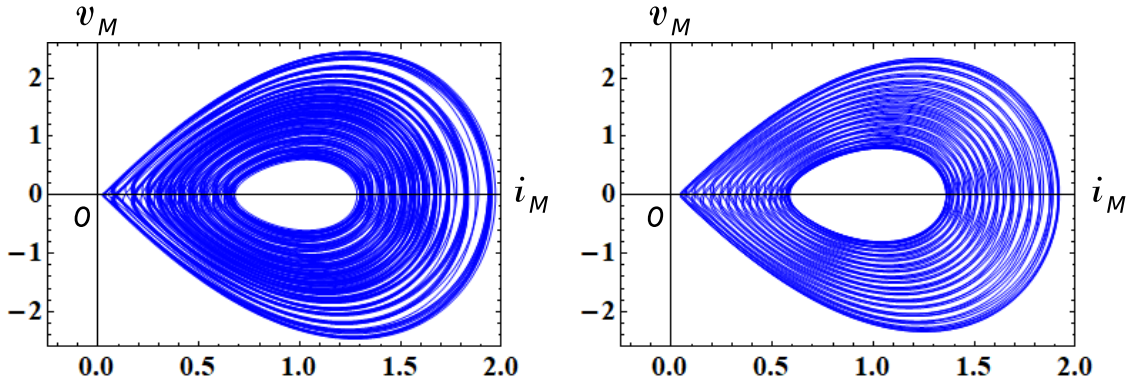

(a) non-periodic (b) quasi-periodic

Figure 66: The $i_M - v_M$ loci of the forced 4-dimensional memristor Lotka-Volterra equations (144). Here, v_M and i_M denote the terminal voltage and the terminal current of the current-controlled generic memristor. Parameters: $r = 0.1,\ \omega = 2$. Initial conditions: (a) $i(0) = 0.6072$, $x_1(0) = 1.2$, $x_2(0) = 1.3$, $x_3(0) = 1.3$. (b) $i(0) = 0.585$, $x_1(0) = 1.2$, $x_2(0) = 1.3$, $x_3(0) = 1.3$.

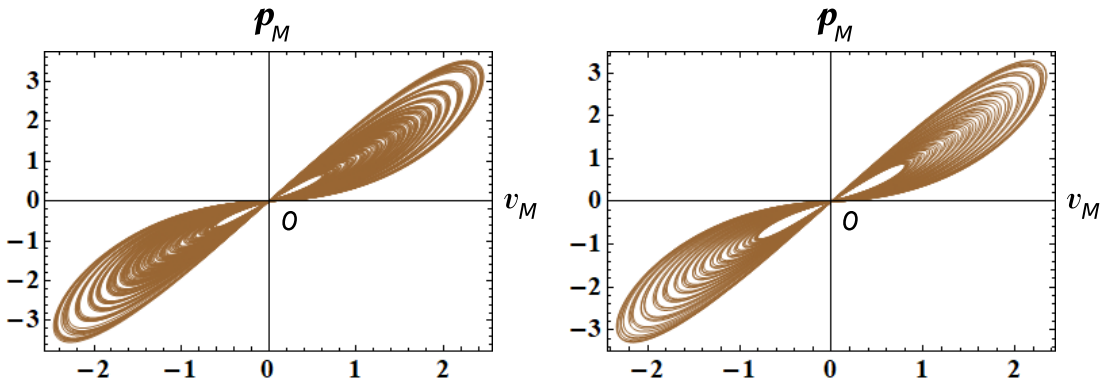

(a) non-periodic (b) quasi-periodic

Figure 67: The $v_M - p_M$ locus of the forced 4-dimensional memristor Lotka-Volterra equations (144). Here, $p_M(t)$ is an instantaneous power defined by $p_M(t) = i_M(t)v_M(t)$, and $v_M(t)$ and $i_M(t)$ denote the terminal voltage and the terminal current of the current-controlled generic memristor. Observe that the $v_M - p_M$ locus is pinched at the origin, and the locus lies in the first and the third quadrants. The memristor switches between passive and active modes of operation, depending on its terminal voltage $v_M(t)$. Parameters: $r = 0.1,\ \omega = 2$. Initial conditions: (a) $i(0) = 0.6072$, $x_1(0) = 1.2$, $x_2(0) = 1.3$, $x_3(0) = 1.3$. (b) $i(0) = 0.585$, $x_1(0) = 1.2$, $x_2(0) = 1.3$, $x_3(0) = 1.3$.

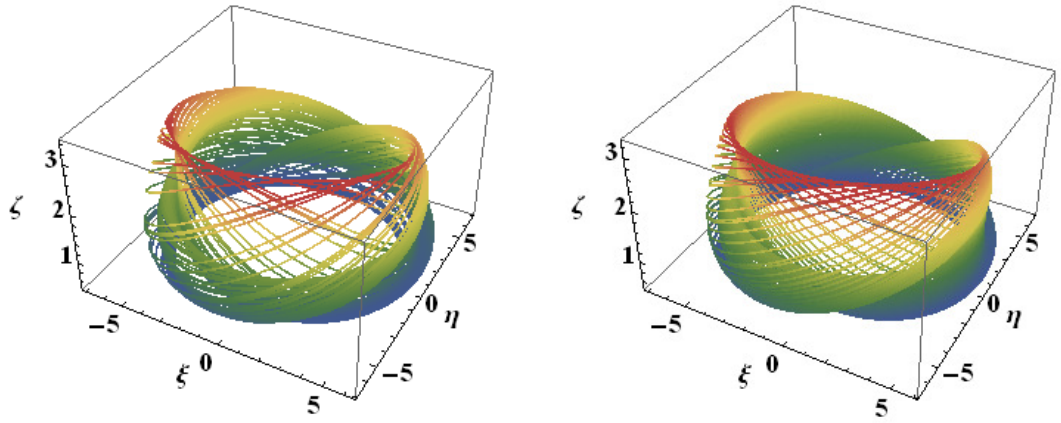

(a) non-periodic (b) quasi-periodic

Figure 68: The two trajectories of the forced 4-dimensional memristor Lotka-Volterra equations (144), which are projected into the (ξ, η, ζ)-space via the coordinate transformation (147). Observe that the trajectory in Figure 68(a) is less dense than Figure 68(b). The trajectories are colored with the *DarkRainbow* color code in Mathematica. Parameters: $r = 0.1$, $\omega = 2$. Initial conditions: (a) $i(0) = 0.6072$, $x_1(0) = 1.2$, $x_2(0) = 1.3$, $x_3(0) = 1.3$. (b) $i(0) = 0.585$, $x_1(0) = 1.2$, $x_2(0) = 1.3$, $x_3(0) = 1.3$.

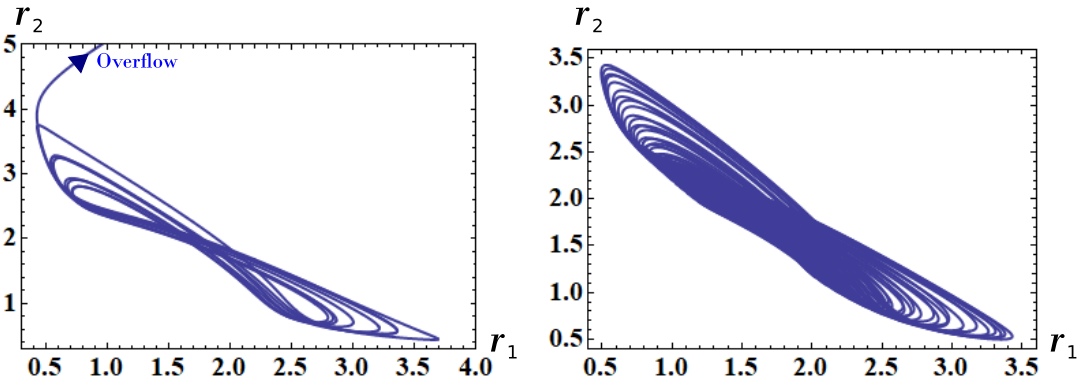

(a) $h = 0.002$ (b) $h = 0.001$

Figure 69: Behavior of the forced memristor Lotka-Volterra equations (144). If $h = 0.002$, then the trajectory rapidly grows for $t \geq 1443$, and an overflow occurs as shown in Figure 29(a). However, if $h = 0.001$, then the trajectory stays in a finite region of the (r_1, r_2)-plane as shown in Figure 29(b). Here, h denotes the maximum step size of the numerical integration, and $r_1 = \sqrt{i^2 + {x_1}^2}$, $r_2 = \sqrt{{x_2}^2 + {x_3}^2}$ Parameters: $r = 0.107$, $\omega = 2$. Initial conditions: $i(0) = 0.608$, $x_1(0) = 1.2$, $x_2(0) = 1.3$, $x_3(0) = 1.3$.

3.3.1 4-dimensional ecological predator-prey model

The 4-dimensional ecological predator-prey model is given by [22]

4-dimensional ecological predator-prey model equations

$$\left.\begin{aligned} \frac{dM_1}{dt} &= (M_4 - M_2){M_1}^2, \\ \frac{dM_2}{dt} &= (M_1 - M_3){M_2}^2, \\ \frac{dM_3}{dt} &= (M_2 - M_4){M_3}^2, \\ \frac{dM_4}{dt} &= (M_3 - M_1){M_4}^2. \end{aligned}\right\} \tag{167}$$

If we change the variables

$$M_1 = i_1,\ M_2 = x_1,\ M_3 = i_2,\ M_4 = x_2, \tag{168}$$

Eq. (167) can be recast into the form

4-dimensional memristor ecological predator-prey model equations

$$\left.\begin{aligned} \frac{di_1}{dt} &= (x_2 - x_1)\,{i_1}^2, \\ \frac{dx_1}{dt} &= (i_1 - i_2)\,{x_1}^2, \\ \frac{di_2}{dt} &= (x_1 - x_2)\,{i_2}^2, \\ \frac{dx_2}{dt} &= (i_2 - i_1)\,{x_2}^2. \end{aligned}\right\} \tag{169}$$

Here, i_1 and i_2 denote the currents of two current-controlled extended memristors in Figure 45. In this case, the small-signal *memristances* of the extended memristors is defined by

$$\left.\begin{aligned} \hat{R}_1(x_1,\, x_2,\, i_1) &= -(x_2 - x_1)\,i_1 \\ \hat{R}_2(x_1,\, x_2,\, i_2) &= -(x_1 - x_2)\,i_2. \end{aligned}\right\} \tag{170}$$

The terminal voltages v_n and the terminal current i_n of these extended memristors are given by ($n = 1,\, 2$)

V-I characteristics of the 2 extended memristors

$$\left.\begin{aligned} v_1 &= \hat{R}_1(x_1,\, x_2,\, i_1)\,i_1 = -(x_2 - x_1)\,{i_1}^2, \\ \frac{dx_1}{dt} &= \tilde{f}_1(x_1,\, i_1,\, i_2) = (i_1 - i_2)\,{x_1}^2 \end{aligned}\right\}$$

$$\left.\begin{aligned} v_2 &= \hat{R}_2(x_1,\, x_2,\, i_2)\,i_2 = -(x_1 - x_2)\,{i_2}^2, \\ \frac{dx_2}{dt} &= \tilde{f}_2(x_2,\, i_1,\, i_2) = (i_2 - i_1)\,{x_2}^2. \end{aligned}\right\} \tag{171}$$

Thus, Eq. (169) can be realized by the 4-element memristor circuit in Figure 45. The forced 4-dimensional memristor ecological predator-prey model is given by

Forced 4-dimensional memristor ecological predator-prey model equations

$$\left.\begin{aligned} \frac{di_1}{dt} &= (x_2 - x_1)\, {i_1}^2 + r\sin(\omega t), \\ \frac{dx_1}{dt} &= (i_1 - i_2)\, {x_1}^2, \\ \frac{di_2}{dt} &= (x_1 - x_2)\, {i_2}^2, \\ \frac{dx_2}{dt} &= (i_2 - i_1)\, {x_2}^2. \end{aligned}\right\} \tag{172}$$

where r and ω are constants.

The memristor circuit equations (163) and (172) exhibit periodic behavior. If an external source is added as shown in Figure 46, then the forced 4-dimensional memristor ecological predator-prey model (172) can exhibit quasi-periodic and non-periodic responses. We show the non-periodic response, quasi-periodic response, Poincaré maps, and $i_j - v_j$ loci of Eq. (172) in Figures 70, 71, 72, and 73, respectively ($j = 1, 2$). The $i_j - v_j$ loci in Figure 73 lie in the first and the fourth quadrants. Thus, the corresponding extended memristor is an active element. We show the $v_j - p_j$ locus in Figure 74, where $p_j(t)$ is an instantaneous power defined by $p_j(t) = i_j(t)v_j(t)$ ($j = 1, 2$). Observe that the $v_j - p_j$ locus is pinched at the origin, and the locus lies in the first and the third quadrants. Thus, the memristor switches between passive and active modes of operation, depending on its terminal voltage. We conclude as follow:

Switching behavior of the memristor

Assume that Eq. (172) exhibits non-periodic or quasi-periodic oscillation. Then the extended memristor defined by Eq. (171) can switch between "passive" and "active" modes of operation, depending on its terminal voltage.

In order to view the Poincaré maps in Figure 72 from a different perspective, let us project the trajectories into the (ξ, η, ζ)-space via the transformation

$$\begin{aligned} \xi(\tau) &= (r_1(\tau) + 5)\cos(\omega\tau), \\ \eta(\tau) &= (r_1(\tau) + 5)\sin(\omega\tau), \\ \zeta(\tau) &= r_2(\tau), \end{aligned} \tag{173}$$

where $r_1 = \sqrt{i_1^2 + {x_1}^2}$ and $r_2 = \sqrt{{i_2}^2 + {x_2}^2}$. Observe that the irregular trajectory exists in Figure 75(a). The following parameters are used in our computer simulations:

$$r = 0.5,\ \omega = 2. \tag{174}$$

Note that in order to generate a non-periodic response, we have to choose the initial conditions carefully. We show its example in Figure 76. Suppose that Eq. (172) has the following parameters and initial conditions:

$$\begin{aligned} &\text{Parameters:} && r = 0.5,\ \ \omega = 2, \\ &\text{Initial conditions:} && i(0) = 0.098,\ x_1(0) = 0.5, \\ & && x_2(0) = 1.1,\ x_3(0) = 1.3. \end{aligned} \tag{175}$$

If we choose $h = 0.01$, then the trajectory rapidly grows for $t \geq 5327$, and an overflow occurs as shown in Figure 76(a). However, if we choose $h = 0.005$, then the trajectory stays in a finite region as shown in Figure 76(b). The maximum step size of the numerical integration greatly affects the behavior of Eq. (172). In this case, noise may considerably affect the behavior of the physical memristor circuit.

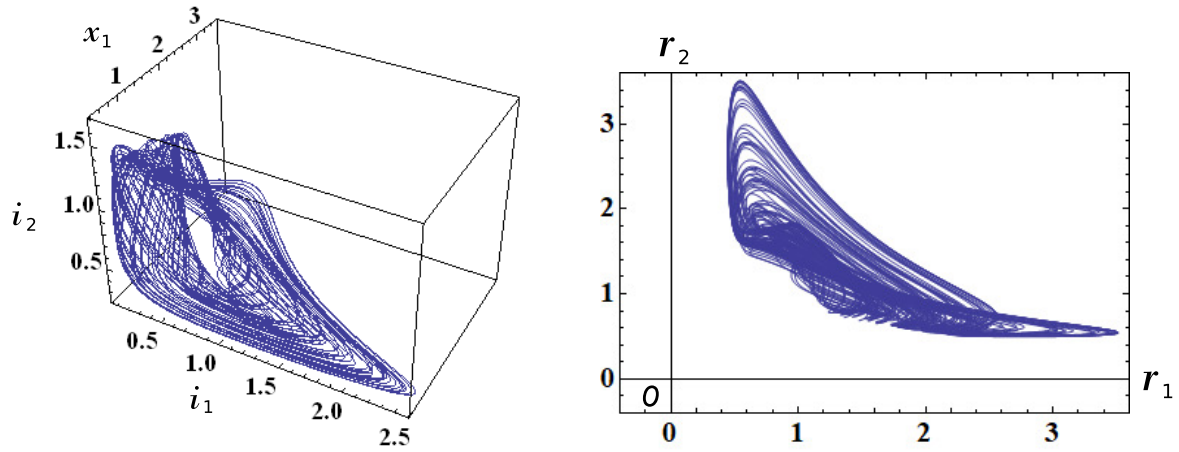

(a) $(i_1,\ x_1,\ i_2)$-space (b) $(r_1,\ r_2)$-plane

Figure 70: Non-periodic response of the forced 4-dimensional memristor ecological predator-prey equations (172), where $r_1 = \sqrt{{i_1}^2 + {x_1}^2}$ and $r_2 = \sqrt{{i_2}^2 + {x_2}^2}$. Parameters: $r = 0.5,\ \omega = 2$. Initial conditions: $i(0) = 0.1,\ x_1(0) = 0.5,\ x_2(0) = 1.1,\ x_3(0) = 1.3$.

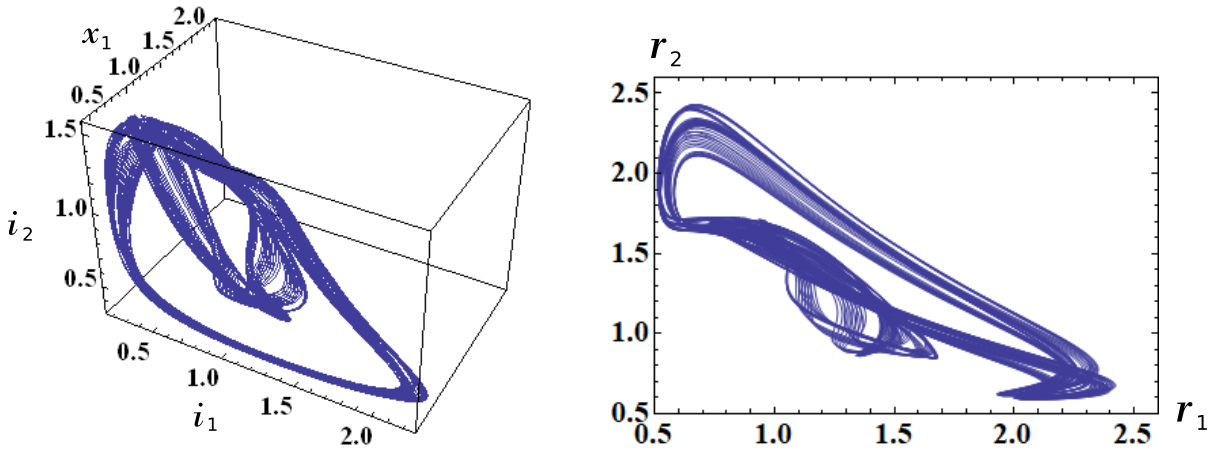

(a) $(i_1,\ x_1,\ i_2)$-space (b) $(r_1,\ r_2)$-plane

Figure 71: Quasi-periodic response of the forced 4-dimensional memristor ecological predator-prey equations (172), where $r_1 = \sqrt{{i_1}^2 + {x_1}^2}$ and $r_2 = \sqrt{{i_2}^2 + {x_2}^2}$. Parameters: $r = 0.5,\ \omega = 2$. Initial conditions: $i_1(0) = 0.2,\ x_1(0) = 0.5,\ i_2(0) = 1.1,\ x_2(0) = 1.3$.

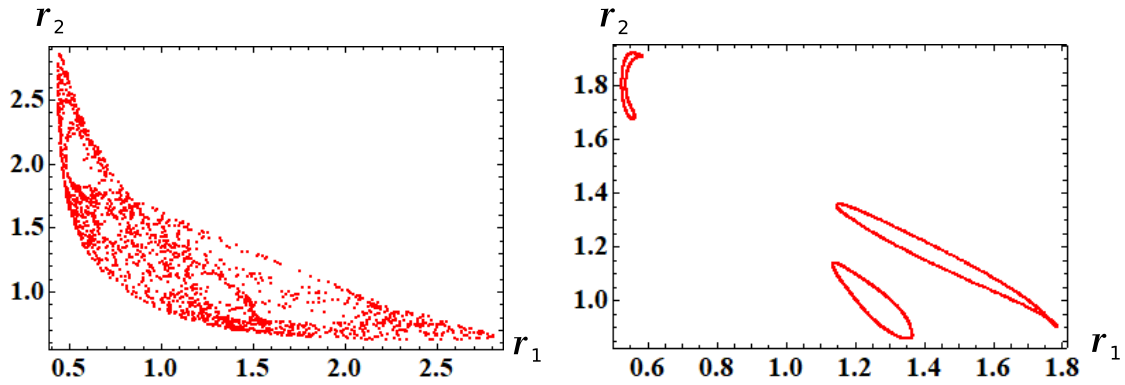

(a) non-periodic (b) quasi-periodic

Figure 72: Poincaré maps of the forced 4-dimensional memristor ecological predator-prey equations (172), where $r_1 = \sqrt{{i_1}^2 + {x_1}^2}$ and $r_2 = \sqrt{{i_2}^2 + {x_2}^2}$. Parameters: $r = 0.5$, $\omega = 2$. Initial conditions: (a) $i_1(0) = 0.1$, $x_1(0) = 0.5$, $i_2(0) = 1.1$, $x_2(0) = 1.3$. (b) $i_1(0) = 0.2$, $x_1(0) = 0.5$, $i_2(0) = 1.1$, $x_2(0) = 1.3$.

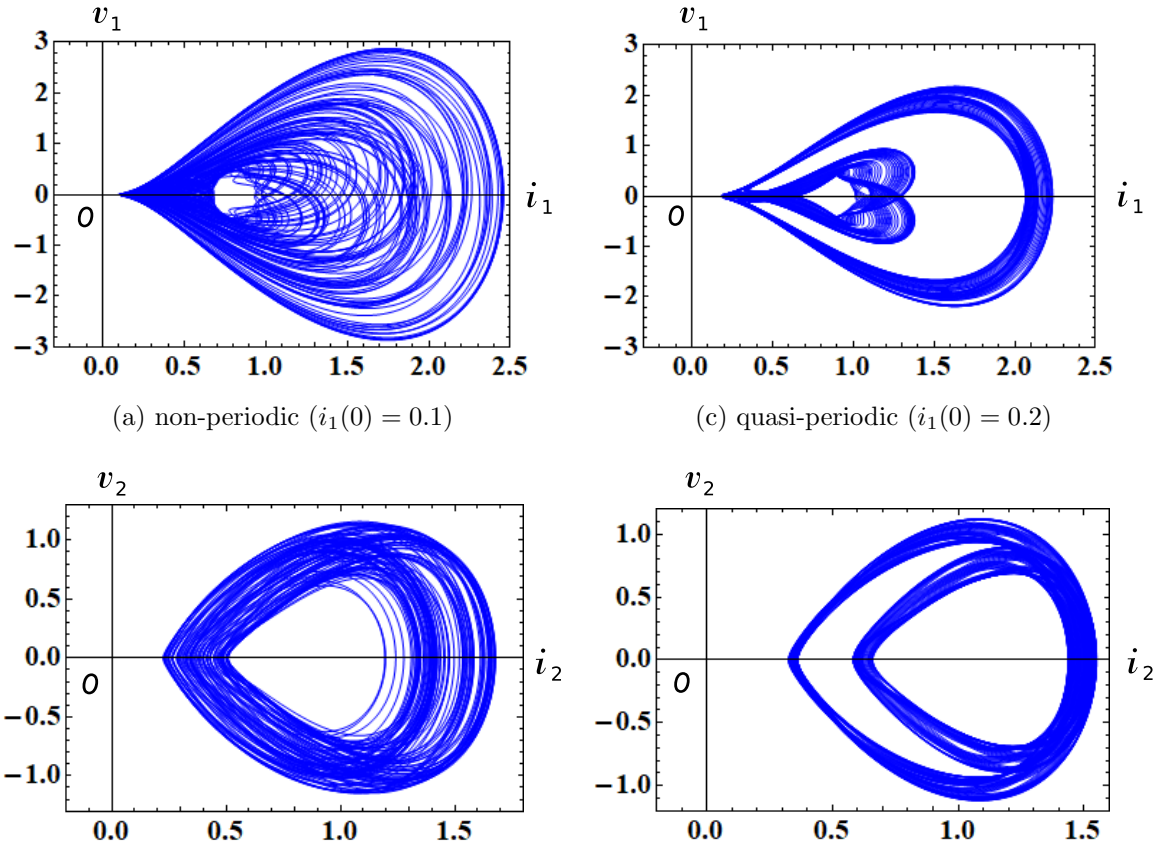

(a) non-periodic ($i_1(0) = 0.1$) (c) quasi-periodic ($i_1(0) = 0.2$)

(b) non-periodic ($i_1(0) = 0.1$) (d) quasi-periodic ($i_1(0) = 0.2$)

Figure 73: The $i_j - v_j$ loci of the forced 4-dimensional memristor ecological predator-prey equations (172). Here, i_j and v_j denote the terminal current and the voltage of the extended memristor, respectively ($j = 1, 2$). Parameters: $r = 0.5$, $\omega = 2$. (a), (b) $i_1(0) = 0.1$, $x_1(0) = 0.5$, $i_2(0) = 1.1$, $x_2(0) = 1.3$. (c), (d) $i_1(0) = 0.2$, $x_1(0) = 0.5$, $i_2(0) = 1.1$, $x_2(0) = 1.3$.

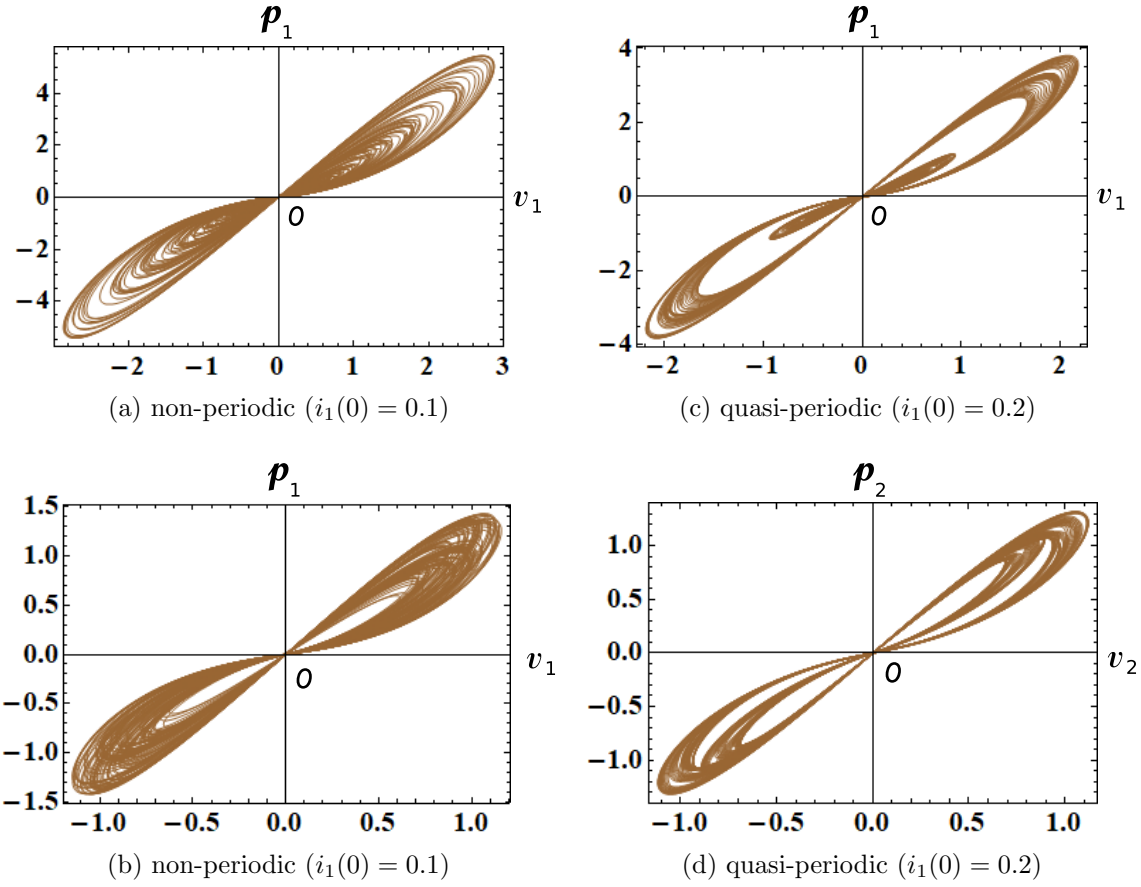

(a) non-periodic ($i_1(0) = 0.1$)

(c) quasi-periodic ($i_1(0) = 0.2$)

(b) non-periodic ($i_1(0) = 0.1$)

(d) quasi-periodic ($i_1(0) = 0.2$)

Figure 74: The $v_j - p_j$ loci of the forced 4-dimensional memristor ecological predator-prey equations (172). Here, $p_j(t)$ is an instantaneous power defined by $p_j(t) = i_j(t)v_j(t)$, and $v_j(t)$ and $i_j(t)$ denote the terminal voltage and the terminal current of the j-th generic memristor, respectively ($j = 1, 2$). Observe that the $v_j - p_j$ loci are pinched at the origin, and the locus lies in the first and the third quadrants. The memristor switches between passive and active modes of operation, depending on its terminal voltage $v_j(t)$. Parameters: $r = 0.1$, $\omega = 2$. Initial conditions: (a), (b) $i_1(0) = 0.1$, $x_1(0) = 0.5$, $i_2(0) = 1.1$, $x_2(0) = 1.3$. (c), (d) $i_1(0) = 0.2$, $x_1(0) = 0.5$, $i_2(0) = 1.1$, $x_2(0) = 1.3$.

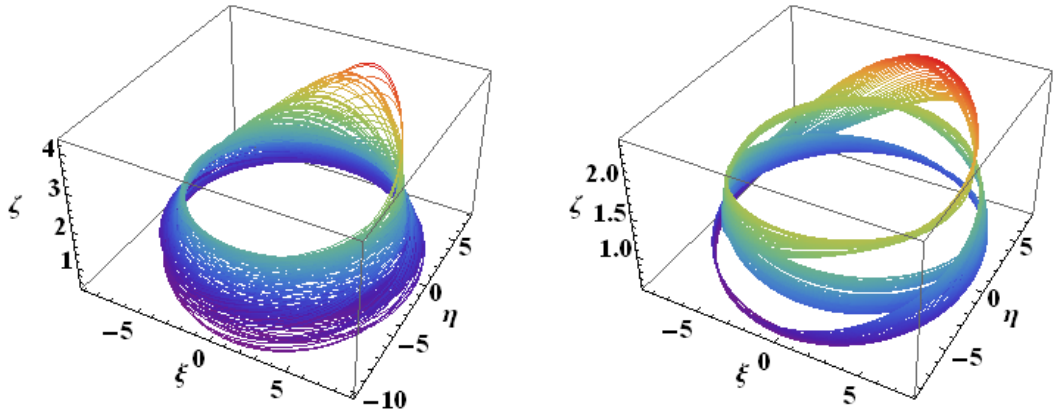

(a) non-periodic (b) quasi-periodic

Figure 75: The two trajectories of the forced 4-dimensional memristor ecological predator-prey equations (172), which are projected into the (ξ, η, ζ)-space via the coordinate transformation (173). We can observe a gap in Figure 75(b). Compare the trajectories in Figure 75 with the Poincaré maps in Figure 72. The trajectories are colored with the *Rainbow* color code in Mathematica. Parameters: $r = 0.1$, $\omega = 2$. Initial conditions: (a) $i_1(0) = 0.1$, $x_1(0) = 0.5$, $i_2(0) = 1.1$, $x_2(0) = 1.3$. (b) $i_1(0) = 0.2$, $x_1(0) = 0.5$, $i_2(0) = 1.1$, $x_2(0) = 1.3$.

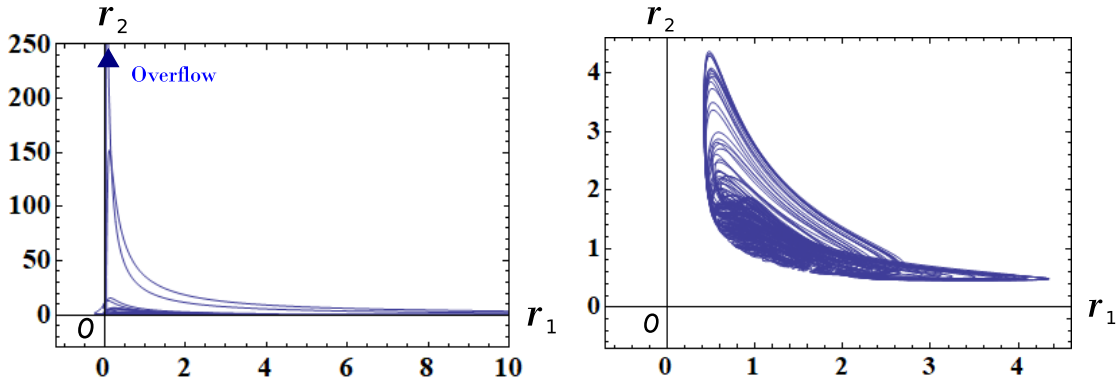

(a) $h = 0.005$ (b) $h = 0.002$

Figure 76: Behavior of the forced 4-dimensional memristor ecological predator-prey model equations (172). If we choose $h = 0.01$, then the trajectory rapidly grows for $t \geq 5327$, and an overflow occurs as shown in Figure 76(a). However, if we choose $h = 0.005$, then the trajectory stays in a finite region as shown in Figure 76(b). Here, h denotes the maximum step size of the numerical integration. Parameters: $r = 0.5$, $\omega = 2$. Initial conditions: $i_1(0) = 0.098$, $x_1(0) = 0.5$, $i_2(0) = 1.1$, $x_2(0) = 1.3$.

4 Exponential Coordinate Transformation

In this section, we show that the dynamics of an n-dimensional autonomous system can be transformed into the dynamics of a three-element memristor circuit by using the exponential coordinate transformation [3, 4].

4.1 Tennis racket equations

The components of the angular momentum of a tennis racket about its center of mass are governed by the following equations [23]:

Tennis racket equations

$$\left.\begin{aligned} \frac{d\omega_1}{dt} &= -\omega_2\,\omega_3, \\ \frac{d\omega_2}{dt} &= \omega_3\,\omega_1, \\ \frac{d\omega_3}{dt} &= -\omega_1\,\omega_2, \end{aligned}\right\} \tag{176}$$

where $\omega_1,\ \omega_2,\ \omega_3$ are the angular velocities about the object's three principal axes.

Equation (176) has the two integrals, since the solution satisfies

Integrals

$$\left.\begin{aligned} \frac{d}{dt}\left({\omega_1}^2 + {\omega_2}^2\right) = 0, \\ \frac{d}{dt}\left({\omega_2}^2 + {\omega_3}^2\right) = 0. \end{aligned}\right\} \tag{177}$$

Substituting

$$\omega_1 = \ln|\,i\,|,\ \omega_2 = x_1,\ \omega_3 = x_2, \tag{178}$$

into Eq. (176), we obtain

Memristor tennis racket equations

$$\left.\begin{aligned} \frac{di}{dt} &= -x_1\,x_2\,i, \\ \frac{dx_1}{dt} &= x_2\,\ln|\,i\,|, \\ \frac{dx_2}{dt} &= -x_1\,\ln|\,i\,|. \end{aligned}\right\} \tag{179}$$

Since $|\,i_1\,| = e^{x_1}$, Eq. (178) indicates an exponential coordinate transformation [4].

Consider the three-element memristor circuit in Figure 1. The dynamics of this circuit given by Eq. (2). Assume that Eq. (2) satisfies

$$\left.\begin{aligned} L = 1, \qquad & E = 0, \\ \hat{R}(x_1,\,x_2,\,i_M) &= x_1\,x_2, \\ \tilde{f}_1(x_1,\ x_2,\ i) &= x_2\,\ln|\,i_M\,|, \\ \tilde{f}_2(x_1,\ x_2,\ i) &= -x_1\,\ln|\,i_M\,|. \end{aligned}\right\} \tag{180}$$

Then Eq. (2) can be recast into Eq. (179). In this case, the extended memristor in Figure 1 can be replaced by the generic memristor. That is,

$$\hat{R}(x_1,\, x_2,\, i_M) = \tilde{R}(x_1,\, x_2) = x_1\, x_2. \tag{181}$$

The terminal voltage v_M and the terminal current i_M of the current-controlled generic memristor are described by

V-I characteristics of the generic memristor

$$\begin{aligned} v_M &= \tilde{R}(x_1,\, x_2)\, i_M = x_1\, x_2\, i_M, \\ \frac{dx_1}{dt} &= x_2\, \ln|\, i_M\,|, \\ \frac{dx_2}{dt} &= -x_1\, \ln|\, i_M\,|. \end{aligned} \tag{182}$$

where $\hat{R}(x_1,\, x_2) = x_1\, x_2$ and $i_M = i$.

Equation (179) has the two integrals, since the solution satisfies

Integrals

$$\left.\begin{aligned} \frac{d}{dt}\left(\ln|\, i\,|^2 + {x_1}^2\right) &= 0, \\ \frac{d}{dt}\left({x_1}^2 + {x_2}^2\right) &= 0, \end{aligned}\right\} \tag{183}$$

where $i \neq 0$.

It can exhibit periodic behavior. When an external source is added as shown in Figure 2, the forced memristor tennis racket equations can exhibit a non-periodic response. The dynamics of this circuit is given by

Forced memristor tennis racket equations

$$\left.\begin{aligned} \frac{di}{dt} &= -x_1\, x_2\, i + r\sin(\omega t), \\ \frac{dx_1}{dt} &= x_2\, \ln|\, i\,|, \\ \frac{dx_2}{dt} &= -x_1\, \ln|\, i\,|, \end{aligned}\right\} \tag{184}$$

where r and ω are constants.

The solution of Eq. (184) satisfies

$$x_1(t)^2 + x_2(t)^2 = K, \tag{185}$$

where K is a constant. We show the non-periodic response, quasi-periodic response, Poincaré maps, and $i_M - v_M$ loci of Eq. (184) in Figures 77, 78, 79, and 80, respectively. The trajectories projected into the $(x_1,\, x_2)$-plane are shown in Figure 77(b) and Figure 78(b), which moves on the circle defined by Eq. (185). Compare the two Poincaré maps in Figure 79. The $i_M - v_M$ loci in Figure 80 lie in the first and the fourth quadrants. Thus, the generic memristor defined by Eq. (182) is an active element. We show the $v_M - p_M$ locus in Figure 81, where $p_M(t)$ is an instantaneous power defined by $p_M(t) = i_M(t) v_M(t)$. Observe that

the $v_M - p_M$ locus is pinched at the origin, and the locus lies in the first and the third quadrants. Thus, the memristor switches between passive and active modes of operation, depending on its terminal voltage. We conclude as follow:

Switching behavior of the memristor

Assume that Eq. (184) exhibits non-periodic or quasi-periodic oscillation. Then the generic memristor defined by Eq. (182) can switch between "passive" and "active" modes of operation, depending on its terminal voltage.

In order to view the above Poincaré maps from a different perspective, let us project the trajectory into the $(\xi,\, \eta,\, \zeta)$-space via the transformation

$$\begin{aligned} \xi(\tau) &= (i(\tau)+5)\cos(\omega\tau), \\ \eta(\tau) &= (i(\tau)+5)\sin(\omega\tau), \\ \zeta(\tau) &= x_1(\tau). \end{aligned} \tag{186}$$

We show the projected trajectories in Figure 82. Observe that the trajectory in Figure 82(a) is less dense than Figure 82(b).

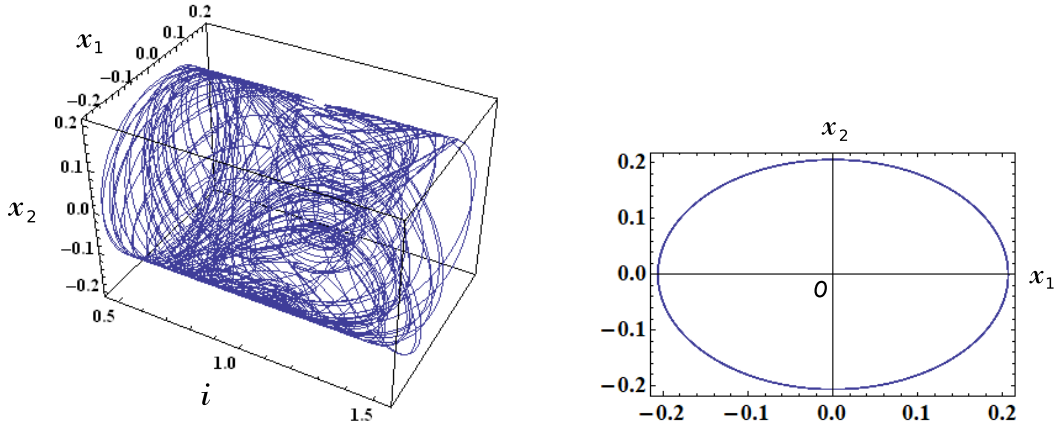

(a) $(i,\, x_1,\, x_2)$-space (b) Projected into the $(x_1,\, x_2)$-plane

Figure 77: Non-periodic response of the forced memristor tennis racket equations (184). (a) A non-periodic trajectory in the $(i,\, x_1,\, x_2)$-space. (b) A trajectory projected into the $(x_1,\, x_2)$-plane. It satisfies a circle equation: $x_1(t)^2 + x_2(t)^2 = 0.0425$. Parameters: $r = 0.087,\ \omega = 0.5$. Initial conditions: $i(0) = e^{0.11},\ x_1(0) = 0.2,\ x_2(0) = 0.05$.

4.2 Pendulum equations

The equation for a pendulum can be written as [10]

$$\frac{d^2u}{dt^2} + \sin u = 0, \tag{187}$$

where u is the angle from the downward vertical. It is equivalent to the sine-Gordon equation in the absence of the diffusion term. Equation (187) can be recast into the form

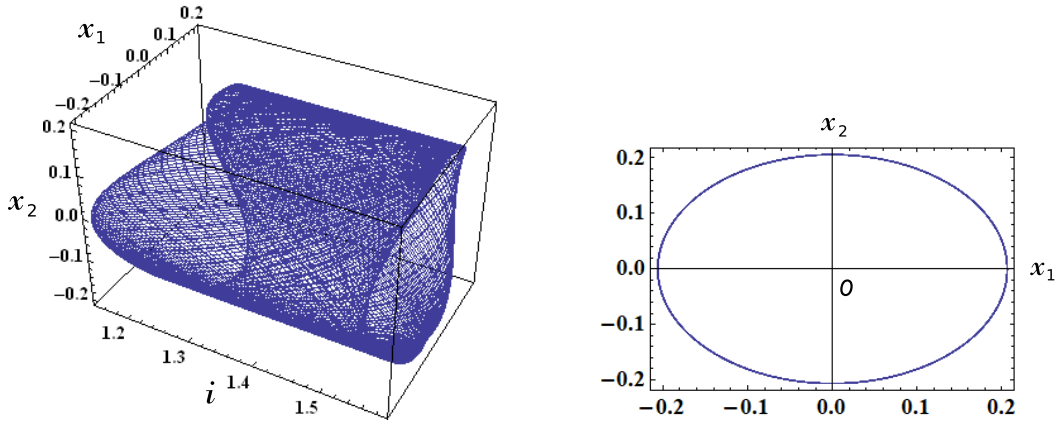

(a) $(i,\, x_1,\, x_2)$-space (b) Projected into the $(x_1,\, x_2)$-plane

Figure 78: Quasi-periodic response of the forced memristor tennis racket equations (184). (a) A quasi-periodic trajectory in the $(i,\, x_1,\, x_2)$-space. (b) A trajectory projected into the $(x_1,\, x_2)$-plane. It satisfies a circle equation: $x_1(t)^2 + x_2(t)^2 = 0.0425$. Parameters: $r = 0.087,\ \omega = 0.5$. Initial conditions: $i(0) = e^{0.15},\ x_1(0) = 0.2,\ x_2(0) = 0.05$.

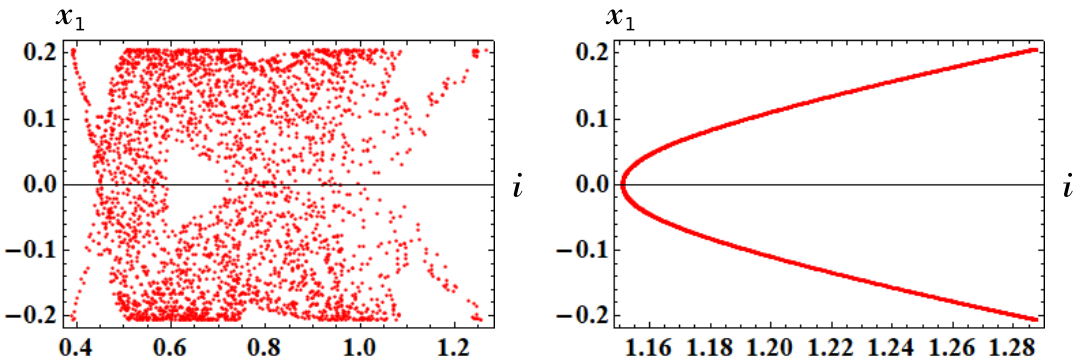

(a) non-periodic (b) quasi-periodic

Figure 79: Poincaré maps of the forced memristor tennis racket equations (184). Parameters: $r = 0.087$, $\omega = 0.5$. Initial conditions: (a) $i(0) = e^{0.11},\ x_1(0) = 0.2,\ x_2(0) = 0.05$. (b) $i(0) = e^{0.15},\ x_1(0) = 0.2,\ x_2(0) = 0.05$.

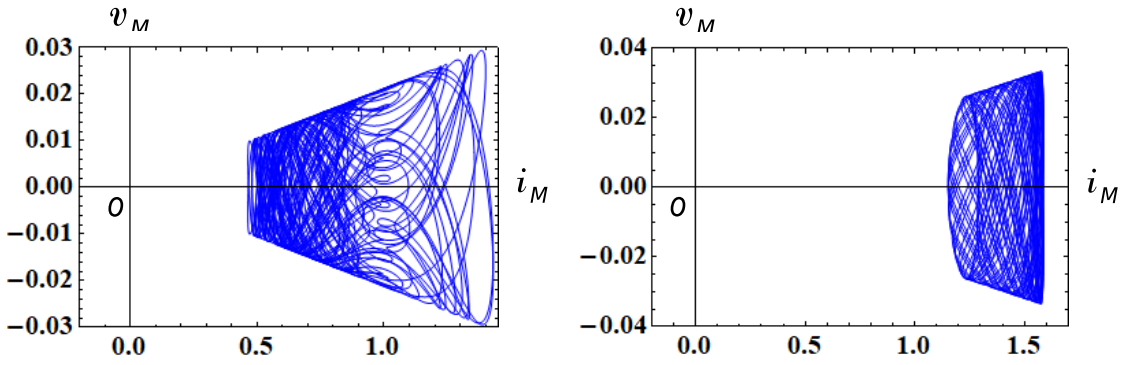

(a) non-periodic (b) quasi-periodic

Figure 80: The $i_M - v_M$ loci of the forced memristor tennis racket equations (184). Here, v_M and i_M denote the terminal voltage and the terminal current of the current-controlled generic memristor. Parameters: $r = 0.087,\ \omega = 0.5$. Initial conditions: (a) $i(0) = e^{0.11},\ x_1(0) = 0.2,\ x_2(0) = 0.05$. (b) $i(0) = e^{0.15},\ x_1(0) = 0.2,\ x_2(0) = 0.05$.

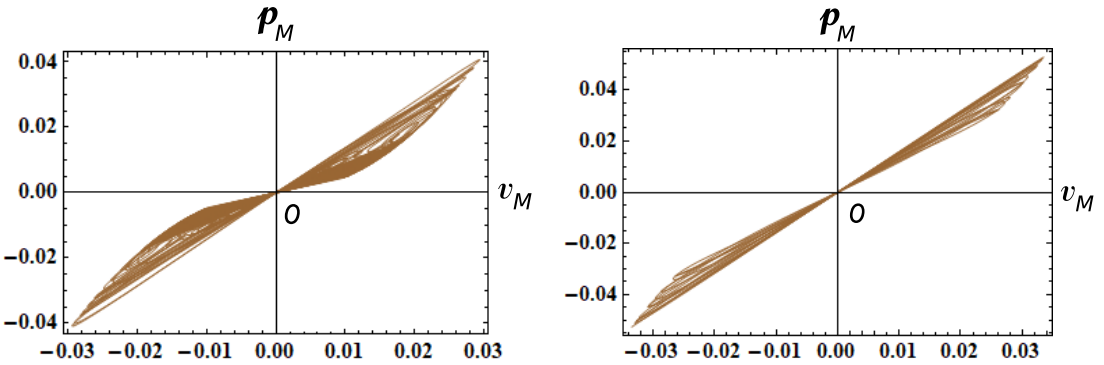

(a) non-periodic (b) quasi-periodic

Figure 81: The $v_M - p_M$ loci of the forced memristor tennis racket equations (184). Here, $p_M(t)$ is an instantaneous power defined by $p_M(t) = i_M(t)v_M(t)$, and $v_M(t)$ and $i_M(t)$ denote the terminal voltage and the terminal current of the current-controlled generic memristor. Observe that the $v_M - p_M$ locus is pinched at the origin, and the locus lies in the first and the third quadrants. The memristor switches between passive and active modes of operation, depending on its terminal voltage $v_M(t)$. Parameters: $r = 0.087,\ \omega = 0.5$. Initial conditions: (a) $i(0) = e^{0.11},\ x_1(0) = 0.2,\ x_2(0) = 0.05$. (b) $i(0) = e^{0.15},\ x_1(0) = 0.2,\ x_2(0) = 0.05$.

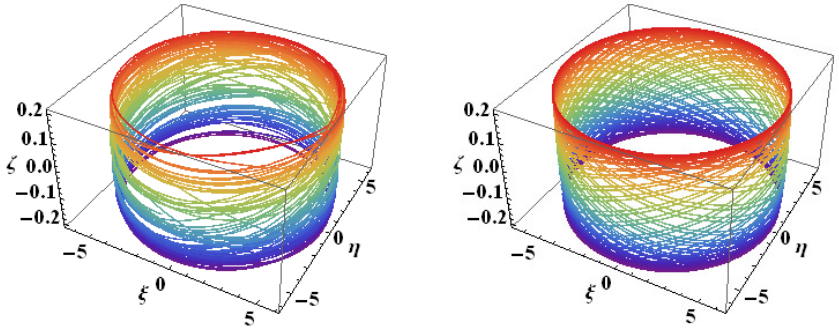

(a) non-periodic (b) quasi-periodic

Figure 82: The two trajectories of the forced memristor tennis racket equations (184, which are projected into the $(\xi,\, \eta,\, \zeta)$-space via the coordinate transformation (186). Observe that the trajectory in Figure 82(a) is less dense than Figure 82(b). Compare the trajectories in Figure 82 with the Poincaré maps in Figure 79. The trajectories are colored with the *Rainbow* color code in Mathematica. Parameters: $r = 0.087,\ \omega = 0.5$. Initial conditions: (a) $i(0) = e^{0.11},\ x_1(0) = 0.2,\ x_2(0) = 0.05$. (b) $i(0) = e^{0.15},\ x_1(0) = 0.2,\ x_2(0) = 0.05$.

Pendulum equations

$$\begin{aligned} \frac{du}{dt} &= v, \\ \frac{dv}{dt} &= -\sin u. \end{aligned} \tag{188}$$

Substituting $v = \ln|\,i\,|$ and $u = x$ into Eq. (187), we obtain

Memristor pendulum equations

$$\begin{aligned} \frac{di}{dt} &= -i\sin x, \\ \frac{dx}{dt} &= \ln|\,i\,|. \end{aligned} \tag{189}$$

Consider the three-element memristor circuit in Figure 1. The dynamics of this circuit given by Eq. (3). Assume that Eq. (3) satisfies

$$\left.\begin{aligned} E &= 0, \\ \hat{R}(x,\, i_M) &= \sin x, \\ f_1(x,\, i) &= \ln|\,i\,|. \end{aligned}\right\} \tag{190}$$

Then, Eq. (3) can be recast into Eq. (189). In this case, the extended memristor in Figure 1 can be replaced by by the generic memristor. Thus,

$$\hat{R}(x,\, i_M) = \tilde{R}(x) = \sin x. \tag{191}$$

The terminal voltage v_M and the terminal current i_M of the memristor are described by

V-I characteristics of the generic memristor

$$\begin{aligned} v_M &= \tilde{R}(x)\, i_M = (\sin x)\, i_M, \\ \frac{dx}{dt} &= \ln |\, i_M \,|, \end{aligned} \tag{192}$$

where $\hat{R}(x) = \sin x$ and $i_M = i$.

Equation (189) has the integral, since the solution satisfies

Integral

$$\frac{dt}{dt}\left\{ \frac{(\ln |\, i \,|)^2}{2} + \cos x \right\} = 0. \tag{193}$$

The memristor pendulum equations (189) exhibit periodic behavior. If an external source is added as shown in Figure 2, then the forced memristor pendulum equations can exhibit non-periodic and quasi-periodic responses. The dynamics of this circuit is given by

Forced memristor pendulum equations

$$\begin{aligned} \frac{di}{dt} &= -i \sin x + r \sin(\omega t), \\ \frac{dx}{dt} &= \ln |\, i \,|, \end{aligned} \tag{194}$$

where r and ω are constants.

Equation (194) is invariant under the transformation $x \rightarrow x + 2\pi$. We show their trajectories, Poincaré maps, and $i_M - v_M$ loci in Figures 83, 84, and 85, respectively. The following parameters are used in our computer simulations:

$$r = 0.04452,\ \omega = 1. \tag{195}$$

The $i_M - v_M$ loci in Figure 85 lie in the first and the fourth quadrant. Thus, the generic memristor defined by Eq. (192) is an active element. We next show the $v_M - p_M$ locus in Figure 86, where $p_M(t)$ is an instantaneous power defined by $p_M(t) = i_M(t) v_M(t)$. Observe that the $v_M - p_M$ locus is pinched at the origin, and the locus lies in the first and the third quadrants. Thus, the memristor switches between passive and active modes of operation, depending on its terminal voltage. We conclude as follow:

Switching behavior of the memristor

Assume that Eq. (194) exhibits non-periodic or quasi-periodic oscillation oscillation. Then the generic memristor defined by Eq. (192) can switch between "passive" and "active" modes of operation, depending on its terminal voltage.

In order to view the above Poincaré maps in Figure 84 from a different perspective, let us project the trajectory into the (ξ, η, ζ)-space via the transformation

$$\begin{aligned} \xi(\tau) &= (i(\tau) + 5) \cos(\omega\tau), \\ \eta(\tau) &= (i(\tau) + 5) \sin(\omega\tau), \\ \zeta(\tau) &= x_1(\tau). \end{aligned} \tag{196}$$

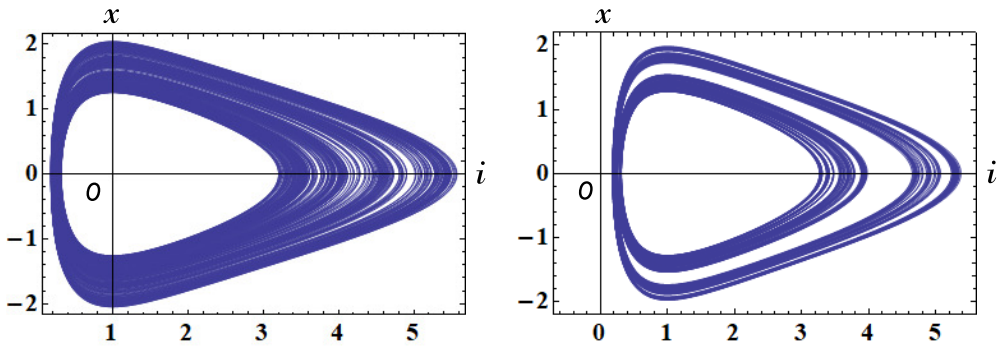

(a) non-periodic (b) quasi-periodic

Figure 83: Non-periodic and quasi-periodic responses of the forced memristor pendulum equations (194). Parameters: $r = 0.04452,\ \omega = 1$. Initial conditions: (a) $i(0) = 0.187,\ x(0) = 0.21$. (b) $i(0) = 0.187,\ x(0) = 0.2$.

Compare the trajectories in Figure 87 with the Poincaré maps in Figure 84. We can observe a wide gap in Figure 87(b).

Note that in order to obtain the Poincaré map in Figure 84(a), we have to choose the parameters and initial conditions carefully. Furthermore, the maximum step size h of the numerical integration must be sufficiently small ($h = 0.003$) because of the numerical instability in long-time simulations. We show an interesting example in Figure 88. Suppose that Eq. (194) has the following parameters and initial conditions:

$$\begin{aligned} &\text{Parameters: } r = 0.0445,\ \ \omega = 1, \\ &\text{Initial conditions: } i(0) = 0.187,\ x(0) = 0.187. \end{aligned} \tag{197}$$

If we choose $h = 0.0005$, then $x(t)$ decreases gradually as time t increases as shown in Figure 88(a). However, if we choose $h = 0.0003$, then the trajectory stays in a finite region of the $(i,\ x)$-plane as shown in Figure 88(b). The maximum step size of the numerical integration greatly affects the behavior of Eq. (194).

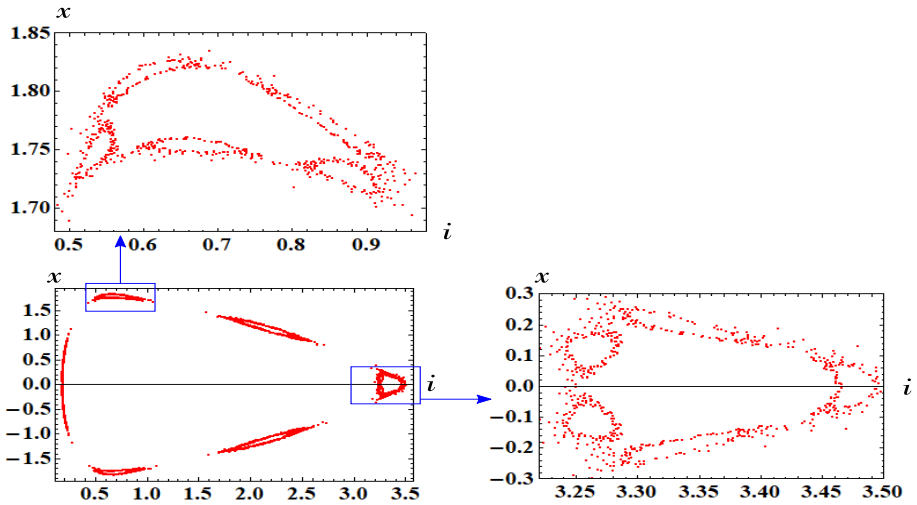

(a) non-periodic

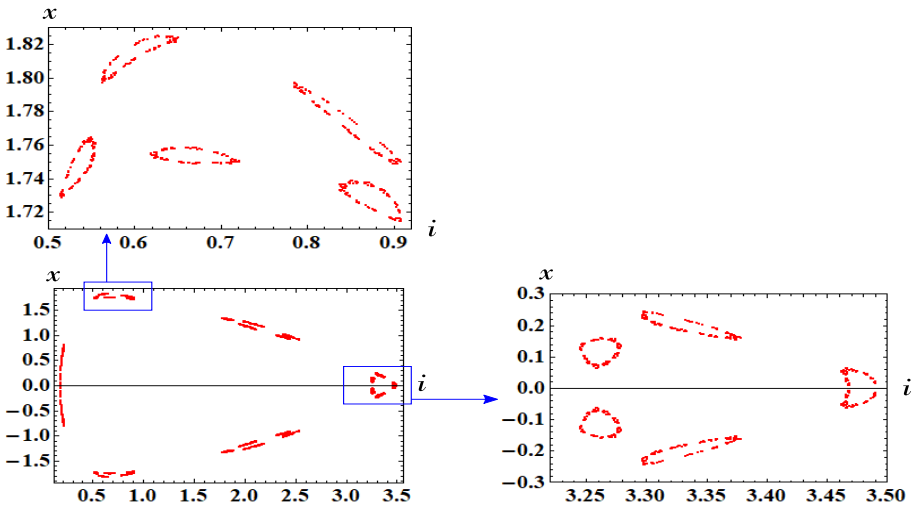

(b) quasi-periodic

Figure 84: Poincaré maps of the forced memristor pendulum equations (194). Parameters: $r = 0.04452$, $\omega = 1$. Initial conditions: (a) $i(0) = 0.187,\ x(0) = 0.21$. (b) $i(0) = 0.187,\ x(0) = 0.2$.

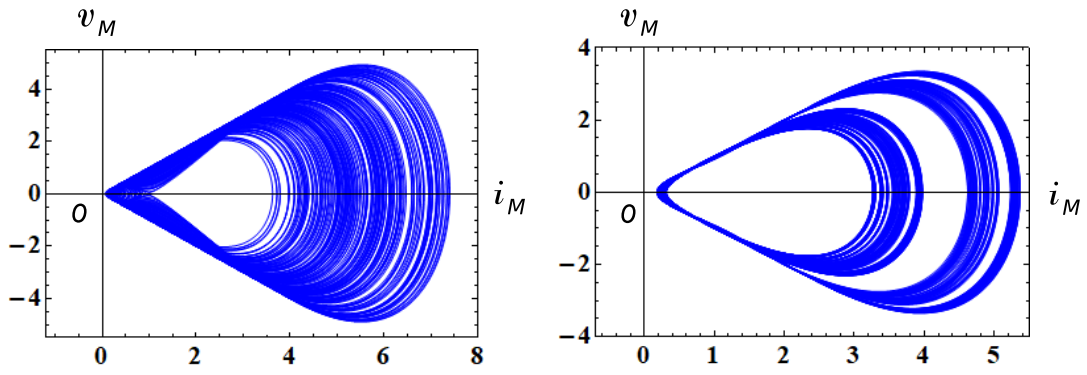

(a) non-periodic (b) quasi-periodic

Figure 85: The $i_M - v_M$ loci of the forced memristor pendulum equations (194). Here, v_M and i_M denote the terminal voltage and the terminal current of the current-controlled generic memristor. Parameters: $r = 0.04452,\ \omega = 1$. Initial conditions: (a) $i(0) = 0.187,\ x(0) = 0.21$. (b) $i(0) = 0.187,\ x(0) = 0.2$.

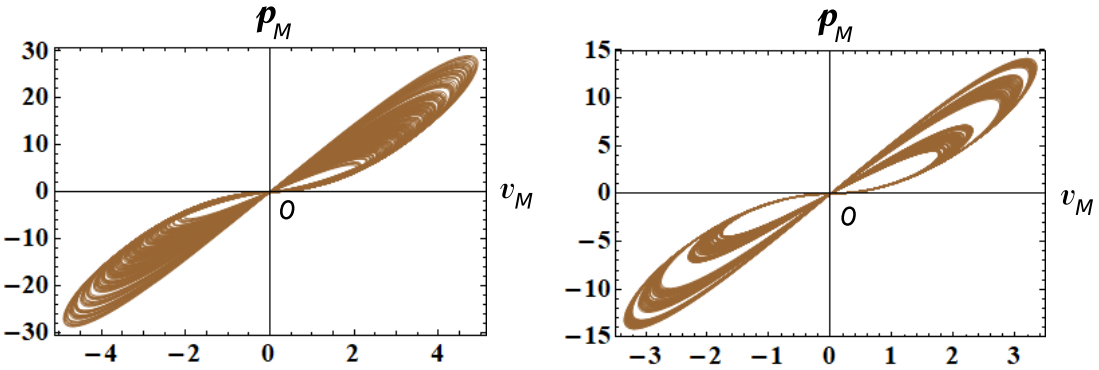

(a) non-periodic (b) quasi-periodic

Figure 86: The $v_M - p_M$ locus of the forced memristor pendulum equations (194). Here, $p_M(t)$ is an instantaneous power defined by $p_M(t) = i_M(t)v_M(t)$, and $v_M(t)$ and $i_M(t)$ denote the terminal voltage and the terminal current of the current-controlled generic memristor. Observe that the $v_M - p_M$ locus is pinched at the origin, and the locus lies in the first and the third quadrants. The memristor switches between passive and active modes of operation, depending on its terminal voltage $v_M(t)$. Parameters: $r = 0.04452,\ \omega = 1$. Initial conditions: (a) $i(0) = 0.187,\ x(0) = 0.21$. (b) $i(0) = 0.187,\ x(0) = 0.2$.

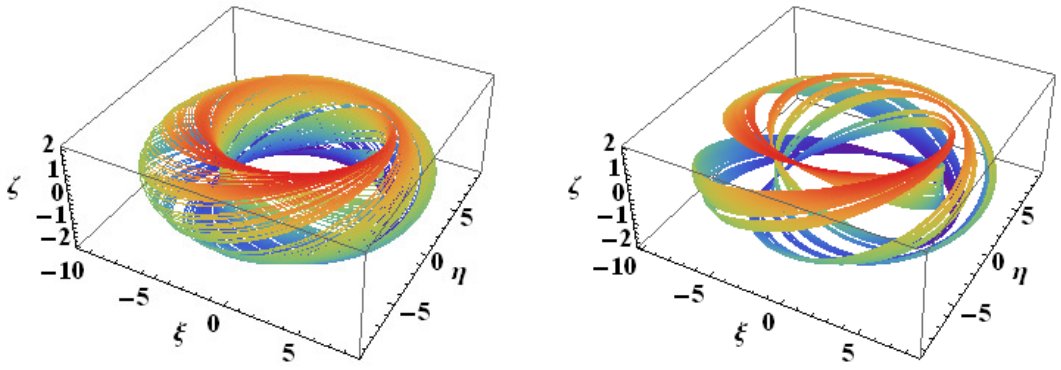

(a) non-periodic (b) quasi-periodic

Figure 87: The two trajectories of the forced memristor pendulum equations (194), which are projected into the (ξ, η, ζ)-space via the coordinate transformation (196). We can observe a wide gap in Figure 87(b). Compare the trajectories in Figure 87 with the Poincaré maps in Figure 84. The trajectories are colored with the *Rainbow* color code in Mathematica. Parameters: $r = 0.04452,\ \omega = 1$. Initial conditions: (a) $i(0) = 0.187,\ x(0) = 0.21$. (b) $i(0) = 0.187,\ x(0) = 0.2$.

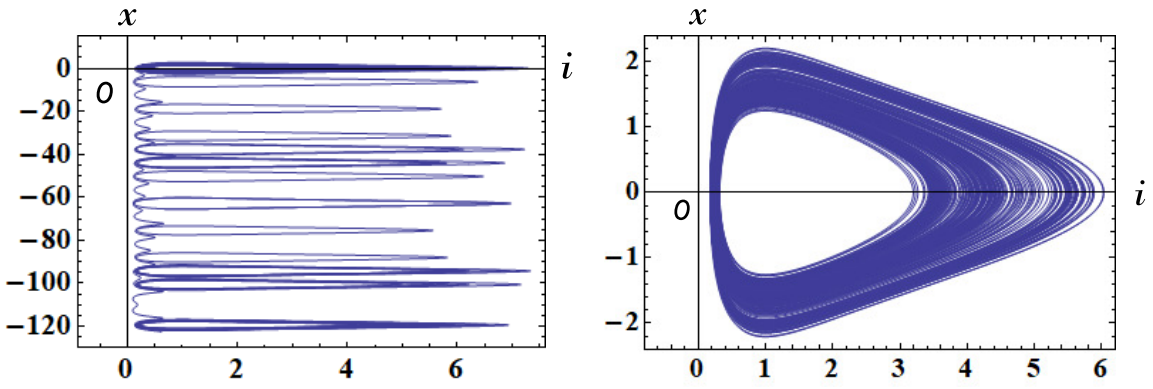

(a) $h = 0.0005$ (b) $h = 0.0003$

Figure 88: Behavior of the forced memristor pendulum equations (194) for $0 \le t \le 2000$. Observe the difference between the two trajectories. If we choose $h = 0.0005$, then $x(t)$ decreases gradually as time t increases as shown in Figure 88(a), where $x(2000) \approx -122.7$. However, if we choose $h = 0.0003$, then the trajectory stays in a finite region of the $(i,\ x)$-plane as shown in Figure 88(b), where $x(2000) \approx -1.815$. Here, h denotes the maximum step size of the numerical integration. Parameters: $r = 0.0445,\ \omega = 1$. Initial conditions: $i(0) = 0.187,\ x(0) = 0.187$.

4.3 Lorenz system

The dynamics of the *Lorenz system* [16] is defined by a system of three ordinary differential equations:

Lorenz system

$$\left.\begin{aligned} \frac{dx}{dt} &= \sigma\,(y-x), \\ \frac{dy}{dt} &= x\,(\rho-z)-y, \\ \frac{dz}{dt} &= xy-\beta\,z, \end{aligned}\right\} \tag{198}$$

where $\sigma = 10$, $\beta = \frac{8}{3}$, and $\rho = 28$.

The Lorenz system (198) is a simplified model of convection rolls in the atmosphere. When $\sigma = 10$, $\beta = \frac{8}{3}$, and $\rho = 28$, Eq. (198) has chaotic solutions, which resemble a butterfly or figure eight.

Substituting $x = \ln|\,i\,|$, $y = x_1$, and $z = x_2$ into Eq. (198), we obtain

Memristor Lorenz equations for Eq. (198)

$$\left.\begin{aligned} \frac{di}{dt} &= \sigma\,(x_2-\ln|\,i\,|\,)\,i, \\ \frac{dx_1}{dt} &= (\rho-x_2)\,\ln|\,i\,|-x_1, \\ \frac{dx_2}{dt} &= x_1-\beta\,x_2, \end{aligned}\right\} \tag{199}$$

where $\sigma = 10$, $\beta = \frac{8}{3}$, and $\rho = 28$.

Consider the three-element memristor circuit in Figure 1. The dynamics of this circuit given by Eq. (2). Assume that Eq. (2) satisfies

$$\left.\begin{aligned} L = 1, \qquad & E = 0, \\ \hat{R}(x_1,\,x_2,\,i_M) &= -\sigma\,(x_2-\ln|\,i_M\,|\,) \\ \tilde{f}_1(x_1,\;x_2,\;i) &= (\rho-x_2)\,\ln|\,i_M\,|-x_1, \\ \tilde{f}_2(x_1,\;x_2,\;i) &= x_1-\beta\,x_2. \end{aligned}\right\} \tag{200}$$

Then Eq. (2) can be recast into Eq. (199). Thus, the terminal voltage v_M and the terminal current i_M of the current-controlled extended memristor in Figure 1 are described by

V-I characteristics of the extended memristor

$$\begin{aligned} v_M &= \hat{R}(x_1,\,x_2,\,i_M)\,i_M \\ &= -\sigma\,(x_2-\ln|\,i_M\,|\,)\,i_M, \\ \frac{dx_1}{dt} &= (\rho-x_2)\,\ln|\,i_M\,|-x_1, \\ \frac{dx_2}{dt} &= x_1-\beta\,x_2, \end{aligned} \tag{201}$$

where $\hat{R}(x_1,\,x_2,\,i_M) = -\sigma\,(x_2-\ln|\,i_M\,|\,)$.

Note that $i = 0$ and $i_M = 0$ are not well-defined in Eq. (199) and Eq. (201), respectively. Furthermore, the condition for the extended memristor, that is, $\hat{R}(x_1,\, x_2,\, 0) \neq \infty$ is not satisfied, since

$$\lim_{i_M \to 0} |\hat{R}(x_1,\, x_2,\, i_M)| = \lim_{i_M \to 0} \left| -\sigma\,(x_2 - \ln|\, i_M\,|\,) \right| \to \infty. \tag{202}$$

However, if $i_M \to 0$, then v_M satisfies

$$v_M = \hat{R}(x_1,\, x_2,\, i_M)\, i_M = -\sigma\,(x_2 - \ln|\, i_M\,|\,)\, i_M \to 0. \tag{203}$$

Therefore, without loss of generality, we can regard this kind of memristor as the extended memristor. For more details, see [1].

For $\sigma = 10$, $\beta = \frac{8}{3}$, and $\rho = 28$, the memristor Lorenz equations (199) also exhibit chaotic oscillation. Thus, an external periodic forcing is *unnecessary* to generate chaotic oscillation. We show the chaotic attractor, Poincaré map, and $i_M - v_M$ locus in Figures 89, 90, and 91, respectively. We can easily observe the folding action of the chaotic attractor as shown in Figure 90. The $i_M - v_M$ locus in Figure 91 lies in the first and the fourth quadrants. Thus, the extended memristor defined by Eq. (201) is an active element. Let us show the $v_M - p_M$ locus in Figure 92, where $p_M(t)$ is an instantaneous power defined by $p_M(t) = i_M(t)v_M(t)$. Observe that the $v_M - p_M$ locus is pinched at the origin, and the locus lies in the first and the third quadrants. Thus, when $v_M > 0$, the instantaneous power p_M delivered from the forced signal and the inductor is dissipated in the memristor. However, when $v_M < 0$, the instantaneous power p_M is not dissipated in the memristor. Hence, the memristor switches between passive and active modes of operation, depending on its terminal voltage. We conclude as follow:

Switching behavior of the memristor

Assume that Eq. (199) exhibits chaotic oscillation. Then the extended memristor defined by Eq. (201) can switch between "passive" and "active" modes of operation, depending on its terminal voltage.

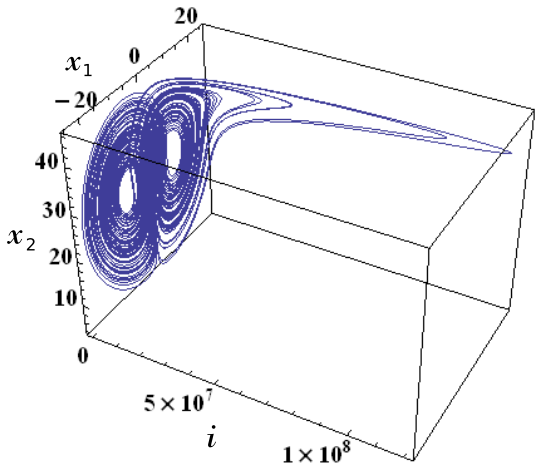

Figure 89: Chaotic attractor of the memristor Lorenz equations (199). Parameters: $a = 0.2,\ b = 0.2,\ c = 5.7$. Initial conditions: $i(0) = 0.1,\ x_1(0) = 0.1,\ x_2(0) = 0.1$.

4.4 Two-variable Oregonator model

Two-variable Oregonator model [27] is defined by

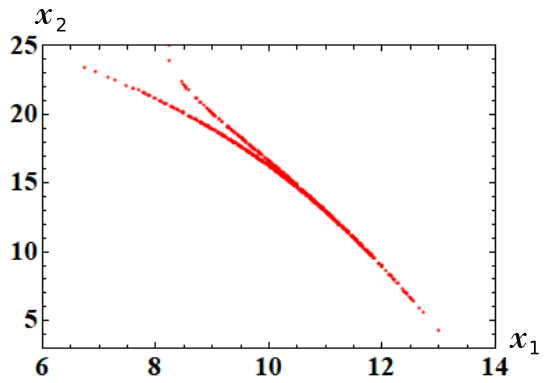

Figure 90: Poincaré map of the memristor Lorenz equations (199). The Poincaré cross-section is defined by $\{(i,\, x_1,\, x_2) \in R^3 \mid i = 500\}$. The chaotic trajectory of Eq. (199) crosses the above Poincaré cross-section (plane) many times. Observe the folding action of the chaotic attractor. Parameters: $a = 0.2,\ b = 0.2,\ c = 5.7$. Initial conditions: $i(0) = 0.1,\ x_1(0) = 0.1,\ x_2(0) = 0.1$.

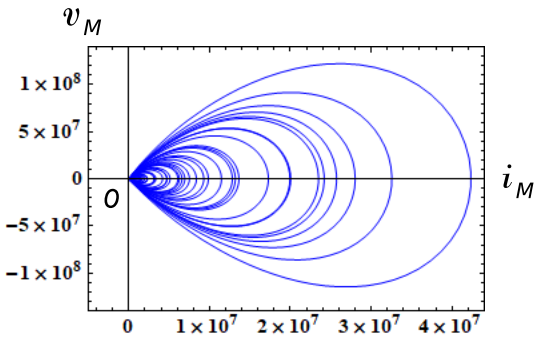

Figure 91: The $i_M - v_M$ locus of the memristor Lorenz equations (199). Here, v_M and i_M denote the terminal voltage and the terminal current of the current-controlled extended memristor. Parameters: $a = 0.2,\ b = 0.2,\ c = 5.7$. Initial conditions: $i(0) = 0.1,\ x_1(0) = 0.1,\ x_2(0) = 0.1$.

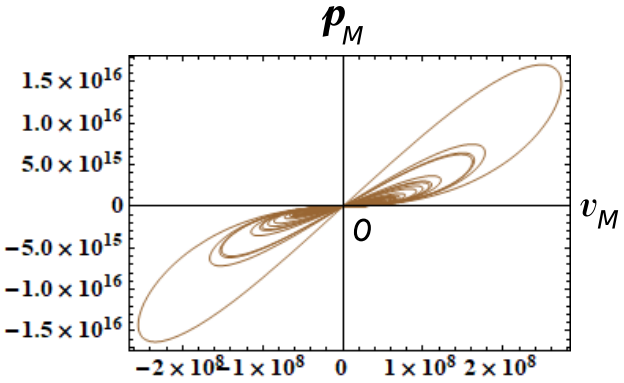

Figure 92: The $v_M - p_M$ locus of the memristor Lorenz equations (199). Here, $p_M(t)$ is an instantaneous power defined by $p_M(t) = i_M(t)v_M(t)$, and $v_M(t)$ and $i_M(t)$ denote the terminal voltage and the terminal current of the current-controlled extended memristor. Observe that the $v_M - p_M$ locus is pinched at the origin, and the locus lies in the first and the third quadrants. The memristor switches between passive and active modes of operation, depending on its terminal voltage $v_M(t)$. Parameters: $a = 0.2,\ b = 0.2,\ c = 5.7$. Initial conditions: $i(0) = 0.1,\ x_1(0) = 0.1,\ x_2(0) = 0.1$.

Two-variable Oregonator model equations

$$\begin{aligned} \frac{du}{dt} &= \frac{1}{\epsilon}\left(u - u^2 - \frac{fv(u-q)}{u+q}\right), \\ \frac{dv}{dt} &= u - v, \end{aligned} \tag{204}$$

where $f = 1$, $q = 0.001$, and $\epsilon = 0.7$.

Substituting $u = \ln|\,i\,|$ and $v = x$, into Eq. (204), we obtain

Memristor two-variable Oregonator model equations

$$\begin{aligned} L\frac{di}{dt} &= \left\{\ln|\,i\,| - (\ln|\,i\,|)^2 - \frac{f\,x\,(\ln|\,i\,| - q)}{\ln|\,i\,| + q}\right\} i, \\ \frac{dx}{dt} &= \ln|\,i\,| - x, \end{aligned} \tag{205}$$

where $f = 1$, $q = 0.001$, and $L = 0.7$.

Consider the three-element memristor circuit in Figure 1. The dynamics of this circuit given by Eq. (3). Assume that Eq. (3) satisfies

$$\begin{aligned} E &= 0, \\ \hat{R}(x,\, i_M) &= -\left\{\ln|\,i_M\,| - (\ln|\,i_M\,|)^2 - \frac{f\,x\,(\ln|\,i_M\,| - q)}{\ln|\,i_M\,| + q}\right\}, \\ f_1(x,\, i) &= \ln|\,i_M\,| - x. \end{aligned} \tag{206}$$

Then Eq. (3) can be recast into Eq. (205). The terminal voltage v_M and the terminal current i_M of the current-controlled extended memristor in Figure 1 are described by

V-I characteristics of the extended memristor

$$\begin{aligned} v_M &= \hat{R}(x,\, i_M)\, i_M \\ &= -\left\{\ln|\,i_M\,| - (\ln|\,i_M\,|)^2 - \frac{f\,x\,(\ln|\,i_M\,| - q)}{\ln|\,i_M\,| + q}\right\} i_M, \\ \frac{dx}{dt} &= f_1(x,\, i) = \ln|\,i_M\,| - x, \end{aligned} \tag{207}$$

where

$$\hat{R}(x, i_M) = -\left\{\ln|\,i_M\,| - (\ln|\,i_M\,|)^2 - \frac{f\,x\,(\ln|\,i_M\,| - q)}{\ln|\,i_M\,| + q}\right\}.$$

Note that $\lim_{i_M \to 0} |\hat{R}(x,\, i_M)| \to \infty$. Hence, the above memristor does not satisfy the condition of the extended memristor, that is, $\hat{R}(x,\, 0) \neq \infty$. Furthermore, $i = 0$ and $i_M = 0$ are not well-defined in Eq. (205) and Eq. (207). However, if $i_M \to 0$, then $v_M \to 0$. Thus, without loss of generality, we can regard this kind of memristor as the extended memristor. For more details, see [1].

The memristor two-variable Oregonator model equations (205) exhibit periodic oscillation. When an external source is added as shown in Figure 2, the forced two-variable Oregonator model equations can exhibit chaotic oscillation. The dynamics of this circuit is given by

Forced memristor two-variable Oregonator model equations

$$\begin{aligned} L\frac{di}{dt} &= \left\{\ln|i| - (\ln|i|)^2 - \frac{f\,x\,(\ln|i| - q)}{\ln|i| + q}\right\} i \\ &\quad + r\sin(\omega t), \\ \frac{dx}{dt} &= \ln|i| - x, \end{aligned} \tag{208}$$

where r and ω are constants.

We show their chaotic attractor, Poincaré map, and $i_M - v_M$ locus in Figures 93, 94, and 95, respectively. The following parameters are used in our computer simulations:

$$\left.\begin{array}{lll} f = 1, & q = 0.001, & L = 0.7. \\ r = 0.01, & \omega = 0.79. & \end{array}\right\} \tag{209}$$

The $i_M - v_M$ locus in Figure 95 lies in the first and the fourth quadrants. Thus, the extended memristor defined by Eq. (207) is an active element. Let us show the $v_M - p_M$ locus in Figure 96, where $p_M(t)$ is an instantaneous power defined by $p_M(t) = i_M(t)v_M(t)$. Observe that the $v_M - p_M$ locus is pinched at the origin, and the locus lies in the first and the third quadrants. Thus, the memristor switches between passive and active modes of operation, depending on its terminal voltage. We conclude as follow:

Switching behavior of the memristor

Assume that Eq. (208) exhibits chaotic oscillation. Then the extended memristor defined by Eq. (207) can switch between "passive" and "active" modes of operation, depending on its terminal voltage.

In order to obtain the above results, we have to choose the initial conditions carefully. It is due to the fact that a periodic response (drawn in magenta) coexists with a chaotic attractor (drawn in blue) as shown in Figure 97.

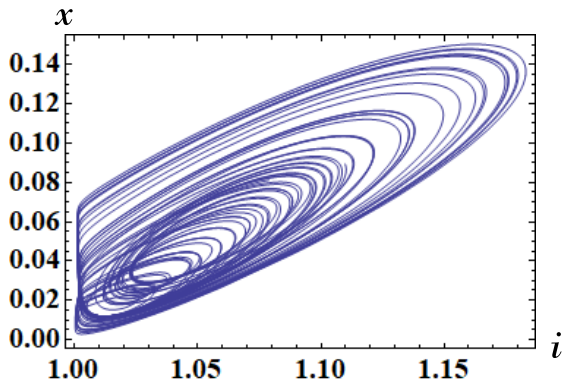

Figure 93: Chaotic attractor of the forced two-variable Oregonator model equations (208). Parameters: $f = 1,\ q = 0.001,\ L = 0.7,\ r = 0.01,\ \omega = 0.79$. Initial conditions: $i(0) = e^{0.1},\ x(0) = 0.1$.

5 Ideal Memristor Circuit

In this section, we realize the dynamics of the systems by using *ideal* memristors.

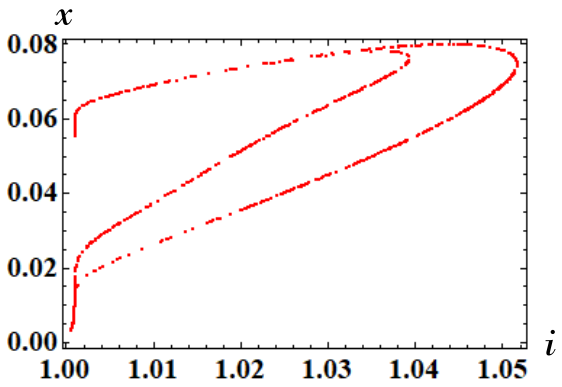

Figure 94: Poincaré map of the forced two-variable Oregonator model equations (208). Parameters: $f = 1,\ q = 0.001,\ L = 0.7,\ r = 0.01,\ \omega = 0.79$. Initial conditions: $i(0) = e^{0.1},\ x(0) = 0.1$.

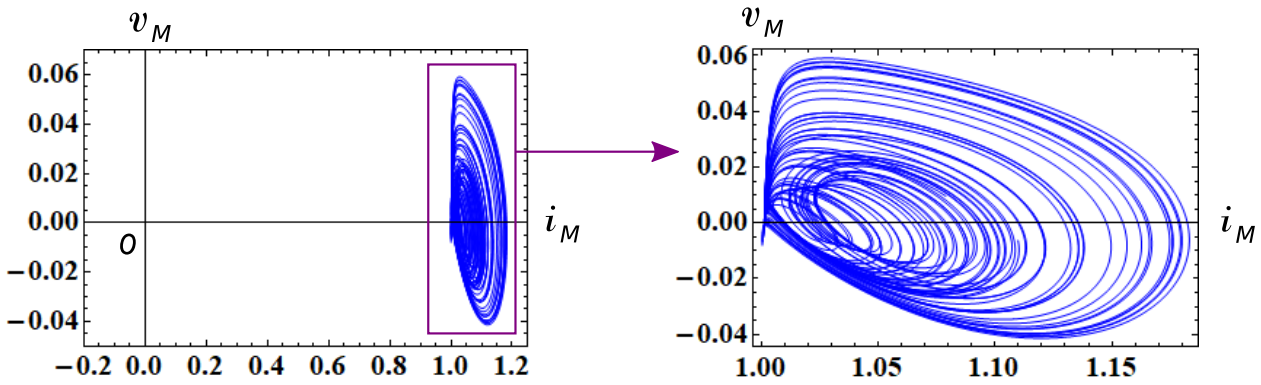

Figure 95: The $i_M - v_M$ locus of the forced two-variable Oregonator model equations (208). Here, v_M and i_M denote the terminal voltage and the terminal current of the current-controlled extended memristor. Parameters: $f = 1,\ q = 0.001,\ L = 0.7,\ r = 0.01,\ \omega = 0.79$. Initial conditions: $i(0) = e^{0.1},\ x(0) = 0.1$.

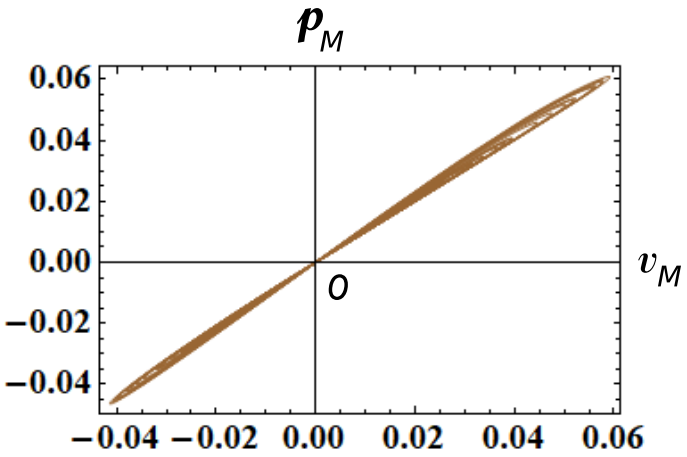

Figure 96: The $v_M - p_M$ locus of the forced two-variable Oregonator model equations (208). Here, $p_M(t)$ is an instantaneous power defined by $p_M(t) = i_M(t)v_M(t)$, and $v_M(t)$ and $i_M(t)$ denote the terminal voltage and the terminal current of the current-controlled extended memristor. Observe that the $v_M - p_M$ locus is pinched at the origin, and the locus lies in the first and the third quadrants. The memristor switches between passive and active modes of operation, depending on its terminal voltage $v_M(t)$. Parameters: $f = 1,\ q = 0.001,\ L = 0.7,\ r = 0.01,\ \omega = 0.79$. Initial conditions: $i(0) = e^{0.1},\ x(0) = 0.1$.

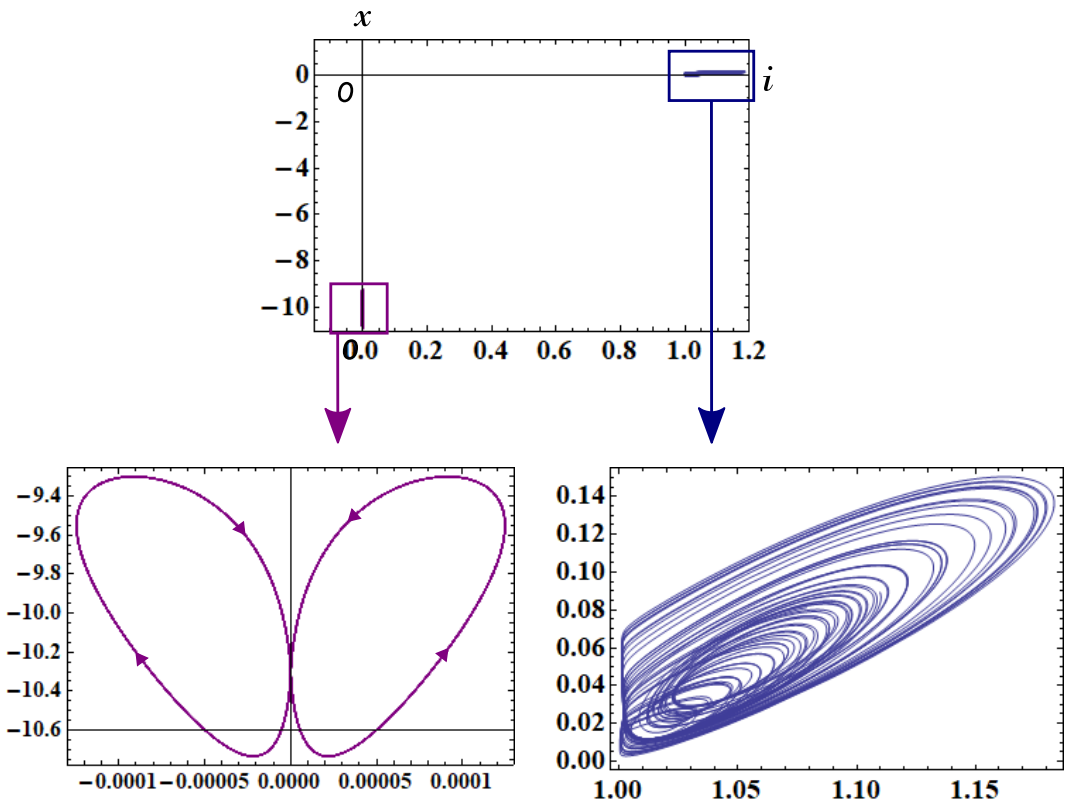

Figure 97: A periodic response (purple) coexists with a chaotic attractor (blue). Parameters: $f = 1,\ q = 0.001,\ L = 0.7,\ r = 0.01,\ \omega = 0.79$. Initial conditions for a periodic response: $i(0) = e^{-0.1},\ x(0) = 0.1$. Initial conditions for a chaotic attractor: $i(0) = e^{0.1},\ x(0) = 0.1$.

5.1 Van der Pol oscillator

The Van der Pol oscillator is defined by the second-order differential equations

Van der Pol equations

$$\left.\begin{aligned} \frac{dx}{dt} &= y - f(x), \\ \frac{dy}{dt} &= -x, \end{aligned}\right\} \tag{210}$$

where $f(x)$ is a scalar function of a single variable x defined by

$$f(x) = \frac{x^3}{3} - x. \tag{211}$$

Equation (210) can be realized by the circuit in Figure 98 [2]. The circuit equations are given by

Memristor Van der Pol equations

$$\left.\begin{aligned} L\frac{dq}{dt} &= \varphi - f(q), \\ C\frac{d\varphi}{dt} &= -q. \end{aligned}\right\} \tag{212}$$

Here, $L = C = 1$, q and φ denote the charge of the inductor L and the flux of the capacitors C, respectively, that is,

$$\left.\begin{aligned} q(t) &\stackrel{\triangle}{=} \int_{-\infty}^{t} i(t)dt, \\ \varphi(t) &\stackrel{\triangle}{=} \int_{-\infty}^{t} v(t)dt, \end{aligned}\right\} \tag{213}$$

and the $q - \varphi$ curve of the charge-controlled memristor is given by

$q - \varphi$ curve of the charge-controlled memristor

$$\varphi = f(q) = \frac{q^3}{3} - q. \tag{214}$$

Differentiating Eq. (212) with respect to time t, we obtain a set of differential equations

Derivative of Eq. (212)

$$\left.\begin{aligned} L\frac{di}{dt} &= v - M(q)i, \\ C\frac{dv}{dt} &= -i, \\ \frac{dq}{dt} &= i. \end{aligned}\right\} \tag{215}$$

Here, $L = C = 1$, i and v denote the current of the inductor L and the voltage of the capacitor C, respectively, and $M(q)$ is the small-signal memristance defined by

$$M(q) \stackrel{\triangle}{=} \frac{df(q)}{dq} = q^2 - 1. \tag{216}$$

The terminal voltage v_M and the terminal current i_M of the ideal memristor in Figure 98 are given by

V-I characteristics of the ideal memristor

$$v_M = M(q)\, i_M = (q^2 - 1)\, i_M. \qquad (217)$$

Equations (212) and (215) exhibit periodic oscillation (limit cycle). If an external source is added as shown in Figure 99, then the forced memristor Van der Pol equations can exhibit quasi-periodic oscillation [28]. The dynamics of this circuit is given by

Forced memristor Van der Pol equations

$$\left.\begin{aligned} L\frac{di}{dt} &= v - M(q)i + r\sin(\omega t), \\ C\frac{dv}{dt} &= -i, \\ \frac{dq}{dt} &= i. \end{aligned}\right\} \qquad (218)$$

We show the quasi-periodic attractor, Poincaré map, and $i_M - v_M$ locus of Eq. (218) in Figures 100, 101, and 102, respectively. The $i_M - v_M$ locus in Figure 102 lies in the all quadrants. Thus, the ideal memristor defined by Eq. (214) or Eq. (217) is an active element.

Let us next show the $v_M - p_M$ locus in Figure 103, where $p_M(t)$ is an instantaneous power defined by $p_M(t) = i_M(t)v_M(t)$. Observe that the $v_M - p_M$ locus is pinched at the origin, and the locus lies in all quadrants, which is similar to the locus in Figure 54(a). The memristor switches between four modes of operation:

$$(v_M,\, p_M) = (+,\, +),\ (+,\, -),\ (-,\, +),\ (-,\, -). \qquad (219)$$

Here, $(v_M,\, p_M) = (+,\, +)$ is read as $v_M > 0$ and $p_M > 0$, $(v_M,\, p_M) = (+,\, -)$ is read as $v_M > 0$ and $p_M < 0$, and we excluded the special case where $(v_M,\, p_M) = (0,\, 0)$. Thus, the operation of the memristor has the high complexity. The operation modes (219) can be coded by two bits:

$$(0,\, 0),\ (0,\, 1),\ (1,\, 0),\ (1,\, 1),$$

where $+$ is coded to a binary number 0 and $-$ to 1.

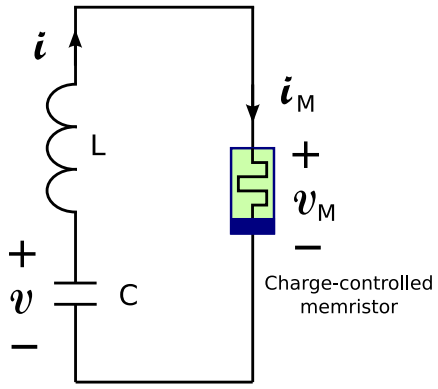

Figure 98: Memristor Van der Pol oscillator. The $q-\varphi$ curve of the charge-controlled memristor is given by $\varphi = f(q) = \frac{q^3}{3} - q$. Parameters: $L = C = 1$.

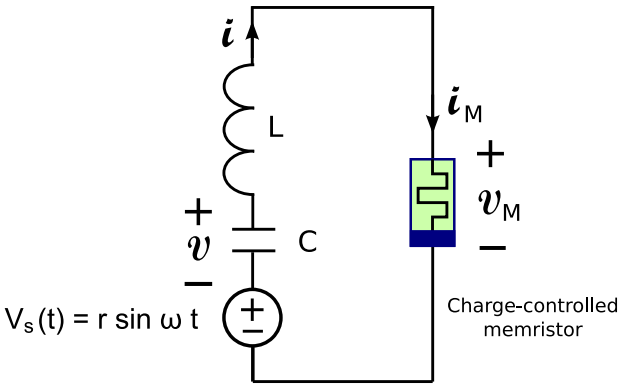

Figure 99: Memristor circuit driven by a periodic voltage source $v_s(t) = r\sin(\omega t)$, where r and ω are constants.

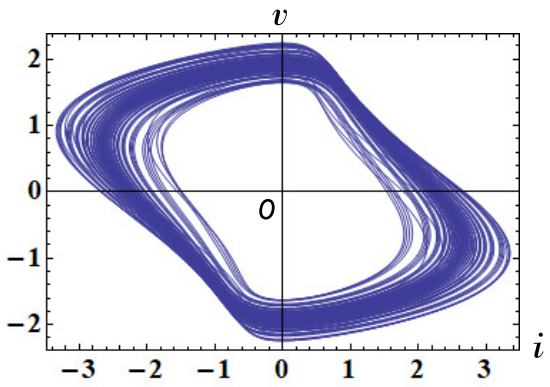

Figure 100: Quasi-periodic attractor of the forced memristor Van der Pol equations (218). Parameters: $r = 0.59,\ \omega = 1.1$. Initial conditions: $i(0) = 0.5,\ x(0) = 0$.

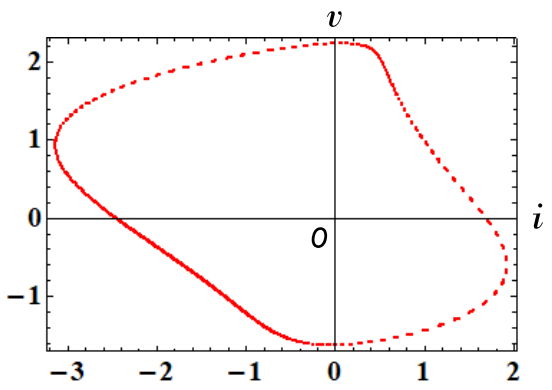

Figure 101: Poincaré map of the forced memristor Van der Pol equations (218). Parameters: $r = 0.59,\ \omega = 1.1$. Initial conditions: $i(0) = 0.5,\ x(0) = 0$.

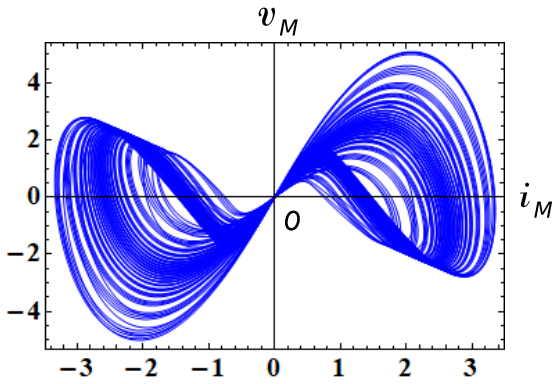

Figure 102: The $i_M - v_M$ locus of the forced memristor Van der Pol equations (218). Here, v_M and i_M denote the terminal voltage and the terminal current of the charge-controlled memristor. Observe that the ideal memristor defined by Eq. (214) or Eq. (217) is an active element. Parameters: $r = 0.59,\ \omega = 1.1$. Initial conditions: $i(0) = 0.5,\ x(0) = 0$.

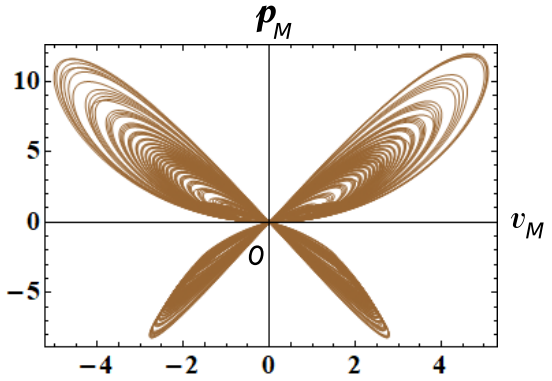

Figure 103: The $v_M - p_M$ locus of the forced memristor Van der Pol equations (218). Here, $p_M(t)$ is an instantaneous power defined by $p_M(t) = i_M(t)v_M(t)$. and $v_M(t)$ and $i_M(t)$ denote the terminal voltage and the terminal current of the charge-controlled memristor. Observe that the $v_M - p_M$ locus is pinched at the origin, and the locus lies in all quadrants. Parameters: $r = 0.59,\ \omega = 1.1$. Initial conditions: $i(0) = 0.5,\ x(0) = 0$.

5.2 Chua Circuit

The dynamics of the Chua circuit [14, 29] is defined by

Chua circuit equations

$$\left.\begin{aligned} \frac{dx_1}{dt} &= \alpha\big(x_2 - x_1 - g(x_1)\big), \\ \frac{dx_2}{dt} &= x_1 - x_2 + x_3, \\ \frac{dx_3}{dt} &= -\beta x_2. \end{aligned}\right\} \tag{220}$$

Here, α and β are parameters, and $g(x_1)$ is a scalar function of a single variable x_1 defined by

$$g(x_1) = \frac{1}{16}x_1^3 - \frac{7}{6}x_1, \tag{221}$$

which is a generalization from a continuous piecewise-linear function to a smooth function [14]. The original Chua circuit equations possess a piecewise-linear nonlinearity [29]. That is, $g(x_1)$ is a piecewise-linear function with discontinuous derivatives at the breakpoints. Equation (220) has a chaotic attractor similar to a double scroll attractor for certain values of the parameters α and β [14, 29]. This equation can also have a stable closed orbit outside of a chaotic attractor.

Equation (220) can be realized by the circuit in Figure 104 [2].

Memristor Chua circuit equations

$$\left.\begin{aligned} C_1\frac{d\varphi_1}{dt} &= \frac{\varphi_2 - \varphi_1}{R} - f(\varphi_1), \\ C_2\frac{d\varphi_2}{dt} &= q_3 - \frac{\varphi_2 - \varphi_1}{R}, \\ L\frac{dq_3}{dt} &= -\varphi_2. \end{aligned}\right\} \tag{222}$$

Here, φ_1, φ_2, and q_3 denote the flux of the capacitor C_1, the flux of the capacitor C_2, and the charge of the inductor L, respectively, and the $\varphi - q$ curve of the flux-controlled memristor is given by

$\varphi - q$ curve of the ideal memristor

$$q = g(\varphi) = \frac{\varphi^3}{16} - \frac{7\varphi}{6}. \tag{223}$$

Differentiating Eq. (220) with respect to time t, we obtain

Derivative of Eq. (220)

$$\left.\begin{aligned} C_1\frac{dv_1}{dt} &= \frac{v_2 - v_1}{R} - W(\varphi_1)v_1, \\ C_2\frac{dv_2}{dt} &= i_3 - \frac{v_2 - v_1}{R}, \\ L\frac{di_3}{dt} &= -v_2. \end{aligned}\right\} \tag{224}$$

Here, v_1, v_2, and i_3 denote the voltage across the capacitor C_1, the voltage across the capacitor C_2, and the current through the inductor L, respectively, and $W(\varphi_1)$ is the small-signal *memductance* defined by

$$W(\varphi_1) \triangleq \frac{dg(\varphi_1)}{d\varphi_1} = \frac{3}{16}\varphi^2 - \frac{7}{6}. \tag{225}$$

The terminal voltage v_M and the terminal current i_M of the ideal memristor in Figure 104 are given by

V-I characteristics of the ideal memristor

$$i_M = W(\varphi_1)\, v_M = \left(\frac{3}{16}\varphi^2 - \frac{7}{6}\right) v_M. \tag{226}$$

We show the chaotic attractor, Poincaré map, and $v_M - i_M$ locus in Figures 105, 106, and 107, respectively. The following parameters are used in our computer simulations:

$$\left.\begin{array}{l} C_1 = \dfrac{1}{\alpha}, \quad C_2 = 1, \quad L = \dfrac{1}{\beta}, \quad R = 1. \\ \alpha = 10, \quad \beta = 14. \end{array}\right\} \tag{227}$$

Observe the folding action of the chaotic attractor in Figure 106. The $v_M - i_M$ locus in Figure 107 lies in the second and the fourth quadrants. Thus, the ideal memristor defined by Eq. (223) or Eq. (226) is an active element.

Let us next show the $i_M - p_M$ locus in Figure 103, where $p_M(t)$ is an instantaneous power defined by $p_M(t) = i_M(t)v_M(t)$. Observe that the $i_M - p_M$ locus is pinched at the origin, and the locus lies in the third and the fourth quadrants. The memristor switches between two operation modes:

$$(i_M,\, p_M) = (+,\, -),\ (-,\, -). \tag{228}$$

Here, $(i_M, p_M) = (+, -)$ is read as $i_M > 0$ and $p_M < 0$, $(i_M, p_M) = (-, -)$ is read as $i_M < 0$ and $p_M < 0$, and we excluded the special case where $(i_M, p_M) = (0, 0)$. These memristor's operation modes are quite different from those of the other systems. The operation modes (228) can be coded by two bits:

$$(0,\, 1),\ (1,\, 1),$$

where $+$ is coded to a binary number 0 and $-$ to 1.[8]

[8]Similarly, the forced memristor Brusselator equations (9) have the different operation modes, which are given by $(v_M, p_M) = (+, +)$. It can be coded by $(0, 0)$. It is due to the reason that the extended memristor is passive. See the $v_M - p_M$ locus shown in Figure 109 and Appendix B for more details.

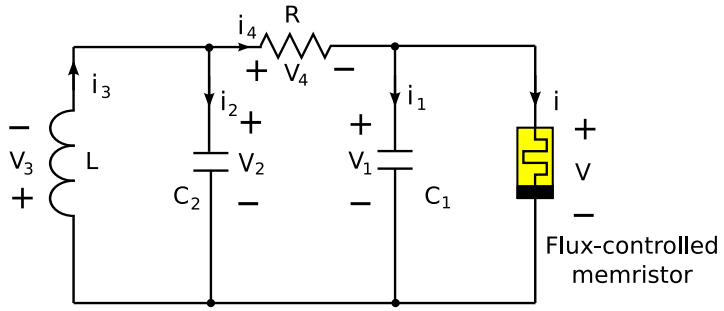

Figure 104: Memristor Chua circuit. It contains five circuit elements: two passive capacitors, one passive inductor, one passive resistor, and one flux-controlled memristor.

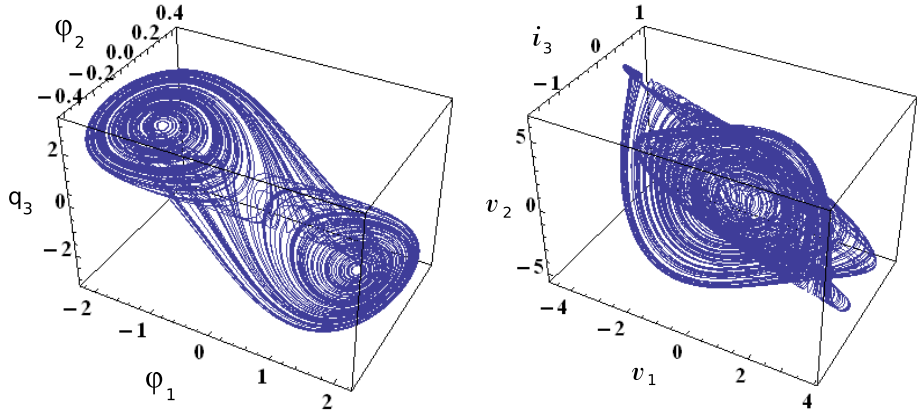

(a) $(\varphi_1, \varphi_1, q_3)$-space (b) (v_1, v_2, i_3)-space

Figure 105: Chaotic attractors of the memristor Chua circuit equations. (a) Chaotic attractor of Eq. (222). (b) Chaotic attractor of Eq. (224). Parameters: $C_1 = \frac{1}{10}$, $C_2 = 1$, $L = \frac{1}{14}$, $R = 1$. Initial conditions: $(v_1(0),\ v_2(0),\ i_3(0),\ \varphi_1(0)) = (0.1,\ 0.1,\ 0.1,\ 0)$.

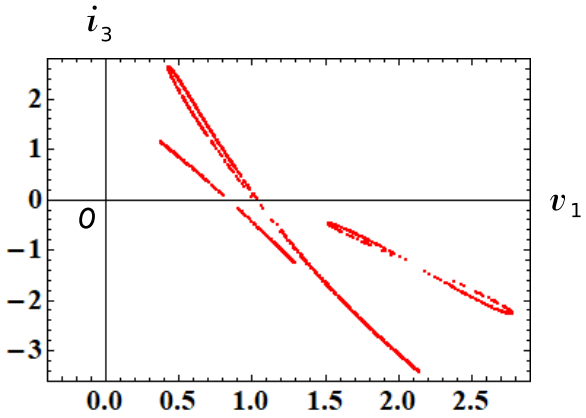

Figure 106: Poincaré map of the chaotic attractor for the memristor Chua circuit equations (224). The Poincaré cross-section is defined by $\{(v_1,\, v_2,\, i_3) \in R^3 \mid v_2 = 0.8\}$. The chaotic trajectory of Eq. (224) crosses the above Poincaré cross-section (plane) many times. Observe the folding action of the chaotic attractor. Parameters: $C_1 = \dfrac{1}{10}$, $C_2 = 1$, $L = \dfrac{1}{14}$, $R = 1$. Initial conditions: $(v_1(0),\ v_2(0),\ i_3(0),\ \varphi_1(0)) = (0.1,\ 0.1,\ 0.1,\ 0)$.

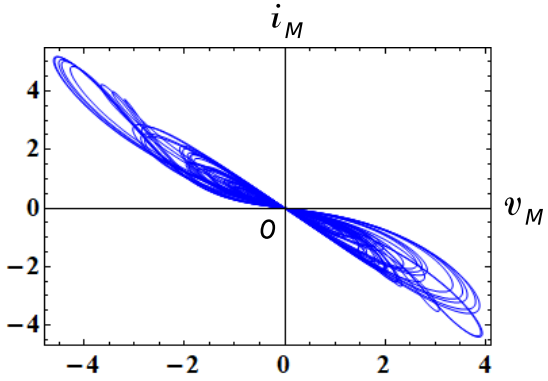

Figure 107: The $v_M - i_M$ locus of the memristor Chua circuit equations (224). Here, v_M and i_M denote the terminal voltage and the terminal current of the flux-controlled memristor. Observe that the ideal memristor defined by Eq. (223) or Eq. (226) is an active element, since the locus lies in the second and the fourth quadrants. Parameters: $C_1 = \dfrac{1}{10}$, $C_2 = 1$, $L = \dfrac{1}{14}$, $R = 1$. Initial conditions: $(v_1(0),\ v_2(0),\ i_3(0),\ \varphi_1(0)) = (0.1,\ 0.1,\ 0.1,\ 0)$.

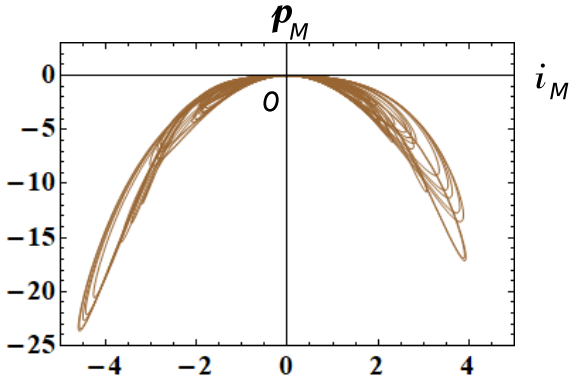

Figure 108: The $i_M - p_M$ locus of the memristor Chua circuit equations (224). Here, $p_M(t)$ is an instantaneous power defined by $p_M(t) = i_M(t)v_M(t)$, and $v_M(t)$ and $i_M(t)$ denote the terminal voltage and the terminal current of the flux-controlled memristor. Observe that the $i_M - p_M$ locus is pinched at the origin, and the locus lies in the third and the fourh quadrants. Parameters: $C_1 = \dfrac{1}{10}$, $C_2 = 1$, $L = \dfrac{1}{14}$, $R = 1$. Initial conditions: $(v_1(0),\ v_2(0),\ i_3(0),\ \varphi_1(0)) = (0.1,\ 0.1,\ 0.1,\ 0)$.

6 Conclusion

We have shown that the dynamics of a wide variety of nonlinear systems such as engineering, physical, chemical, biological, and ecological systems, can be simulated or modeled by the dynamics of memristor circuits. The resulting memristor circuits can exhibit quasi-periodic, non-periodic, or chaotic behavior by supplying the external source. If they have an integral invariant, their behavior greatly depends on the initial conditions, the circuit parameters, and the maximum step size of the numerical integration. Furthermore, an overflow (outside the range of data) is likely to occur due to the numerical instability in long-time simulations. We have also shown that we can reconstruct chaotic attractors by using the terminal voltage and current of the memristor. Furthermore, in many circuits, the active memristor switches between passive and active modes of operation, depending on its terminal voltage. However, we found that the memristor's operation modes exhibit the higher complexity in the forced memristor Toda lattice equations and the forced memristor Van der Pol equations. We note that almost all results in this paper were obtained by using "NDSolve" in Mathematica (32 bit version). If we use other softwares to solve differential equations, we might obtain slightly different results.

References

[1] Itoh, M. and Chua, L. (2017) Dynamics of Hamiltonian systems and memristor circuits. *Int. J. Bifurcation and Chaos* **27**(2), 1730005-1–66.

[2] Itoh, M. and Chua, L. O. (2013) Duality of memristor circuits. *Int. J. Bifurcation and Chaos* **23**(1), 1330001-1–50.

[3] Itoh, M. and Chua, L. O. (2011) Memristor Hamiltonian circuits. *Int. J. Bifurcation and Chaos* **21**(9), 2395-2425.

[4] Itoh, M. and Chua, L. O. (2014) Dynamics of memristor circuits. *Int. J. Bifurcation and Chaos* **24**(5), 1430015-1–44.

[5] Bashkirtseva, I. and Ryashko, L. (2005) Sensitivity and chaos control for the forced nonlinear oscillations. *Chaos, Solitons and Fractals*, **26**(5). 1437-1451.

[6] Packard, N. H., Crutchfield, J. P., Farmer, J. D., and Shaw, R. S. (1980) Geometry from a Time Series", Phys. Rev. Lett. **45**(9), 712-716.

[7] Gierer, A. and H. Meinhardt (1972) A theory of biological pattern formation. *Kybernetic* **12**, 30-39.

[8] Gonpot, P., GonpotCollet, J.S.A., and Sookia, N.U.H. (2008) Meinhardt Model: Bifurcation Analysis and Pattern Formation. Trends in Applied Sciences Research **3**(2), 115-128.

[9] Li, Y., Wang, J., and Hou, X. (2017) Stripe and spot patterns for the Gierer-Meinhardt model with saturated activator production. *J. Math. Anal. Appl.* **449**(2), 1863-1879.

[10] Andronov, A. A., Vitt, A. A., and Khaikin, S. E. (1987) *Theory of oscillators* (Dover, NY).

[11] Guckenheimer, J. and Holmes, P. (1983) *Nonlinear Oscillations, Dynamical Systems, and Bifurcations of Vector Fields* (Springer-Verlag, NY).

[12] Chua, L. O. (2012) The fourth element. *Proc. IEEE* **100**(6), 1920-1927.

[13] Tyson, J. and Kauffman, S. J. (1975) "Control of Mitosis by a Continuous Biochemical Oscillation: Synchronization; Spatially Inhomogeneous Oscillations. *Math. Biology* **1**(4), 289-310.

[14] Hirsch, M. W., Smale, S., and Devaney, R. L. (2003) *Differential Equations, Dynamical Systems and An Introduction to Chaos, Second Edition* (Elsevier Academic Press, Amsterdam).

[15] Itoh, M. and Chua, L. (2017b) Chaotic oscillation via edge of chaos criteria. *Int. J. Bifurcation and Chaos* **27**(11), 1730035-1–79.

[16] Peitgen, H., Jurgens, H., and Saupe, D. (2004) *Chaos and Fractals: New Frontiers of Science* (Springer-Verlag, New York).

[17] Letellier, C. and Rossler, O. E. (2006) 'Rossler attractor. *Scholarpedia* **1**(10), 1721.

[18] Pisarchik, A. N., Meucci, R., and Arecchi, F. T. (2001) Theoretical and experimental study of discrete behavior of Shilnikov chaos in a CO 2 laser. Eur. Phys. J. D **13**(3), 385-391.

[19] Toda, M. (1986) *Non-linear wave and soliton* (in Japanese) (Nihon-hyouron-sha, Tokyo).

[20] Toda, M. (1989) *Theory of Nonlinear Lattices (2nd ed.)* (Springer, Berlin).

[21] Hénon, M. (1974) Integrals of the Toda lattice. *Phys. Rev. B* **9**, 1921-1923.

[22] Hirota, R. (1985) Soliton. *Surikagaku (Mathematical Sciences - Special Issues)* **10**, 22-29 (in Japanese).

[23] Toda, M. (1995) *Thirty lectures on waves and non-linear problems* (in Japanese) (Asakura-shoten, Tokyo).

[24] Teschl, G. (2001) Almost everything you always wanted to know about the Toda equation. Jahresber. Deutsch. Math.-Verein. **103**(4), 149-162.

[25] Fernandes, R. L., and Oliva, W. M. (1998) Hamiltonian dynamics of the Lotka-Volterra equations. International Conference on Differential Equations (Lisboa, 1995) 327-334 (World Sci. Publ., River Edge, NJ).

[26] He, Y. and Sun, Y. (2012) On an integrable discretisation of the Lotka-Volterra system. AIP Conference Proceedings **1479**, 1295-1298.

[27] Zemskov, E. P., Vanag, V. K., and Epstein, I. R. (2011) Amplitude equations for reaction-diffusion systems with cross diffusion. *Phys. Rev. E* **84**, 036216-1–13.

[28] Thompson, J. M. T. and Stewart, H. B. (1986) *Nonlinear Dynamics and Chaos, Geometrical Methods for Engineers and Scientists*, (Wiley, Chichester).

[29] Madan, R. N. (1993) *Chua's Circuit: A Paradigm for Chaos* (World Scientific, Singapore).

[30] Chua, L. O. (1971) Memristor–The missing circuit element", *IEEE Trans. Circuit Th.* **CT-18** (5), 507-519.

[31] Chua, L. O. and Kang, S. M. (1976) Memristive devices and systems. *Proc. IEEE* **64**(2), 209-223.

[32] Chua, L. (2015) Everything you want to know about memristors, but are afraid to ask", *Radioengineering* **24**(2), 319-368.

Appendix A *Classification of Memristors*

Memristor is a 2-terminal electronic device, which was postulated in [12, 30, 31]. An *ideal* memristor can be described by a constitutive relation between the charge q and the flux φ,

$$q = g(\varphi) \;\; \text{or} \;\; \varphi = f(q), \tag{229}$$

where $g(\cdot)$ and $f(\cdot)$ are differentiable scalar-valued functions. Its terminal voltage v and terminal current i are described by

$$i = G(\varphi)v \;\; \text{or} \;\; v = R(q)i, \tag{230}$$

where

$$v = \frac{d\varphi}{dt} \;\; \text{and} \;\; i = \frac{dq}{dt}, \tag{231}$$

which represent *Faraday's induction law* and its dual law, respectively. The nonlinear functions $G(\varphi)$ and $R(\varphi)$, called the small-signal *memductance* and small-signal *memristance*, respectively, are defined by, is defined by

$$G(\varphi) \stackrel{\triangle}{=} \frac{dg(\varphi)}{d\varphi}, \tag{232}$$

and

$$R(q) \stackrel{\triangle}{=} \frac{df(q)}{dq}, \tag{233}$$

representing the *slope* of the scalar function $q = g(\varphi)$, and $\varphi = f(q)$, respectively, called the *memristor constitutive relation*.

All voltage-controlled memristors can be classified into four classes [32]:

- voltage-controlled ideal memristor

$$\begin{array}{rcl} i & = & G(\varphi)v, \\ \dfrac{d\varphi}{dt} & = & v. \end{array} \tag{234}$$

- voltage-controlled ideal generic memristor

$$\begin{array}{rcl} i & = & G(x)v, \\ \dfrac{dx}{dt} & = & \hat{g}(x)v. \end{array} \tag{235}$$

- voltage-controlled generic memristor

$$\begin{aligned} i &= \tilde{G}(\boldsymbol{x})v, \\ \frac{d\boldsymbol{x}}{dt} &= \tilde{\boldsymbol{g}}(\boldsymbol{x},\ v). \end{aligned} \tag{236}$$

- voltage-controlled extended memristor

$$\begin{aligned} i &= \hat{G}(\boldsymbol{x},\ v)v, \\ &\quad \hat{G}(\boldsymbol{x},\ 0) \neq \infty, \\ \frac{d\boldsymbol{x}}{dt} &= \tilde{\boldsymbol{g}}(\boldsymbol{x},\ v). \end{aligned} \tag{237}$$

Here, $G(\cdot)$, $\tilde{G}(\cdot)$, $\hat{G}(\cdot)$, and $\hat{g}(\cdot)$ are continuous scalar-valued functions, $\boldsymbol{x} = (x_1,\ x_2,\ \cdots,\ x_n) \in \mathbb{R}^n$, and $\tilde{\boldsymbol{g}} = (\tilde{g}_1,\ \tilde{g}_2,\ \cdots,\ \tilde{g}_n) : \mathbb{R}^n \to \mathbb{R}^n$.

Similarly, all current-controlled memristors can be classified into four classes [32]:

- current-controlled ideal memristor

$$\begin{aligned} v &= R(q)i, \\ \frac{dq}{dt} &= i. \end{aligned} \tag{238}$$

- current-controlled ideal generic memristor

$$\begin{aligned} v &= R(x)i, \\ \frac{dx}{dt} &= \hat{f}(x)i. \end{aligned} \tag{239}$$

- current-controlled generic memristor

$$\begin{aligned} v &= \tilde{R}(\boldsymbol{x})i, \\ \frac{d\boldsymbol{x}}{dt} &= \tilde{\boldsymbol{f}}(\boldsymbol{x},\ i). \end{aligned} \tag{240}$$

- current-controlled extended memristor

$$\begin{aligned} v &= \hat{R}(\boldsymbol{x},\ i)i, \\ &\quad \hat{R}(\boldsymbol{x},\ 0) \neq \infty, \\ \frac{d\boldsymbol{x}}{dt} &= \tilde{\boldsymbol{f}}(\boldsymbol{x},\ i). \end{aligned} \tag{241}$$

Here, $R(\cdot)$, $\tilde{R}(\cdot)$, $\hat{R}(\cdot)$, and $\hat{f}(\cdot)$ are continuous scalar-valued functions, $\boldsymbol{x} = (x_1,\ x_2,\ \cdots,\ x_n) \in \mathbb{R}^n$, and $\tilde{\boldsymbol{f}} = (\tilde{f}_1,\ \tilde{f}_2,\ \cdots,\ \tilde{f}_n) : \mathbb{R}^n \to \mathbb{R}^n$.

Appendix B $v_M - p_M$ *locus of the forced memristor Brusselator equations*

Consider the forced memristor Brusselator equations defined by Eq. (9), that is,

$$\left.\begin{array}{rcl} L\dfrac{di}{dt} &=& A + \big\{ix - (B+1)\big\}i + r\sin(\omega t), \\ \dfrac{dx}{dt} &=& B\,i - i^2\,x, \end{array}\right\} \tag{242}$$

where

$$A = 0.4,\ B = 1.2,\ r = 0.05,\ \omega = 0.81. \tag{243}$$

Assume that the terminal voltage v_M and the terminal current i_M of the extended memristor are given by Eq. (8), that is,

$$\left.\begin{array}{rcl} v_M &=& \hat{R}(x,\, i_M)\, i_M, \\ \dfrac{dx}{dt} &=& B\, i_M - {i_M}^2\, x, \end{array}\right\} \tag{244}$$

where $\hat{R}(x,\, i_M) = -\big\{i_M\, x - (B+1)\big\}$ and $i_M = i$. Then the forced Brusselator equations (242) can be realized by the circuit in Figure 2, where $L = 1$ and $E = A = 0.4$.

As stated in Sec. 2.1, the $i_M - v_M$ locus moves in the first quadrant only, that is, it moves in the *passive* region (see Figure 5(a)). Consider next the instantaneous power of the extended memristor, which is defined by

$$p_M(t) = i_M(t) v_M(t). \tag{245}$$

Then the $v_M - p_M$ locus of Eq. (242) is not pinched at the origin, and the locus lies in the first quadrant only as shown in Figure 109(a). Thus, the memristor's operation mode is given by

$$(v_M,\, p_M) = (+,\, +), \tag{246}$$

where $(v_M,\, p_M) = (+,\, +)$ is read as $v_M > 0$ and $p_M > 0$. The operation mode (246) can be coded by

$$(0,\, 0), \tag{247}$$

where $+$ is coded to a binary number 0 and $-$ to 1. The binary mode (247) is equivalent to the one-bit coding defined by (0).

Define next the instantaneous power of the two elements, that is, the instantaneous power of the extended memristor and the battery by

$$p_{ME}(t) = i_M(t)\, v_{ME}(t), \tag{248}$$

where E denotes the voltage of the battery and $v_{ME}(t) = v_M(t) - E$. That is, $v_{ME}(t)$ denotes the voltage across the extended memristor and the battery. We show the $v_{ME} - p_{ME}$ locus in Figure 109(b). Observe that the locus is pinched at the origin, and it lies in the first and the third quadrants. Thus, the instantaneous power p_{ME} delivered from the forced signal and the inductor is dissipated when $v_M(t) - E > 0$. However, the instantaneous power p_{ME} is *not* dissipated when $v_M(t) - E < 0$. Thus, the operation modes of the two elements is given by

$$(v_{ME},\ p_{ME}) = (+,\, +),\ (-,\, -). \tag{249}$$

They are coded by

$$(0,\, 0),\ (1,\, 1), \tag{250}$$

which are equivalent to the one bit coding defined by

$$(0),\ (1). \tag{251}$$

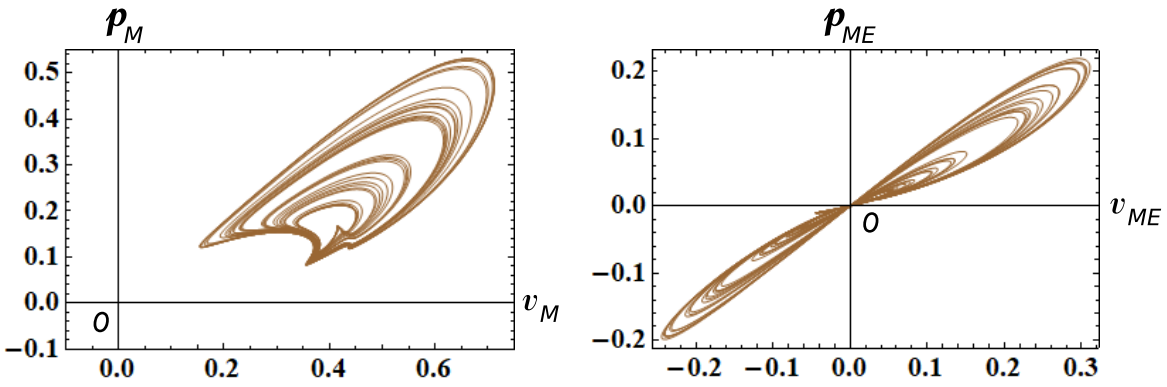

(a) $v_M - p_M$ locus (b) $v_{ME} - p_{ME}$ locus

Figure 109: The $v_M - p_M$ and $v_{ME} - p_{ME}$ loci of the forced memristor Brusselator equations (9). Here, $p_M(t)$ and $p_{ME}(t)$ are the instantaneous powers defined by $p_M(t) = i_M(t)\, v_M(t)$ and $p_{ME}(t) = i_M(t)\, v_{ME}(t)$, respectively, v_M and i_M denote the terminal voltage and the terminal current of the current-controlled extended memristor, $v_{ME}(t) = v_M(t) - E$, and E denotes the voltage of the battery. Observe that the $v_M - i_M$ locus is *not* pinched at the origin, and the locus lies in the first quadrant only. However, the $v_{ME} - p_{ME}$ locus is pinched at the origin, and it lies in the first and the third quadrants. Parameters: $A = 0.4,\ B = 1.2,\ r = 0.05,\ \omega = 0.81$. Initial conditions: $i(0) = 1.1,\ x(0) = 1.1$.